INTERNATIONAL ATOMIC ENERGY AGENCY
UNITED NATIONS EDUCATIONAL, SCIENTIFIC AND CULTURAL ORGANIZATION

INTERNATIONAL CENTRE FOR THEORETICAL PHYSICS
34100 TRIESTE (ITALY) - P.O.B. 586 - MIRAMARE - STRADA COSTIERA 11 - TELEPHONES: 224281/2/3/4/5/6
CABLE: CENTRATOM - TELEX 460392 - I

H4.SMR/164 - 14

WORKSHOP ON CLOUD PHYSICS AND CLIMATE

23 November - 20 December 1985

REMOTE SENSING, SATELLITE & RADAR METEOROLOGY - II
(Extra lecture notes)

G. DUGDALE
University of Reading
U.K.

REMOTE SENSING
RADAR + SATELLITE METEOROLOGY

OBJECTIVES

STUDY SCOPE + LIMITATIONS

SYLLABUS

1. E-M RADIATION + THE ATMOSPHERE
   i) Absorption
   ii) Emmision
   iii) Scattering

2. SATELLITE METEOROLOGY
   i) Satellite characteristics
   ii) Atmospheric soundings
   iii) Soundings of the surface
   iv) Some applications

3. RADAR METEOROLOGY
   i) Principles of radar
   ii) Rainfall measurement
   iii) Special applications

WHY R.S?

ECONOMY

SCALE

WHAT?

1. Routine meteorology
   Sea surface temp.
   Atmospheric soundings
   Surface wind (oceans)
   Atmospheric wind

2. Hydrology
   Rainfall
   Flood forecasting
   Snow cover
   Lake levels

3. Research + special applications
   Energy balance studies
   Crop monitoring
   Pest control
   Storm structure
   Turbulence

HOW?

Interaction with E-M radiation

Table 1

The Global Atmospheric Research Programme of WMO recommended accuracies for atmospheric soundings.

Quantity	Accuracy (r.m.s. error)
Wind component	$\pm$ 3 m s $^{-1}$
Temperature	$\pm$ 1 K
Water vapour pressure	$\pm$ 1 mb
Sea surface temperature	$\pm$ 0.2 K
Pressure reference level	$\pm$ 0.3%

Data required on a 100 km grid, at eight standard levels in the atmosphere

(Surface 900, 700, 500, 200, 100, 50 and 20 mb), twice per day.

TYPES OF SENSOR SYSTEMS

General types of sensor systems

Fig. 1.1

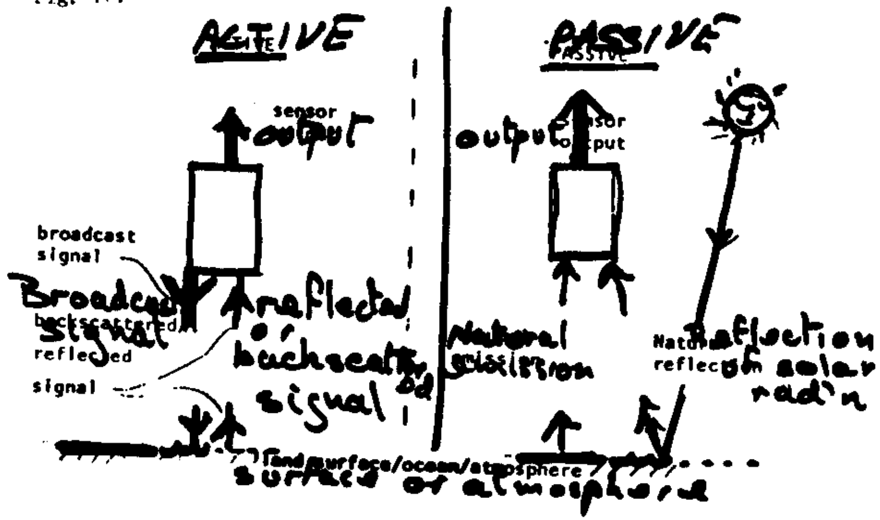

- Passive sensors: passively measure/interpret signal information coming directly from the field of observation. e.g. radiation thermometer.
- Active sensors: transmit a signal towards the field of observation and measure the reflected return signal. e.g. weather radar.

THE R.S PROBLEM

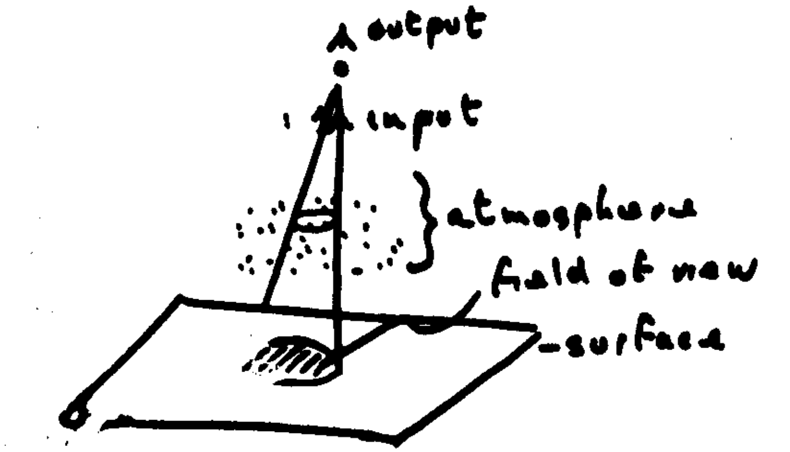

i) Signal may depend on other properties of the source than that one wishes to measure

ii) The input will come from other areas than that one wishes to measure and the effect will depend on many factors.

iii) Sensor calibration may not be constant.

THE E-M SPECTRUM

$\tilde{\nu} = \frac{1}{\lambda}$

$\nu = \frac{c}{\lambda}$

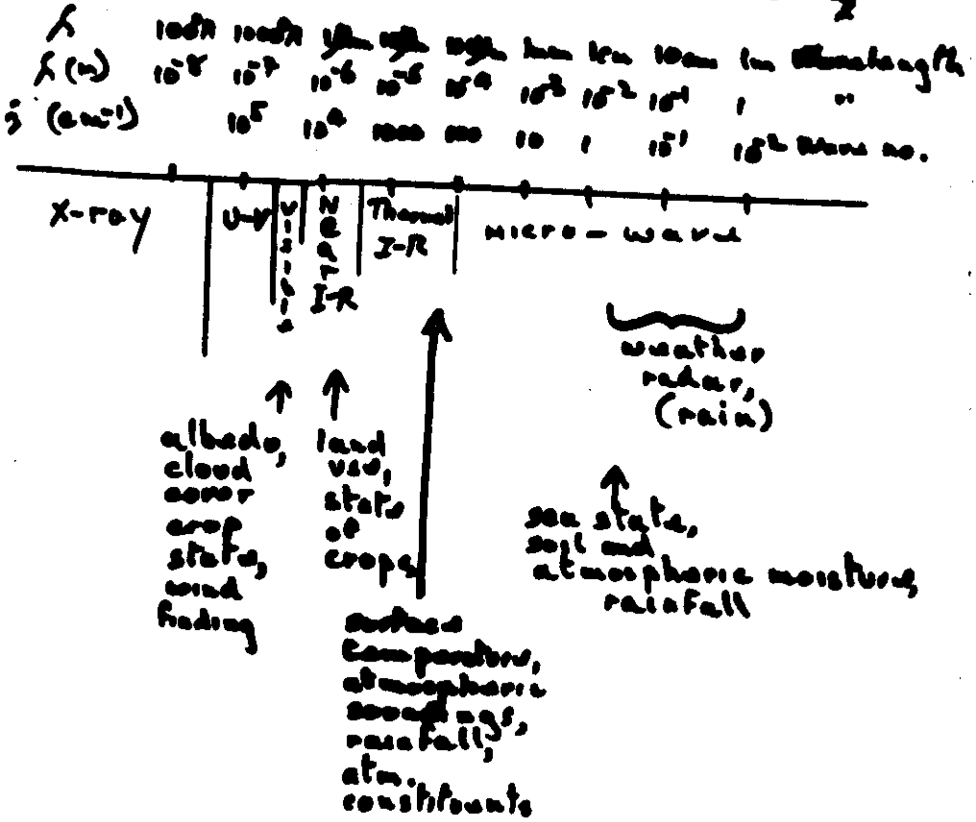

Beer's law MONOCHROMATIC

fractional extinction
$\propto$ ext. coef × path length
× density of absorber or scatterer.

$$\frac{\delta I}{I} = -k\rho\,\delta x$$

Valid for $k\rho\,\delta x \ll 1$

$$\frac{I}{I_0} = \exp(-k\rho x)$$

k abs. coef $[m^2\,kg^{-1}]$ | neglect scattering

$\frac{I}{I_0}$ transmission

$(1 - I/I_0)$ absorption (+ scattering)

Schwarzschild's eq:-

we have absorption and emission in element δS

$$\frac{dN}{dS} = \rho k\,(N_B - N)$$

N is radiance

ABSORPTION + EMISSION OF E.M. RADIATION IN THE ATMOSPHERE

1. ENERGY OF A MOLECULE

Total energy		Electronic energy		Vibrational energy		Rotational energy		Translational energy
E	=	E_e	+	E_V	+	E_R	+	E_T

$\Delta E \Rightarrow$ $<1\,\mu m$ $\quad$ $\underbrace{1\text{–}100\,\mu m \quad 1\text{–}1000\,\mu m}_{\text{Dominate in the atmosphere}}$ $\quad$ continuous

2. LOCAL THERMODYNAMIC EQUILIBRIUM (L.T.E)

IF INTER-MOLECULAR INTERACTION INTERVAL (γ) $\ll$ MOLECULAR DE-EXCITATION TIME THEN AN EXCITED MOLECULE WILL TEND TO INTERACT AND REDISTRIBUTE ITS ENERGY RATHER THAN EMITTING AT THE EXCITATION FREQUENCY.

IN THE ATMOSPHERE L.T.E. USUALLY EXISTS BELOW 80 KM. + ATMOSPHERIC GASES EMIT + ABSORB AT FREQUENCIES CORRESPONDING TO CHANGES IN VIBRATIONAL + ROTATIONAL ENERGY LEVELS.

2.1

2.2. SPECTRAL LINES

a) Intrinsic width

b) Doppler broadening.

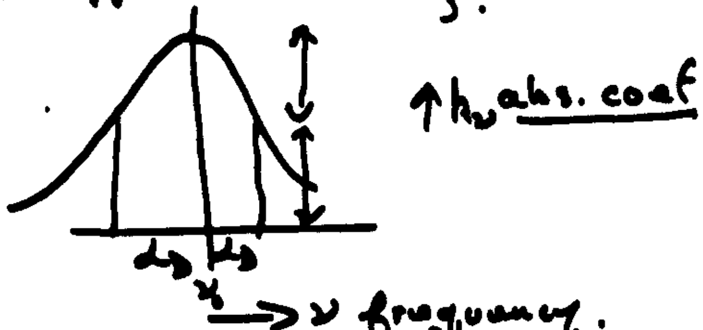

α_D = Doppler half width.

$$\boxed{\begin{array}{c} \Delta\nu = \nu_0 \frac{v}{c} \\ \nu_0 \; \overset{v}{\rightarrow} \qquad \text{Observer.} \end{array}}$$

$$n(\nu_0 \pm \delta\nu) = e^{-(\delta\nu)^2}$$

$$k_\nu = \frac{S}{\alpha_D \pi^{1/2}} \exp -\left[\frac{(\nu-\nu_0)^2}{\alpha_D^2}\right]$$

S = line strength $= \int_{-\infty}^{\infty} k_\nu \, d\nu$

only important high in the atmosphere.

Pressure broadening

α_L the Lorentz half width.

$$k_\nu = \frac{S\alpha_L}{\pi[(\nu-\nu_0)^2+\alpha_L^2]}$$

Interaction frequency depends on T & p. In the atmosphere changes in p are large c.f. changes in T.

$$\& \ \alpha_{Lp} \approx \alpha_{L0}\frac{p}{p_0}$$

where α_{L0} is α_L determined at p_0

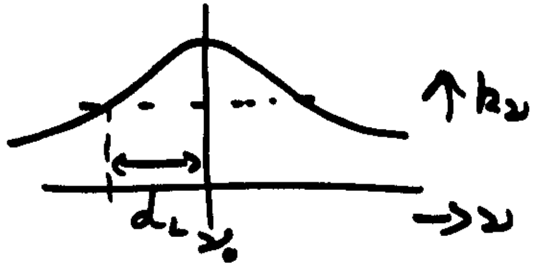

Curtis-Godson approximation

$$\bar{p} \approx \frac{\int \rho p\, dl}{\int \rho\, dl}$$

for determining the effective pressure along an atmospheric path of length L through an absorber of density ρ.

Atmospheric transmission

$$\tau_\nu = \exp[-\int k_\nu \rho\, dl] \quad \text{(Beer's law)}$$

Integrated absorptance of a line W

The total effect of absorption by a line along a defined atmospheric path

$$W = \int_{-\infty}^{\infty}(1-\tau_\nu)\,d\nu$$

"Weak" & "strong" approximations for W for a pressure broadened line

a) $\int \rho k\, dl$ small

$$\tau = \exp -\int k_\nu \rho\, dl \approx 1-\int k_\nu \rho\, dl$$

$$\therefore W = \int k_\nu \rho\, dl$$

i.e. ρ constant

$$W = \rho l S$$

b) $\int \rho k\, dl$ large; there is no transmission near line centre

$$\& \ k_\nu \approx \frac{S\alpha_L}{\pi(\nu_0-\nu)^2}$$

gives $W = 2(S\alpha_L \rho l)^{1/2}$

Fig 2.2

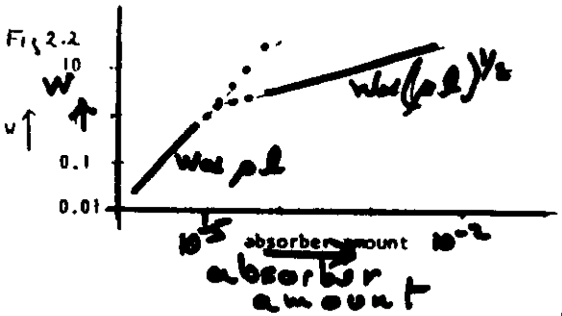

curve of growth

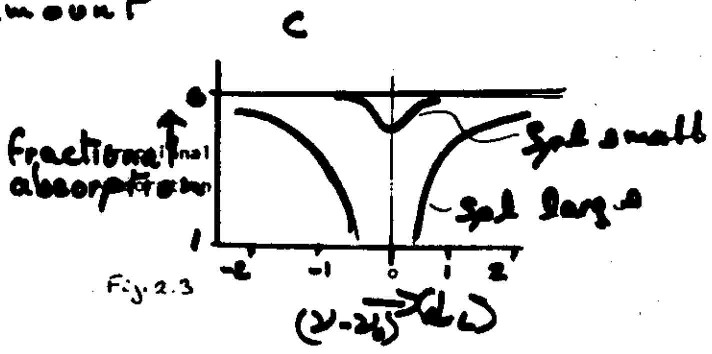

Fig 2.3

C^2

Band Models

a) Elsasser model

$$K_\nu = \sum_{i=-\infty}^{i=\infty} \frac{S}{\pi}\left[\frac{\alpha_L}{(\nu_0-\nu+i\delta)^2+\alpha_L^2}\right]$$

assumes an infinite array of pressure broadened lines of strength S at uniform spaces of δ

If S small

$$\tau \propto \exp(-A) \qquad A \text{ a constant.}$$

If S large

$$\tau = 1-\mathrm{ERF}(\pi\rho l S\alpha_L)$$

CO_2

$$\left[\mathrm{ERF}(x) = \frac{2}{\sqrt{\pi}}\int_0^x e^{-\theta^2}\,d\theta\right]$$

b) Goody model

Infinite array of randomly spaced pressure broadened lines of strength S having a distribution $\mathrm{Prob}\, S = \frac{1}{S_0}\exp\left(-\frac{S}{S_0}\right)$ where S_0 is the $\bar{S}$.

Gives

$$\tau = \exp -\left[\frac{S_0\rho l}{\delta\left(1+\frac{S_0\rho l}{\pi\alpha_L}\right)^{1/2}}\right]$$

H_2O

Black Body emission

a) Total emission

M_B or $B = \sigma T^4$

σ, Stefan const $= \frac{2\pi^5 k^4}{15 c^2 h^3}$ — Boltzmann
Planck

b) **Spectral distribution**

$$B_\lambda = \frac{c_1}{\lambda^5}\,\frac{1}{\left[\exp\left(\frac{c_2}{\lambda T}\right)-1\right]}$$

$c_1 = 2\pi h c^2 = 3.74\times10^{-16}\ \mathrm{W\,m^{-2}}$

$c_2 = \frac{hc}{k} = 1.439\times10^{-2}$ m deg K

diff to give

$$\lambda_{max} T = 2.897\times10^{-3}\ \text{m deg K}$$

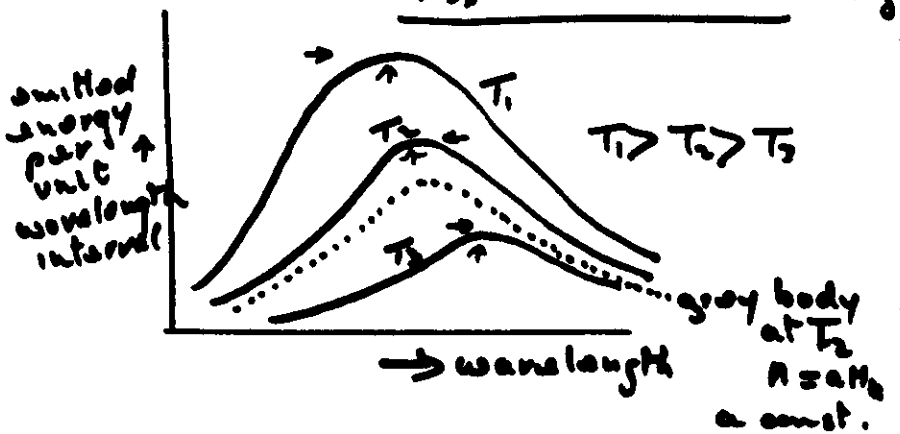

Received from all atmosphere and surface

$$N_R = \underbrace{N_{Bs}\,\epsilon_s\,\tau_{(0,z)}}_{\text{surface}} + \underbrace{\int_0^z N_{Bz'}\,\frac{\partial\tau}{\partial z'}\,dz'}_{\text{atmosphere}}$$

$\frac{\partial\tau}{\partial z}$ is known as the "weighting function"

In an isothermal atmosphere the w.f. indicates the relative contribution of the layer at z' to the total atmosphere radiance received by a radiometer

2. Non vertical transmission

2.1 narrow angle radiometer moving at θ to the vertical

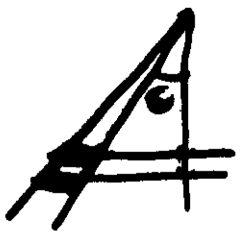

We just use $\rho \sec\theta$ in place of ρ

2.2 wide angle, or flat plate radiome

we can use the diffusive approximation & replace ρ by $\frac{5}{3}\rho$

see notes for full treatment

Monochromatic transmission through a horizontally stratified atmosphere

Define radiance N – radiant flux (energy per unit time), per unit solid angle per unit projected area: emitted or received

1. Vertical transmission

Consider the radiance received by a radiometer with a narrow angle of view looking vertically down.

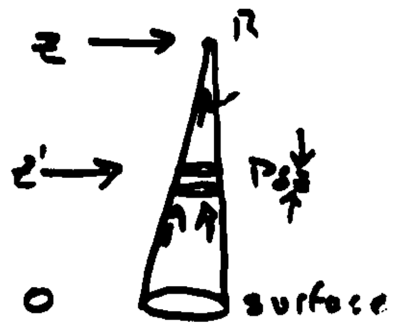

Radiance from the surface

Emitted $N_{Bs}\epsilon$

Received $N_{Bs}\epsilon\,\tau_{(0,z)}$

$$\tau_{(0,z)} = \exp\left[-\int_0^z k\rho\,dz\right]$$

(Beer's law)

Radiance from the atmosphere

Emitted from element δz at P

$$\underbrace{N_{Bz'}\,k\rho\,\delta z}_{\text{emitted}}\ \underbrace{\exp\left[-\int_{z'}^{z} k\rho\,dz\right]}_{\text{transmission } z' \text{ to } z}$$

$$= N_{Bz'}\,\delta z\,\frac{\partial}{\partial z}\left[\exp\left[-\int_{z'}^{z} k\rho\,dz\right]\right]$$

$$= N_{Bz'}\,\delta z\,\frac{\partial \tau_{(z',z)}}{\partial z}$$

Weighting functions

For a vertically viewing radiometer of narrow angle the received radiance is

$$N_\nu = N_{B\nu T_s}\,\epsilon_\nu\,\tau_{(0,z)} - \int_0^z N_{B\nu T}\,\frac{\partial \tau}{\partial z}\Big|_{z'} dz$$

It is computationally convenient to use a vertical scale in y, $y = -\ln\left(\frac{p}{p_0}\right)$

$$dy = -\frac{1}{p}\,dp$$

$$N_\nu = \int_0^\infty N_{B\nu}\,K(y)\,dy - N_{B\nu T_s}\,\tau_{0\infty}$$

where $K(y)$ is the weighting function in terms of y

e.g. ? W.F. for an absorber with k_ν independent of p and T

$$\tau_{y(0,-\infty)} = \exp -\int_p^0 k_\nu \frac{r}{g}\,dp$$ where r is the mass mixing ratio

$$= \exp\left(-\frac{k_\nu r p}{g}\right) \quad \text{for const. } r$$

$$K_y = \frac{\partial \tau}{\partial y} = -p\frac{\partial \tau}{\partial p}$$

$$= \frac{p\,k r}{g}\exp\left(-\frac{k r p}{g}\right)$$

Max. when $\frac{k_\nu r}{g} = p\frac{k^2 r^2}{g^2} \rightarrow p\frac{k r}{g} = 1$ ← UNIT OPTICAL DEPTH

b) Weighting fn in the wing of a pressure broadened line.

$$k_\nu = \frac{S\alpha_L}{\pi\left((\nu-\nu_0)^2+\alpha_L^2\right)}$$

$$\approx \frac{S\alpha_L}{\pi(\nu-\nu_0)^2} \quad \text{in the wing}$$

so $$\tau(y,\infty) = \exp - \int_p^0 \frac{S\alpha_L}{\pi(\nu-\nu_0)^2}\,\frac{r}{g}\,dp$$

Recall $\alpha_L = \alpha_{L0}\frac{p}{p_0}$

so $$\underline{K_y} = \frac{\partial \tau}{\partial y} = -p\frac{\partial \tau}{\partial p} = \underline{A\,p^2 \exp\left(-\frac{Ap^2}{2}\right)}$$

if r is independent of p

where $A = \frac{S\alpha_{L0}\,r}{\pi(\nu-\nu_0)^2 p_0}$

K_y max/min $\quad 2p = Ap^3$

$p_m = \sqrt{2/A}$

$$K_y = 2\left(\frac{p}{p_m}\right)^2 \exp\left(-\frac{p}{p_m}\right)^2$$

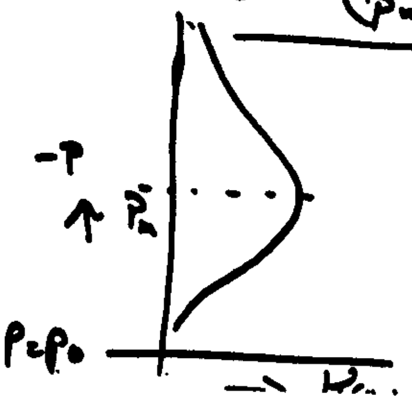

METEOROLOGICAL SATELLITES

I GEOSTATIONARY MET. SATELLITES

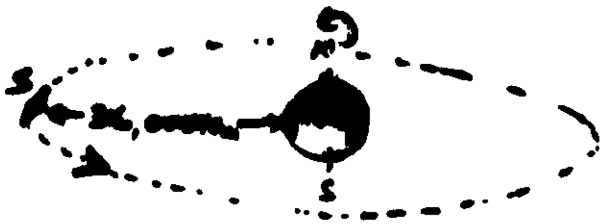

SITED OVER EQUATOR.

ORBITS AT SAME ANGULAR VELOCITY AS THE EARTH.

IMAGES EACH 30 MIN.

GROUND RESOLUTION 1.5 KM.

SCANNING SYSTEM

SPIN STABILIZED, ∥ to POLAR AXIS
100 RPM

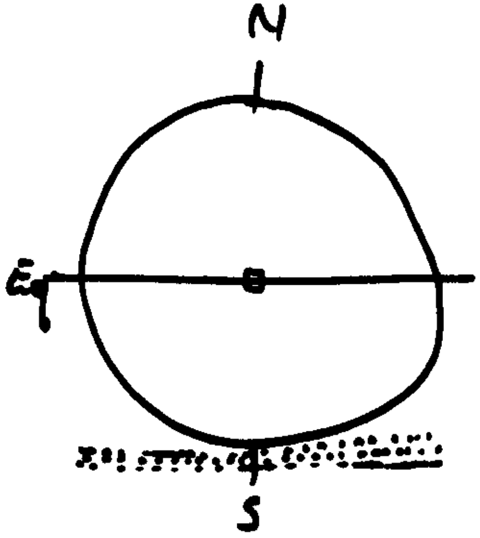

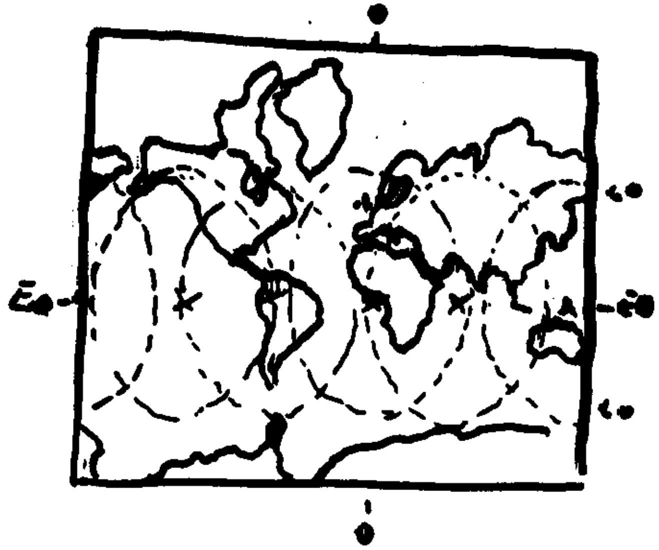

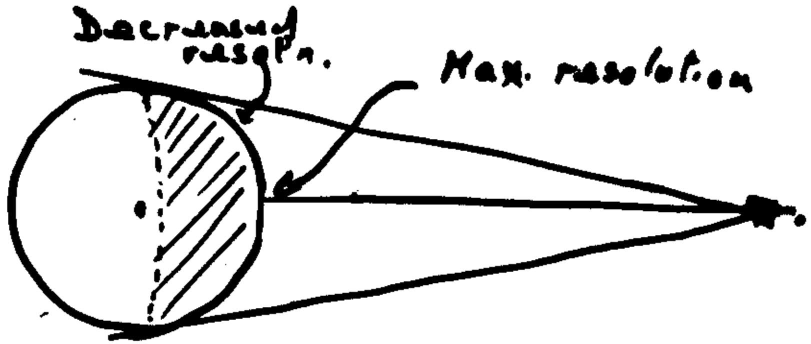

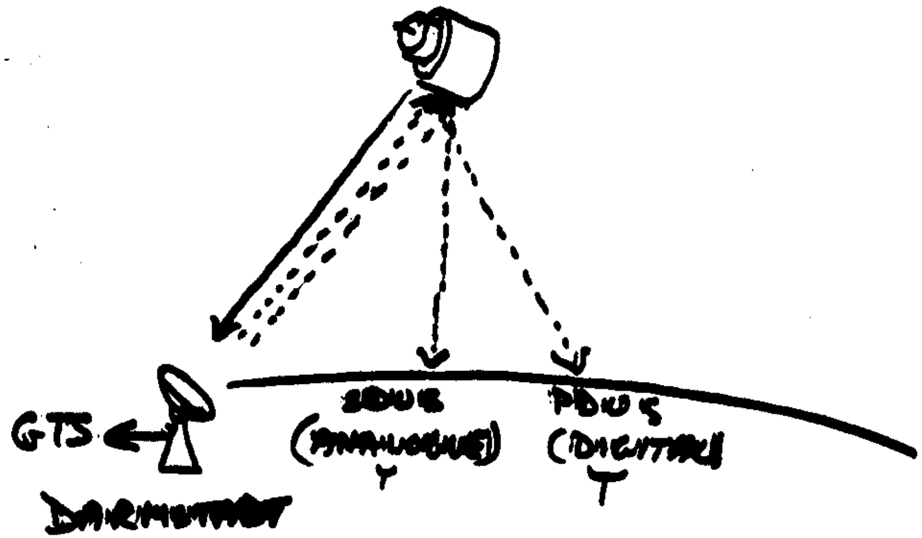

10 DATA.

VIS
NEAR I.R.
THERMAL I.R.

} 256 or 512 levels

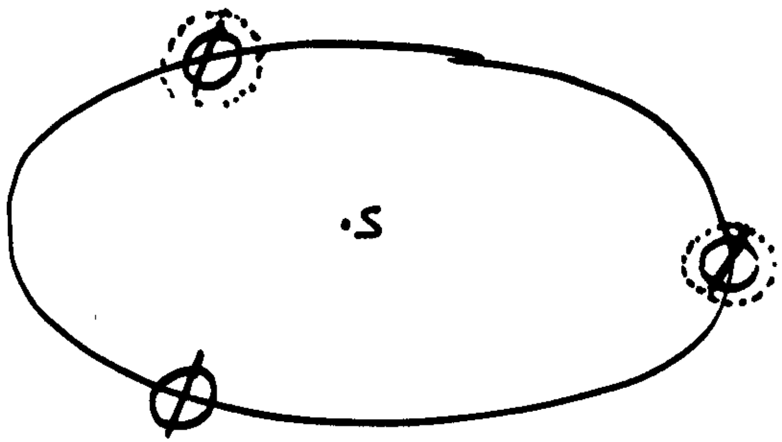

POLAR ORBIT. 1000 – 1500 km

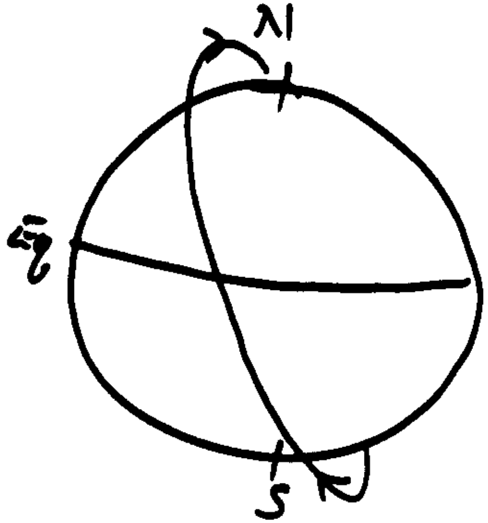

2] Polar orbiting meteorological satellites

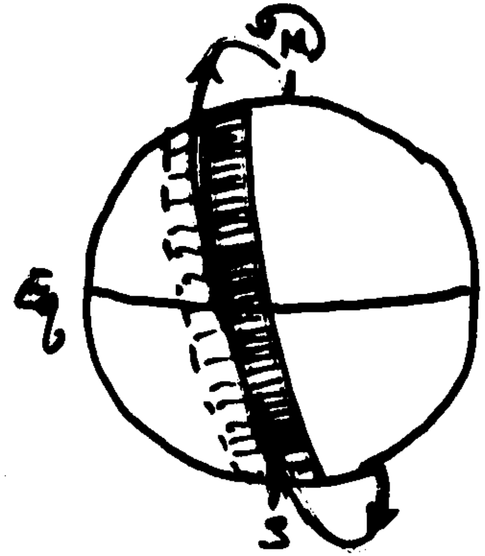

ORBIT ~ 1000 Km

τ ~ 100 min.

SUN SYNCHRONOUS ORBIT.

ORBIT PLANE IS FIXED W.RT. THE LINE JOINING THE CENTRES OF THE SUN AND EARTH HENCE THE SATELLITE CROSSES THE EQUATOR AT THE SAME SOLAR TIMES ON EACH ORBIT. THE ORBIT IS NEAR POLAR.

2 IMAGES /DAY /SATELLITE

RESOLUTION AT SUB-POINT

½ to 1 km

INSTRUMENTATION

VIS - SEVERAL BANDS

NEAR I.R.

H_2O, CO_2, THERMAL IR (2 BANDS) + EXTRA

SCANNING SYSTEMS OF POLAR ORBITERS

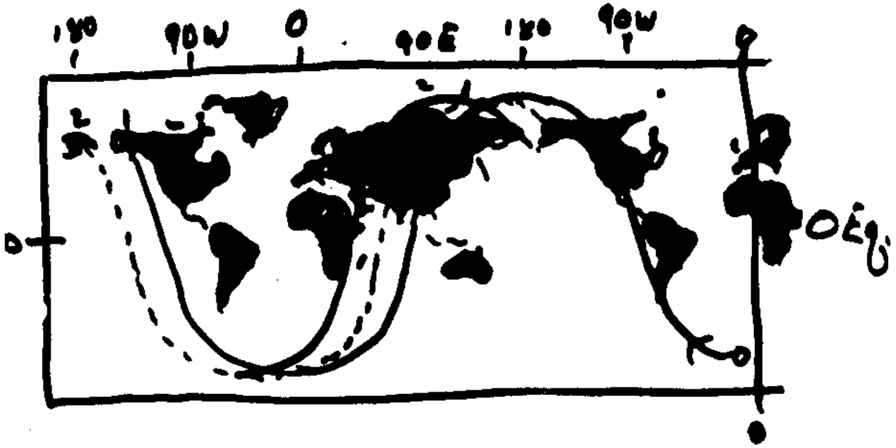

EARLY

SPIN STABILIZED. - SPIN AXIS IN PLANE OF ORBIT. LATER SPIN STABILIZED PERPENDICULAR TO PLANE OF ORBIT.

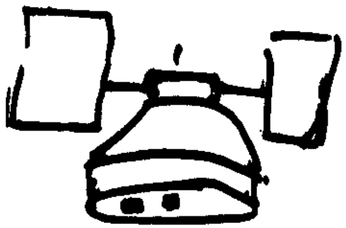

PRESENT - STABILIZED WRT EARTH SO THE SATELLITE BASE, (WHICH CARIES THE INSTRUMENTS) ALWAYS FACES VERTICALLY DOWN-WARDS.

MECHANICAL SCANNING

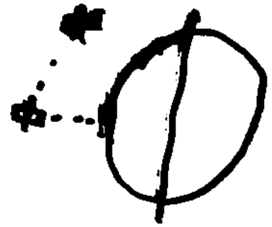

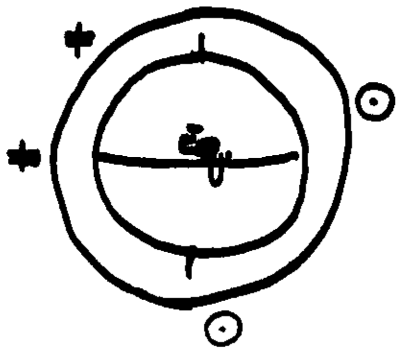

EARTH RESOURCES SATELLITES

e.g. LANDSAT, SPOT

- ORBITS, SUN SYNCHRONOUS ~ 1000 km
- HIGH SURFACE RESOLUTION [20m]
- LOW EARTH SURFACE COVERAGE (~18 days to cover earth)
- SEVERAL BANDS IN VIS AND NEAR I.R.

Meteorological applications in delineating land surface types.

DETECTORS

EARY SYSTEMS – T.V. TYPE CAMERAS FOR VISIBLE

PRESENT – RADIOMETERS
PHOTO-ELECTRIC,
THERMO-ELECTRIC,
PHOTO-CONDUCTIVE,

OPTICS

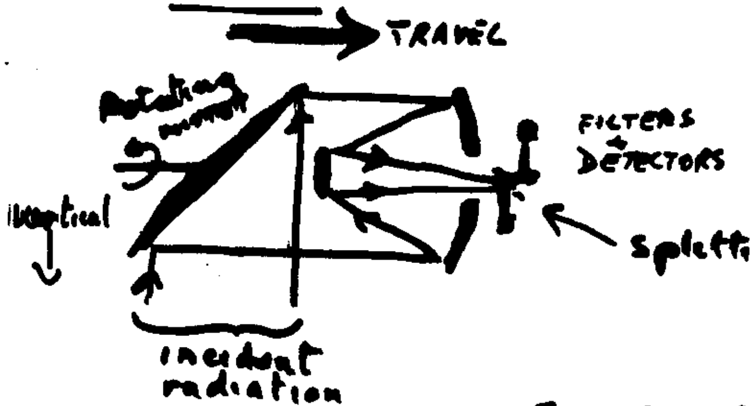

SCHEMATIC OF ONE TYPICAL SYSTEM

LIMITS

SPATIAL RESOLUTION

(i) Diffraction limit

$$\alpha = \frac{1.22\,\lambda}{D}$$

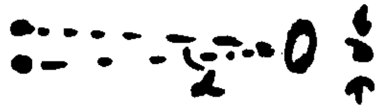

aperture of objective.

ii) Signal to noise ratio

Thermally generated noise in the electronics systems may overshadow the actual signal if emission or reflection is too low

WAVELENGTH RESOLUTION

Often the smaller $\Delta\bar{\nu}$ (the wavenumber interval) the more information can be deduced. But small $\Delta\bar{\nu}$ means low energy hence low S/N ratio.

Filter characteristics also reduce the wavelength resolution

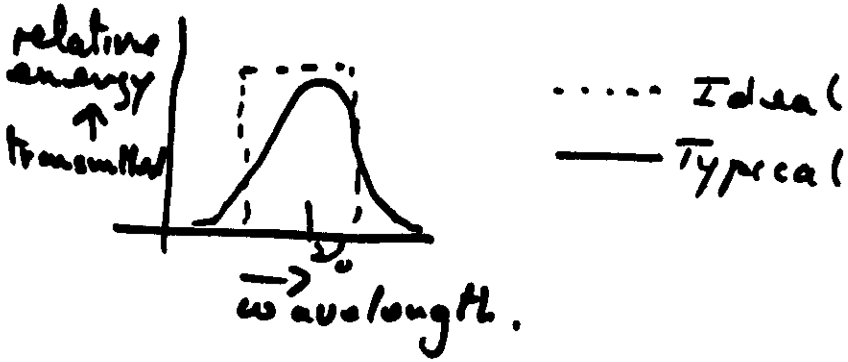

SENSITIVITY (S) OF A RADIOMETER

Fig 3.1

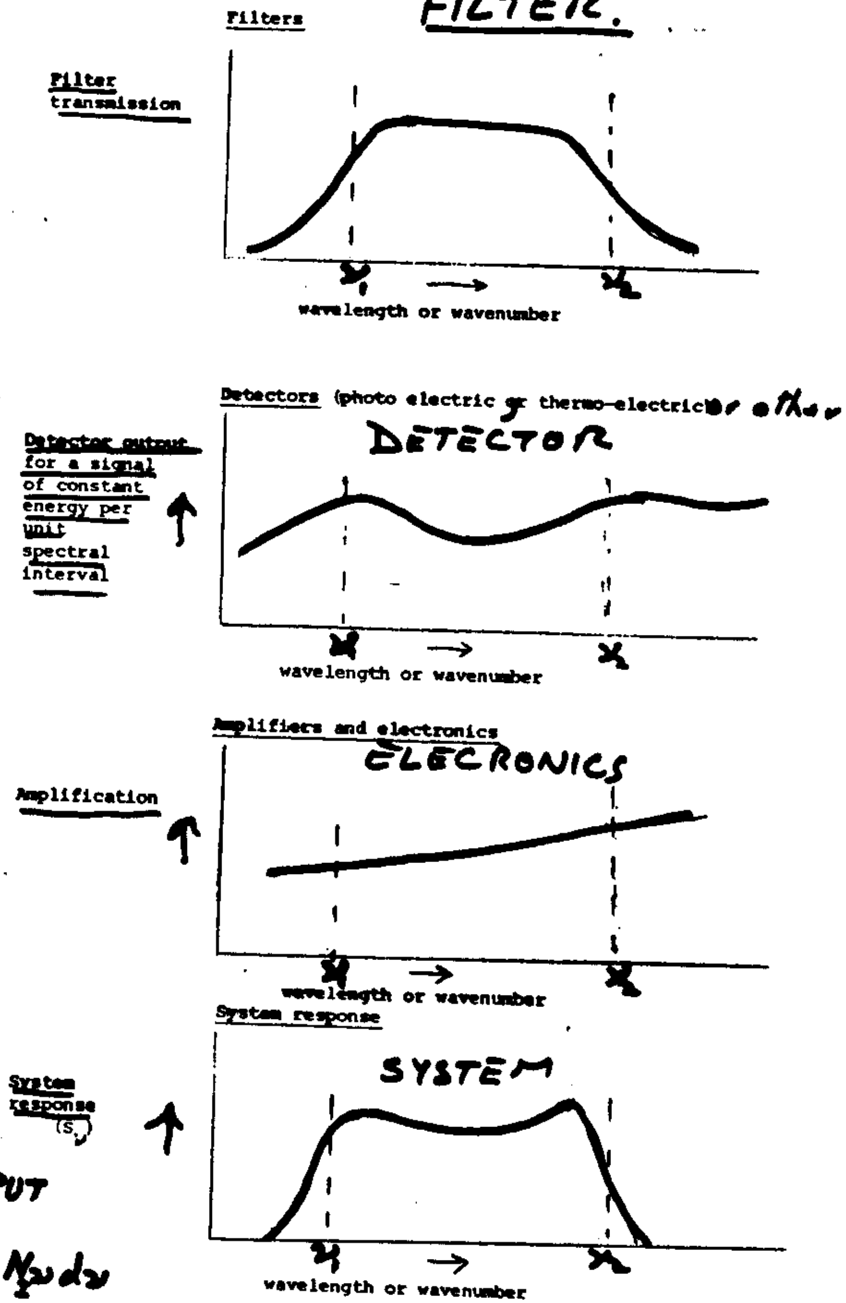

OUTPUT $= \int_{\nu_1}^{\nu_2} S_\nu N_\nu \, d\nu$

The output of the radiometer is given by $\int_{\nu_1}^{\nu_2} N_I S_\nu \, d\nu$ where N_I is the input radiance

N_ν = incident radiance

4.1 TEMPERATURE SOUNDINGS

1. Principles
2. Selecting the waveband
3. Retrieval of temperature profiles
4. Middle and upper atmosphere soundings
5. Instruments for atmospheric temperature sounding.

4.2 Soundings for atmospheric gases

ATMOSPHERIC TEMPERATURE SOUNDING

Vertical monochromatic radiance emerging from the atmosphere $N_{E\nu}$

$$N_{E\nu} = \epsilon_\nu N_{BG} \tau_{(0,1)} + \int_1^0 N_{Bp} \frac{\partial \tau}{\partial p} . dp$$

(Vertical coordinate, pressure p in atmosphere)

Given $\epsilon_\nu, N_{BG}, \tau, N_{Bp}, \frac{\partial \tau}{\partial p}$ one can calculate $N_{E\nu}$

<u>Problem</u> given $N_{E\nu}$ find N_{Bp} hence T_p

If we have an absorber which is uniformly mixed in the atmosphere and only one active absorber at that wavelength and we know the absorptive characteristics of the absorber we can calculate the $\frac{\partial \tau}{\partial p}$ weighting function term. If also $\tau_{(0,1)} \approx 0$ the first term may be neglected

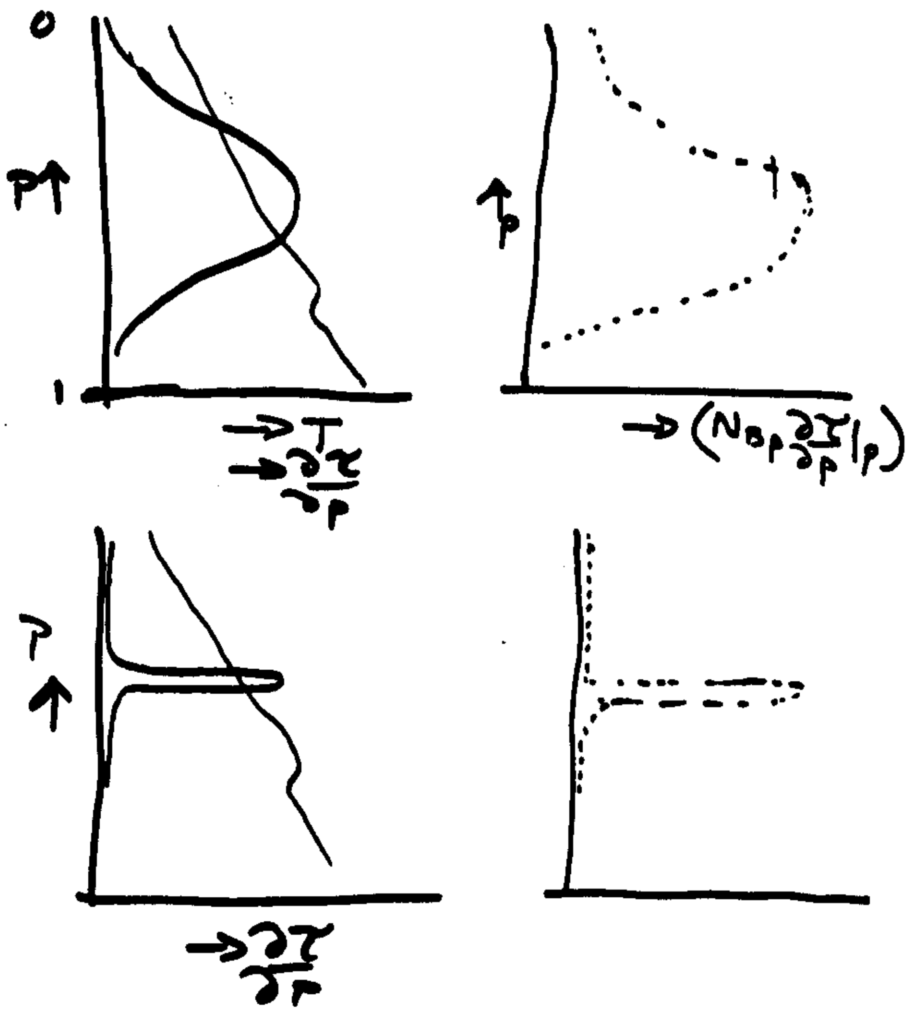

The ideal w.f. is very sharply peaked but this implies a small frequency interval hence not much energy.

REQUIREMENTS

1) A frequency at which only one gas absorbs
2) The absorbing gas should be uniformly mixed in the atmosphere (O_2, CO_2)
3) The frequency should not overlap the solar spectrum
4) L.T.E. should prevail so the Planck fn can be inverted to give temperature
5) The frequency should not be affected by the presence of cloud.

Band	LTE To	Sens	Energy	Spatial resol'n	Solar pumping	Cloud influence
CO_2, 4.2 μm	35 km	$4\%K^{-1}$	GOOD	GOOD	YES	YES
CO_2, 15 μm	80 km	$1\%K^{-1}$	GOOD	GOOD	NO	YES
O_2 5 mm	100 km	$\frac{1}{3}\%K^{-1}$	POOR	LOW	NO	SMALL

Weighting functions (gradient of transmission with respect to log pressure) for instruments sounding the temperature of the lower atmosphere on the Nimbus 6 satellite: (*a*) 15 μm channels of HIRS, (*b*) 4.3 μm channels of HIRS, (*c*) channels of SCAMS (c.f. § 6.9; from Smith and Woolf 1976 and Staelin *et al.* 1975).

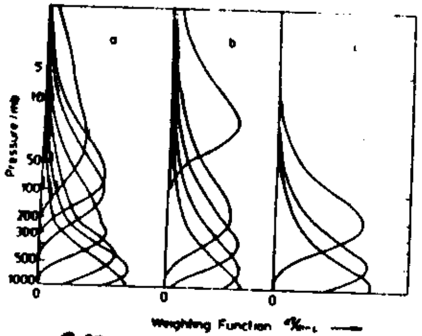

CO_2	CO_2	O_2
15 μm	4·3 μm	5 mm
↑	↑	↑
no solar effect	$\frac{\partial N_B}{\partial T}$	less cloud effect

4·4

15 μm CO_2

Chapman model

$$K(y) = \sqrt{\frac{2}{\pi}}\left(\frac{p}{p_m}\right) \exp\left(-\frac{p}{p_m}\right)^2$$

$p_m \to 0$ as $\tau \to 0$

Gradient Ri.

Ri. Define: Ratio of the rate of ~~[illegible]~~ absorption by the eddy energy ~~against the~~ in working against the stable fluid to the rate of generation of eddy energy by the shear flow.

$$Ri = \frac{g}{\theta}\frac{\partial\theta/\partial z}{(\partial U/\partial z)^2}$$

if $Ri > 0.2$ small turbulence is suppressed

if $Ri \simeq 0$ turbulent energy will increase until the rate of eddy generation = rate of absorption by viscous forces, fully forced

if $Ri < 0$ turbulence enhanced by free convection.

if $Ri < -1$ free convection

$\Rightarrow T, \theta, T_v$

$\Rightarrow$ drag

Rf flux form of the Richardson No.

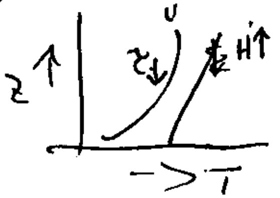

If $(-H)_{ND}$ larger than $(\tau)_{ND}$ turbulence may be expected to be suppressed

$$-\frac{H}{\tau} = \frac{J\,m^{-2}\,s^{-1}}{N\,m^{-2}}\ ;\quad -\frac{H/C_p}{\tau/g} = \frac{s^{-1}\,K\,kg}{kg} = \frac{K}{s}$$

18

$$-\frac{Hg}{\ldots} = R_F \qquad -\frac{H}{C_p}\cdot\frac{g}{\tau}\cdot\frac{1}{T\left(\frac{\partial U}{\partial z}\right)} = ND = R_F$$

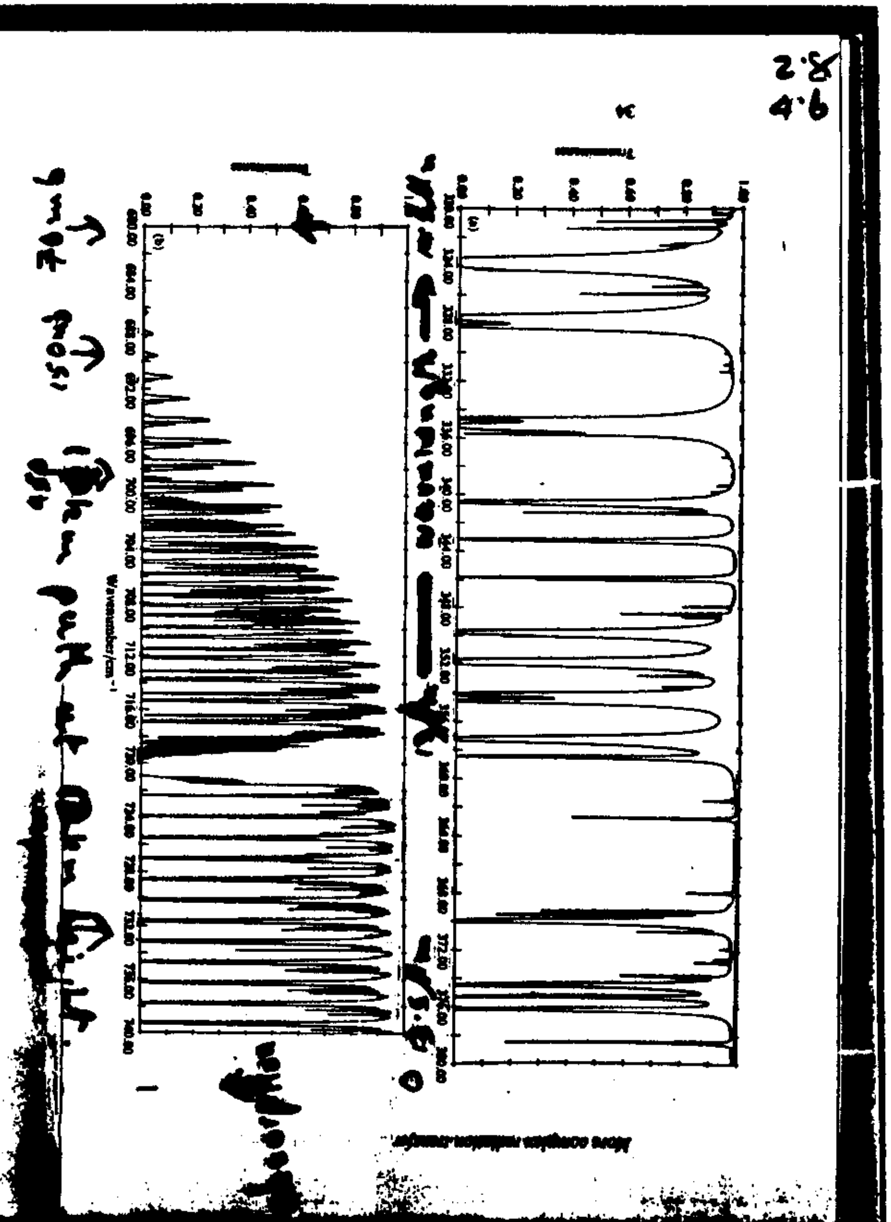

RETRIEVAL OF TEMPERATURE PROFILES

GIVEN a set of radiances from frequency bands of known weighting functions.

"exact" solutions

Assume the temperature profile can be represented by a mathematical function

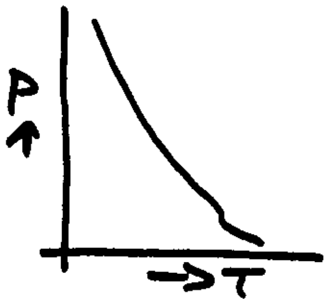

Fourier series, polynomial

eg $T(p) = a + bp + cp^2 + \ldots$

Now $N_B(\nu_0 \pm \delta\nu) = \frac{1}{2\,\delta\nu}\int_{\nu_0-\delta\nu}^{\nu_0+\delta\nu} N_{B\nu}\,d\nu$

Black body radiance in the radiometer band

Monochromatic Planck fn at $T(p)$

So we express $N_{B\nu}$ hence $N_B(\nu_0 \pm \delta\nu)$ in terms of a, b, c etc.

Knowing $K(p)$ we can integrate w.r.t. p to get the radiance arriving at

Vali. 12 – 20 (3)

Digdale (8)

Standards. 7 – 14 (5)

Week	
1	
2	
3	
4.	

Teaching programme:
A.M. – Lectures
P.M. – Projects

	9 M	10 T	11 W	12 T	13 F
Digdale	2				
S	1				

the radiometer in terms of our coefficients. So we can solve for as many coefficients as there are radiometer bands.

Problem errors in measured radiances are amplified in terms of temperature

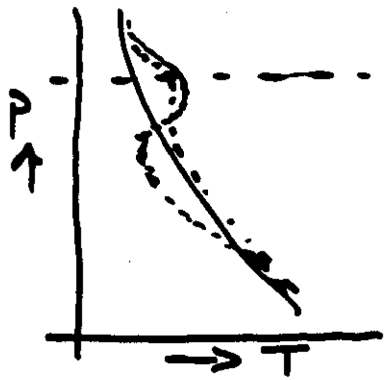

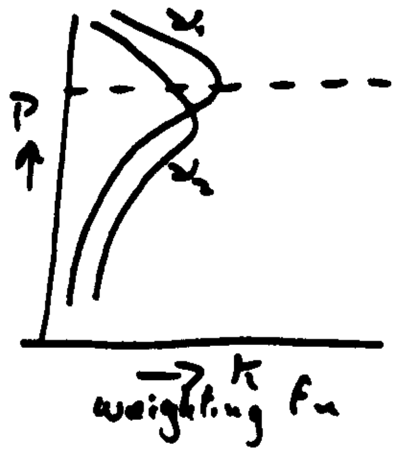

The problem is minimized if the temperature profile is represented by a linear combination of the weighting functions

$$T_z = a K_{\lambda_1}(z) + b K_{\lambda_2}(z) + \dots$$

However a 0.5% radiance error can still give rise to an 8% temperature error.

Non-Exact Solutions

If we have many more sets of information than we have coefficient we can reduce errors by looking for the best fit solution. This data is not usually available from the limited number of weighting functions and their corresponding radiometer readings.

Bogus data

Additional "data points"

climatology
persistence
interpolation { radio-sonde data / or satellite data }

In deriving the profile each type of data is given a weighting according to its expected variance.

Both spurious and real detail may be removed by these techniques.

Iterative methods

A first guess profile is adjusted to fit the data using one radiometer band at a time. The process is re-iterated until the solution converges. The process must be stopped before it produces the "exact" solution with its attendant errors.

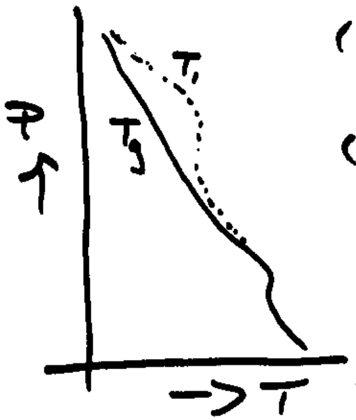

(i) calculate N_E for first guess

(ii) adjust $T(z)$ according to (P/p_{m1}) to give the observed N_E at the κ_2 corresponding to the top level $T(z)$

(iii) adjust $T(z)$ ratiod (P/p_{m2}) to give the observed N_E and $T_1(z)$

(iv) continue through all
⋮
(n) weighting functions

(n+1) Return to (ii)

Regression techniques

Within season and/or climatic zone relate statistically the distribution of the radiometer band readings to radiosonde data.

This empirical method is widely used operationally, it:-

:- fails to identify unusual temperature profiles
:- contains no physics [except in design]
:- is independent of knowledge of the
:- " " " " radiometer calibn.
:- must be calibrated for all synoptic situations

Middle and upper atmosphere soundings

1] L.T.E.? } consider in calculating weighting f'ns
2] Doppler broadening? }

3] Limb sounding

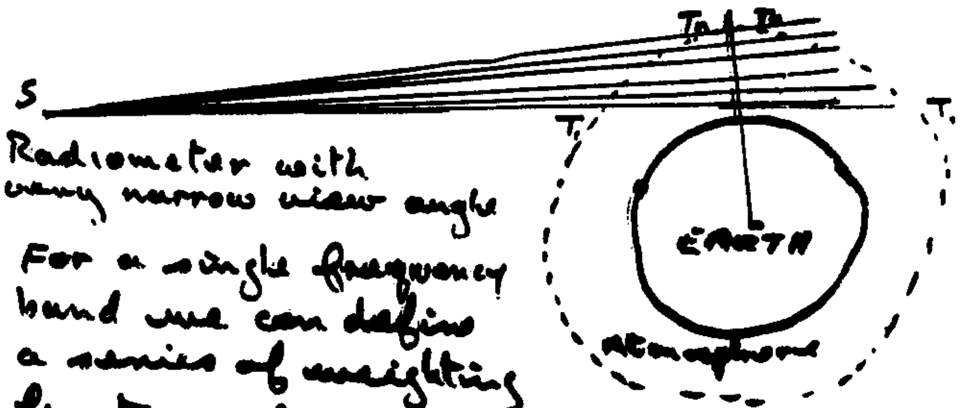

Radiometer with very narrow view angle

For a single frequency band we can define a series of weighting functions along T_1T_1 T_2T_2 etc. These limb weightings are dominated by the contribution close to the tangent point.

So in principle we can start at the top of the atmosphere and progressively work downwards using the temperature already calculated together with each weighting function to estimate the temperature of the next layer.

Fig. 4.3

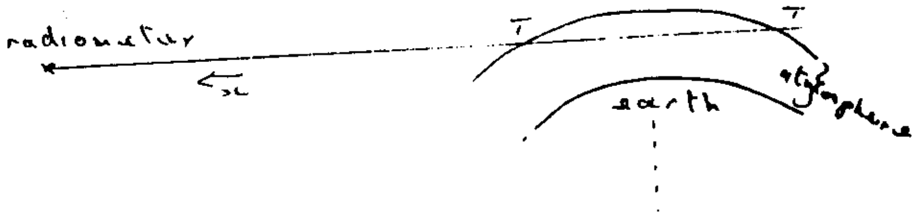

4.4.

Fig. 4.4.

A set of weighting functions for a limb sounder with an infinitesimal field of view (after Gille and House, 1971)

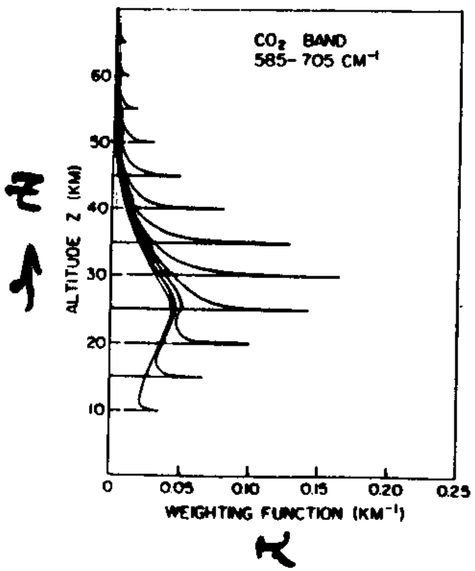

Difficulty – to define the height of the tangent point above the earth. (Navigation problem)

a solution

Use two radiometers with identical view angles and close frequency bands

$$N_1 = \int N_{B1} K_1 \, dx \qquad (x \text{ is atmospheric path})$$
$$N_2 = \int N_{B2} K_2 \, dx$$

If K_1, K_2 are well chosen

$$\frac{N_1}{N_2} \approx \frac{\int K_1 \, dx}{\int K_2 \, dx}$$

This is strongly pressure dependent so $\frac{N_1}{N_2}$ is a function of p and can be used to determine p.

Instruments for atmospheric temperature sounding

Requirements

1] Narrow spectral band ⇒ peaked K

2] Narrow angle of view ⇒ good spatial resolution

3] Large energy capture ⇒ good s/n ratio good temperature resolution

Components

Define view angle and energy capture (Mirrors or germanium lenses for I.R.)

Band width + energy passed

Should give high out/in ratio and be Stable

Filters

	PRISMS	GRATINGS	FABREY PEROT INT.	MICHEL-SON	INTERFERENCE
ENERGY	LOW ENERGY E_1	LOW ENERGY E_1	MORE ENERGY $E_1 \times 10$ to $E_1 \times 100$	AS FABREY	MORE THAN FABREY
BANDWIDTH	NARROW	NARROW	NARROW	NARROW	WIDE
	DETECTOR PER BAND OR SEQUENTIAL READINGS			CHANGE PATH LENGTH TO SCAN BANDS	ADD ANOTHER FILTER *

* SELECTIVE CHOPPER RADIOMETER

PRINCIPLE

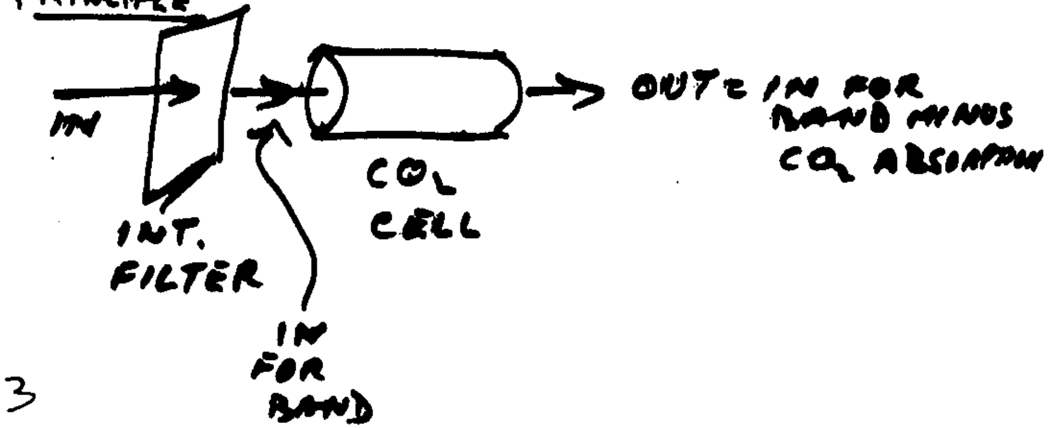

Figure 4.5

Demonstrating the effect of selective absorption, weighting functions for: curve *A*, a 5 cm^{-1} wide interval near 690cm^{-1}; curve *B*, the same interval as for curve *A* but including a path of CO_2; curve *C*, an ideal weighting function for a monochromatic frequency in the wing of a spectral line (from Abel *et al.* 1970).

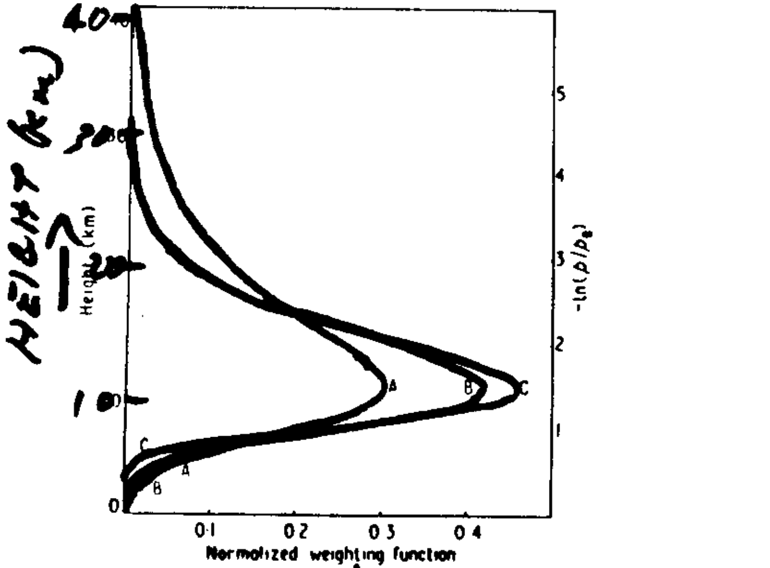

— weighting fn for a 5 cm^{-1} band at 690 cm^{-1}

— Ideal w.f. for a monochromatic freq. in the wing of a p.b. line

— W.f. of 5 cm^{-1} band with a CO_2 cell inserted

selective chopping

Insert two CO_2 cells of different path lengths (or pressures) alternately

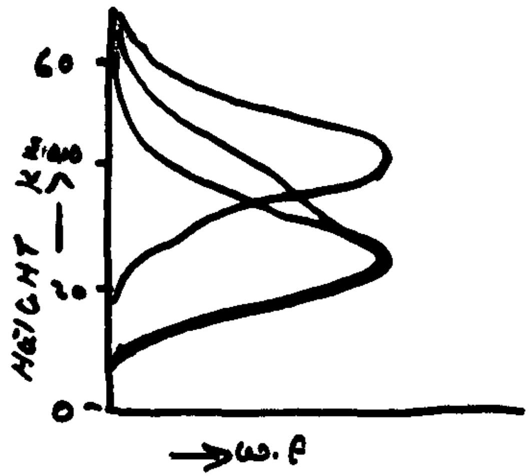

— w.f. 5 cm^{-1} interval at 668 cm^{-1}

— " " " with 1 cm CO_2 at 50 mb

— " chopping between — and —

PRESSURE MODULATED RADIOMETER

Figure 4.8

Weighting functions for a pressure modulator radiometer having a cell ... long operating in the ν_2 band of CO_2 with different cell pressures. The number of the curves is mean cell pressure in mbar (from Curtis et al 1974)

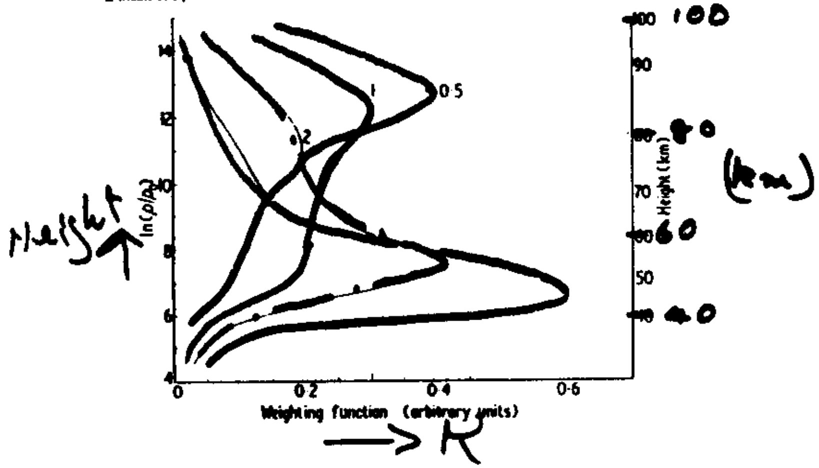

– cell pressure 0·5 mb
— " " 1·0 "
—·— " " 2·0 "

Doppler shifted P.M.R.

The motion along the line of sight of the radiometer shifts the atmospheric emission lines relative to the PMR absorption lines.

This reduces the absorption so the PMR effectively "sees" lower into the atmosphere.

4.20

Figure 4.10

. Weighting-functions for six channels of the SIRS on Nimbus 4 observing in the rotation water vapour band (from Smith 1970).

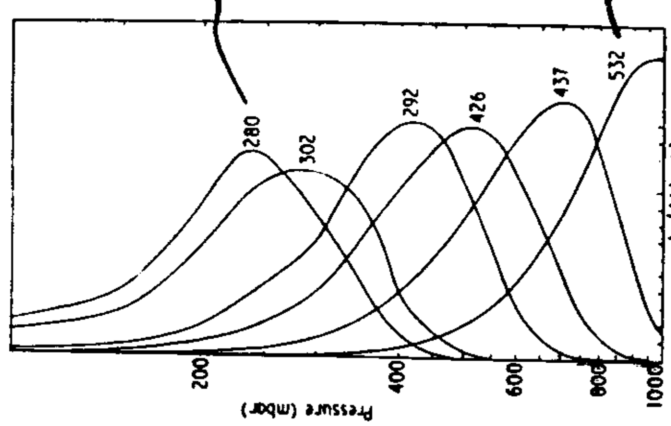

...ed against wavenumber for various vertical atmospheric paths from the level of pressure ...nospheres to top of atmosphere. The number of each curve is the v... of ln p. (*b*) ...mission for PMR cell 6 cm long at pressure 0.7 mbar (curve *A*), 2 mbar (curve *B*). ...e *C* (=curve *A*-curve *B*) is the effective transmission of the radiometer. (*c*) Trans...on for PMR cell 1 cm long and PMR cell pressures 0.25 mbar (curve *A*), and 1.0 ... (curve *B*). Curve *C* (=curve *A* - curve *B*) is the effective transmission of the ...meter. Curve *D* is curve *C* Doppler shifted by the amount which would occur for ...nbus satellite if the radiometer viewed at 10° to the vertical (from Curtis *et al.* ...).

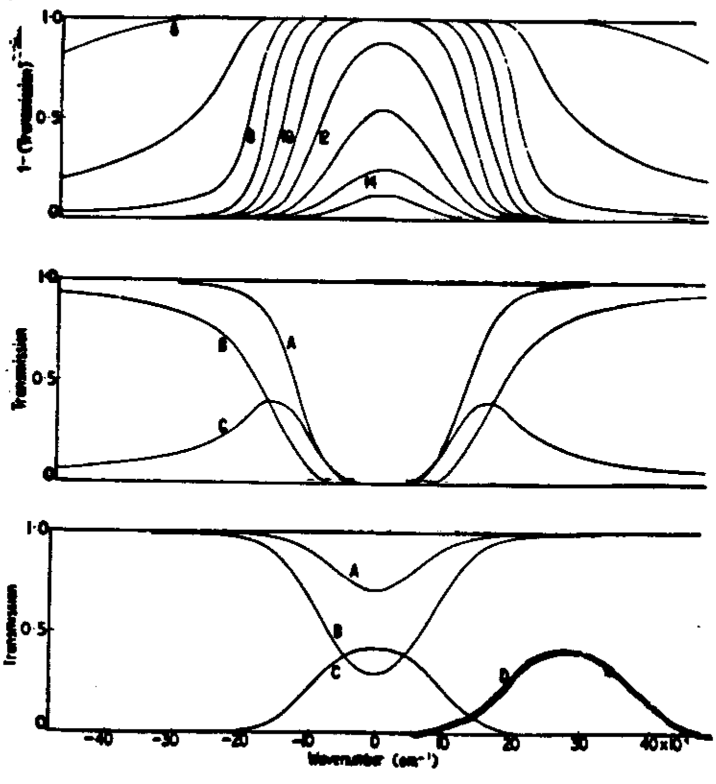

A 0·25 mb
B 1·00 mb.

...be devised is by utilizing the Doppler shift which arises betwe... emiss... lines and the absorption lines of the gas in the cell wh... motion along the line of sight between the radiometer and the ...phere. Since the speed of a Nimbus satellite is about twenty ti... speeds at normal atmospheric temperatures, only about 5% of ... velocity is required to produce a Doppler shift equal to the Do... By varying the Doppler shift it is possible to scan the absorptic... atmospheric emission lines (Fig. 6.19(*c*)). The Nimbus 6 PMR ... designed so that the direction of view could be altered from ve...wards to 15° from the nadir along the direction of flight, thus ...ing Doppler shifts. By this means the optical depth (and hence ... being probed could be varied (Fig. 6.21).

Fig. 6.20 Weighting functions for a pressure modulator radiometer havi... operating in the ν_2 band of CO_2 with different cell pressures. The num... is mean cell pressure in mbar (from Curtis *et al.* 1974).

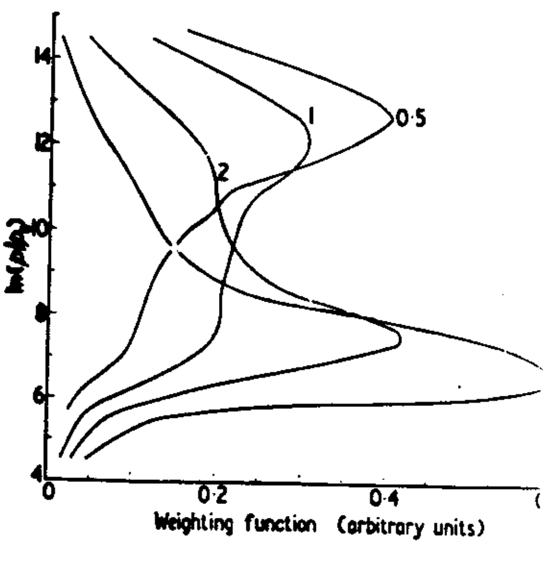

26

Microwave techniques for temperature and humidity sounding

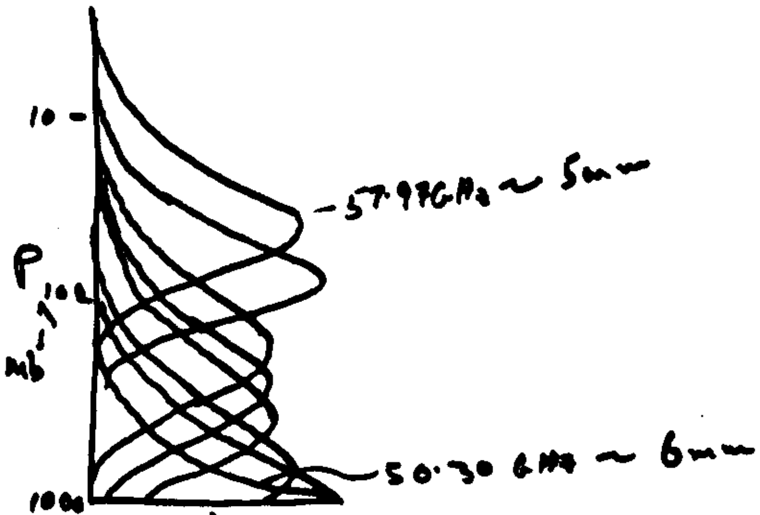

→K

oxygen band   gives Temp profile

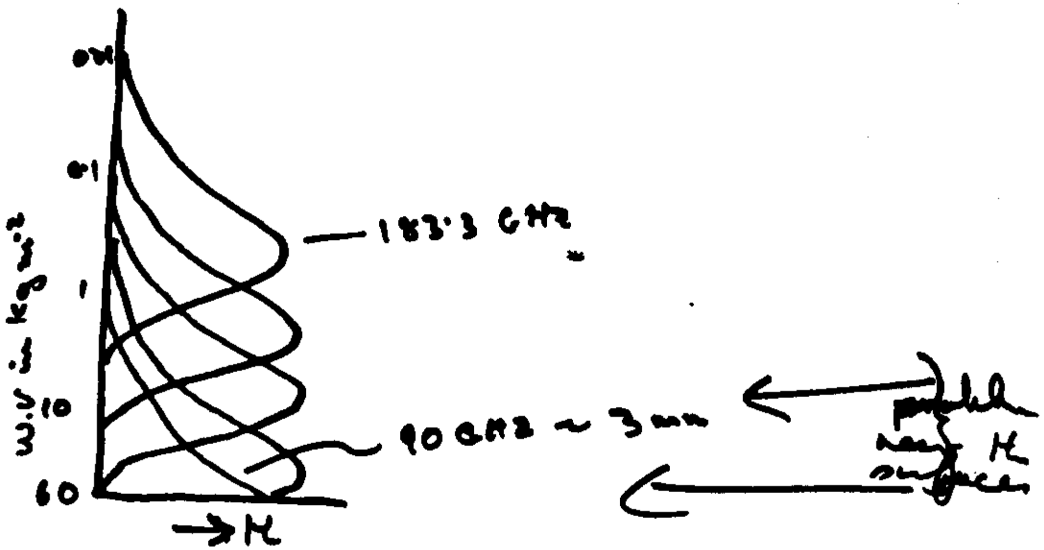

→K

H_2O

gives H_2O profile

27

[redacted]

$B(\nu_i, T_0)$ is the Planck function at frequency ν_i corresponding to atmospheric temperature T at pressure p;
α_i is the frequency independent part of the transmission of the optics;
f_{ν_i} is the frequency dependent part of the optics transmission for the ith radiometer channel normalised to unit maximum;
p_0, T_0 are the pressure and temperature respectively at the lower boundary (ground or cloud).

The assumption has also been made that $B(\nu, T)$ is constant over the pass band of a radiometer channel so that it may be taken outside the integral over ν.

The variation with frequency or wavelength of $\bar{\tau}_i(p_0)$, the transmission of the atmosphere from the ground to space, is plotted in Fig. 5.3 both for the standard atmosphere and for each important constituent separately, showing the

Fig. 5.3 Absorption in the infrared for a vertical atmospheric path by a variety of constituents (from J.H. Shaw).

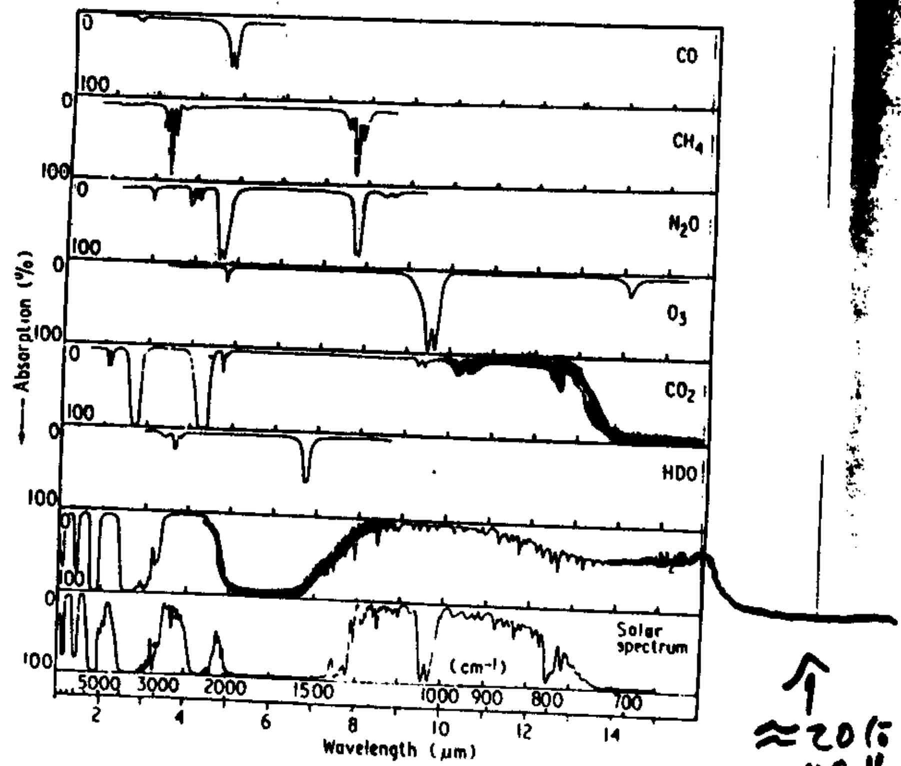

≈ 20 μ
40 ...

1.2. SOUNDINGS FOR ATMOSPHERIC HUMIDITY

Principle – as temperature sounding

given T(z) hence $N_B(z)$

assume a climatic H_2O profile and adjust to give the $\frac{\partial \tau}{\partial z}$ required to fit the observed radiances.

Wavebands

H_2O bands (6·3 μm or 20–40 μm) in I.R. or many micro-wave bands.

$$N_{Atm} = \int_{1}^{0} N_{Bp} \frac{\partial \tau}{\partial p} \cdot dp.$$

DOPPLER SHIFTED P.M.R.

Figure 4.9

Weighting function for a pressure modulator radiometer housing a cell 1cm long containing CO_2 at a mean pressure of 0.5 mbar when viewing at different angles to the nadir, hence allowing scanning of the emitting lines from the atmosphere across the absorbing lines in the cell by the Doppler shift due to the relative motion between atmosphere and instrument. The number of each curve is the angle to the nadir in degrees (from Curtis *et al.* 1974).

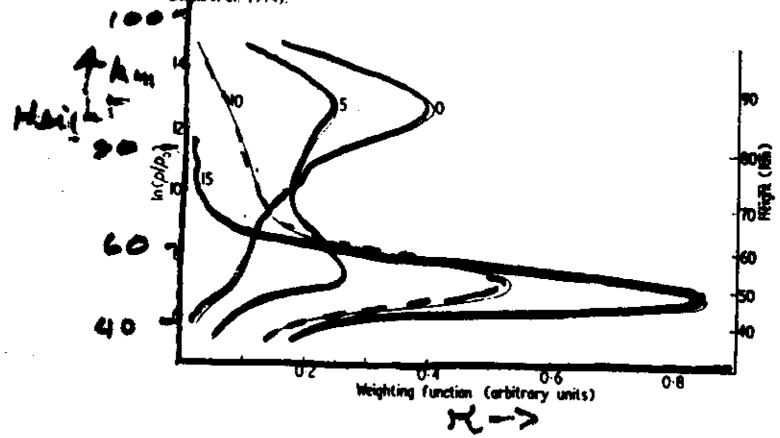

— 0°
— 5°
- - - 10°
— 15°

cell pres = 0·5 mb
cell length = 1 cm.

INFRA-RED SOUNDINGS OF THE SURFACE AND CLOUDS

EMISSION – GENERALLY THE SURFACE AND CLOUDS EMIT AS NON-BLACK BODIES. THE EMISSIVITY ϵ VARIES WITH WAVELENGTH

BRIGHTNESS TEMPERATURE – THE RADIATIVE TEMPERATURE OF A BODY.

$$\int_{\lambda=-\infty}^{\lambda=\infty} N_{BT\lambda} = \int_{\lambda=-\infty}^{\lambda=\infty} \epsilon_\lambda N_{B\lambda}\, d\lambda$$

BRIGHTNESS TEMPERATURE

OFTEN B.T. IS USED OVER A RESTRICTED RANGE i.e. THE ACCEPTANCE BAND OF A RADIOMETER

$$\int_{\lambda_1}^{\lambda_2} N_{BT(\lambda_1-\lambda_2)} = \int_{\lambda_1}^{\lambda_2} \epsilon_\lambda N_{B\lambda}\, d\lambda$$

THE SCENE B.T. IS MEASURED TEMP. OF A SURFACE AND INCLUDES THE EFFECT OF ANY INTERVENING ABSORBER.

Radiometer characteristics

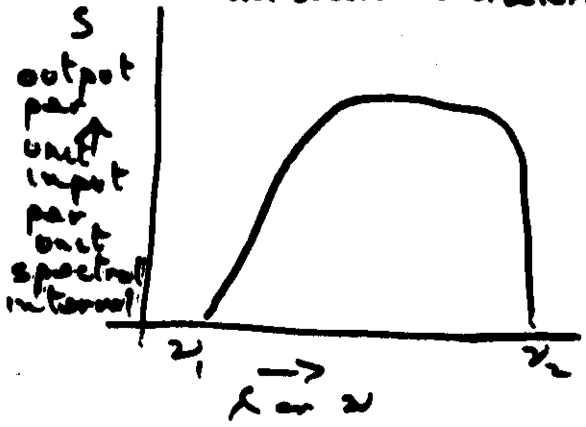

Scene BT is such that

$$\int_{\nu_1}^{\nu_2} N_{BT\nu} S_\nu\, d\nu = \int_{\nu_1}^{\nu_2} N_\nu S\, d\nu$$

where N_ν is the received radiance at ν
" $N_{BS\nu}$ " " " " from a black body.

$$N_\nu = \underbrace{N_{BS\nu} \times \tau_{(0,\infty)\nu}}_{\text{surface}} + \underbrace{\int_0^\infty N_{B\nu} \frac{\partial \tau_\nu}{\partial z} dz}_{\text{atmosphere.}}$$

we wish to remove this effect

remove this also

SURFACE TEMPERATURE MEASUREMENTS

SPECTRUM OF ABSORPTION.

4 μm window	10.5–12.5 μm window
overlaps solar radiation	water vapour dimer

Effects
a) absorption – H_2O dimer

b) absorption + scattering } – aerosols (generally small)

c) sub pixel size clouds

d) thin cirrus

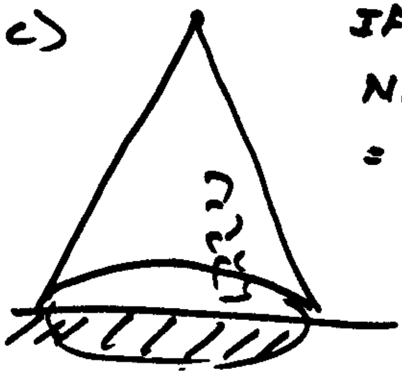

$$k_1\Theta_2 = k_1\Theta_1 \left(\frac{e^*_{\Theta_1}}{e^*_{\Theta_2}}\right) \exp\left(3.5\,kK\left(\frac{1}{\Theta_1}-\frac{1}{\Theta_2}\right)\right)$$

$$k_2 \approx 0.005\, k_1$$

FIG. 3-4. Comparison of the continuum absorption coefficient at three temperatures.

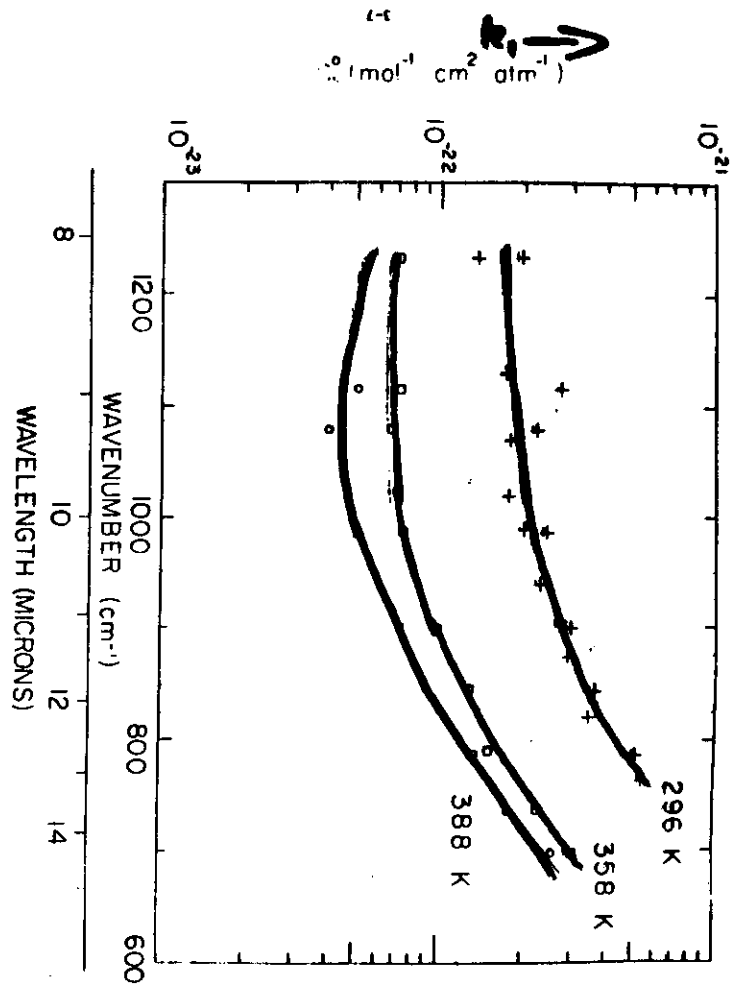

c) If no atmosphere
Nat radiometer
$= \underline{N_{BTS}(1-a) + a N_{BTC}}$
where a is the fraction of cloud cover.

$$\underbrace{\tau \epsilon N_{B\nu}}_{\text{Depends on } T_s} + \int_0^{p_0} N_{B\nu} \frac{\partial \tau}{\partial p} dp$$

independent of surface temp except to the extent that surface & air temp are related

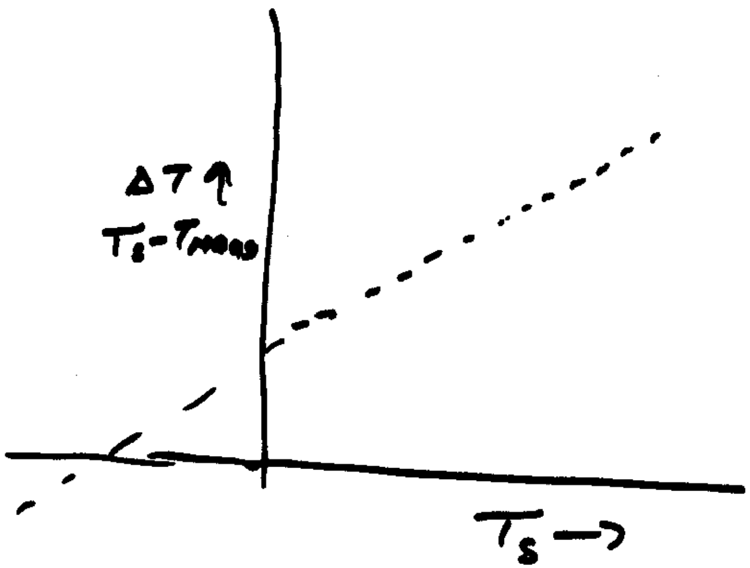

FIGURE 2-5

Atmospheric absorptions (and emissions)

after Goody, R.M., *Atmospheric Radiation*, p.4

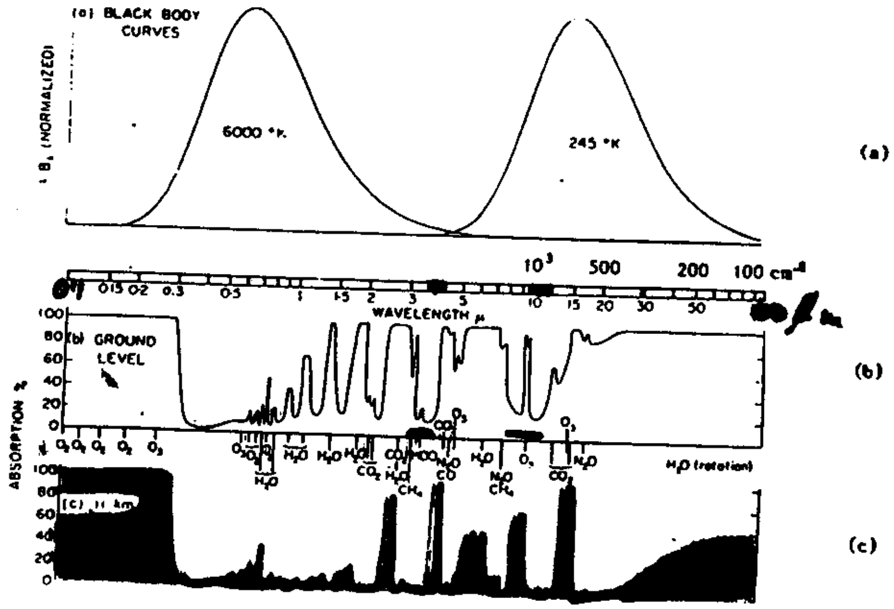

electronic

vibration-rotation transitions

rotation

ABSORPTION BANDS

Atmospheric absorption in the w.v. window 5.5

$$k_\nu = k_{c,\nu}(T)$$

$$k_\nu = \underbrace{\underset{\text{dimer self broadening}}{k_1(\nu,T)\times e} + \underset{\text{dimer foreign broadening}}{k_2(\nu,T)\times p}}_{\text{dominate with self} \gg \text{foreign.}} + \underset{\text{w.v. lines}}{k_3(\nu,T)} + \underset{\text{other gases}}{k_4(\nu,T)\, f(p)}$$

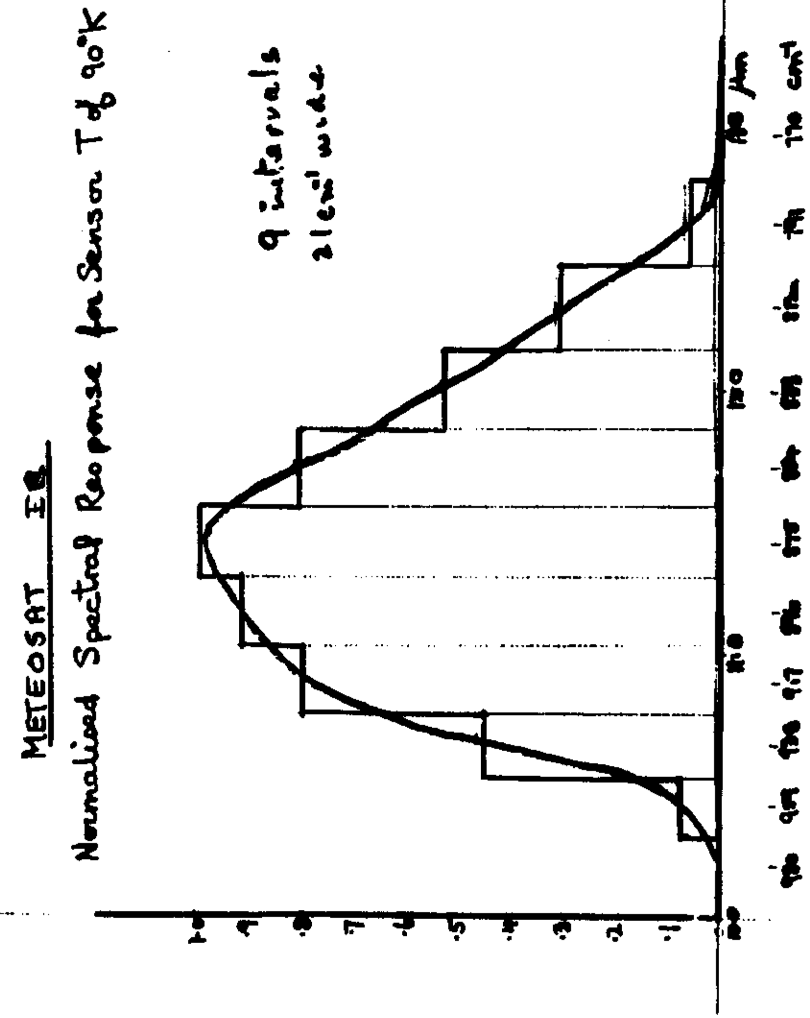

32

Divide radiometer band into "monochromatic" intervals i.e. S_ν & $N_{B\nu}$ considered constant.

Divide atmosphere into horizontal slabs over which p, T, e may be considered constant (20 mb, or 50 mb?)

$P_{(mb)}$	T	e	r	k_ν	$\Delta\tau$	τ_{top}	N_B	N	Δ Atm cont	Surface cont $T_{s1}\,T_{s2}\cdots T_{sn}$
400	TEMP	VAP PRES atm	MIX RATIO	ABS COEF	1	1, $\Delta\tau_1$, $\Delta\tau_1\Delta\tau_2$				
420										
440										
460										
480										
etc.										

From radiosonde

Total atm cont. → N_{SUM}.

Received radiance

Radiance at no atm = measured temp.

$k_\nu = k_1 e + k_2 p$

$k_{1T_2} = k_1(T_1)\left(\frac{e^{n}_{T_2}}{e^{n}_{T_1}}\right)\mathrm{Exp}\left(3570\left(\frac{1}{T_1}-\frac{1}{T_2}\right)\right)$

$k_{996} = 10\,\mathrm{gm^{-1}cm^{2}atm^{-1}}$ for $\nu = 875\,\mathrm{cm^{-1}}$

$k_2 = 0.005 k_1$

$\Delta\tau = 1 - \frac{k r \Delta p}{g}$

$\tau_{TOP} = \pi\,\Delta\tau$

N_B = Planck fn

$N = (1-\Delta\tau) N_B$

Δ Atm. cont $= N\,\tau_{TOP}$

Surface cont $= N_{B T_n}\,\tau_{(0,1)} = N_{0 T_n}(\pi^n \Delta\tau)$

ν_1	T_{s1}	. . . .	T_{sn}
N_{Rec}			
N_{cs}			

Now. Sum wrt ν

$\Sigma[N_{Rec} S]$

$\Sigma[N_{cs} S]$

	T_{s1} ...... T	T_{sn}
Σ_{REC}	X_1	
Σ_{cs}	... X_1	

ΔT the temperature defect or atmospheric correction.

SIMPLIFY

1/ is there a $\Delta\nu$ representative of the waveband?

2/ how many layers are needed? choose layers according to climatic w.v. content?

3/ Relate ΔT to T_s & total atm water

4/ Relate ΔT to T_s for constant atm water.

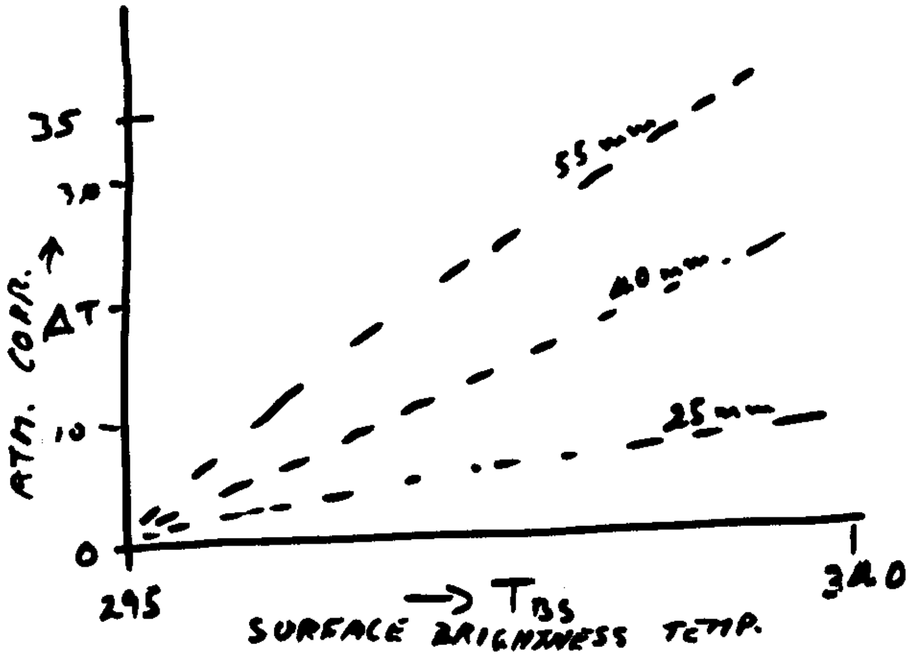
35
30
10
0
ATM. CORR. ΔT
55 mm
40 mm
25 mm
295
320
→ T_BS
SURFACE BRIGHTNESS TEMP.

S.O.

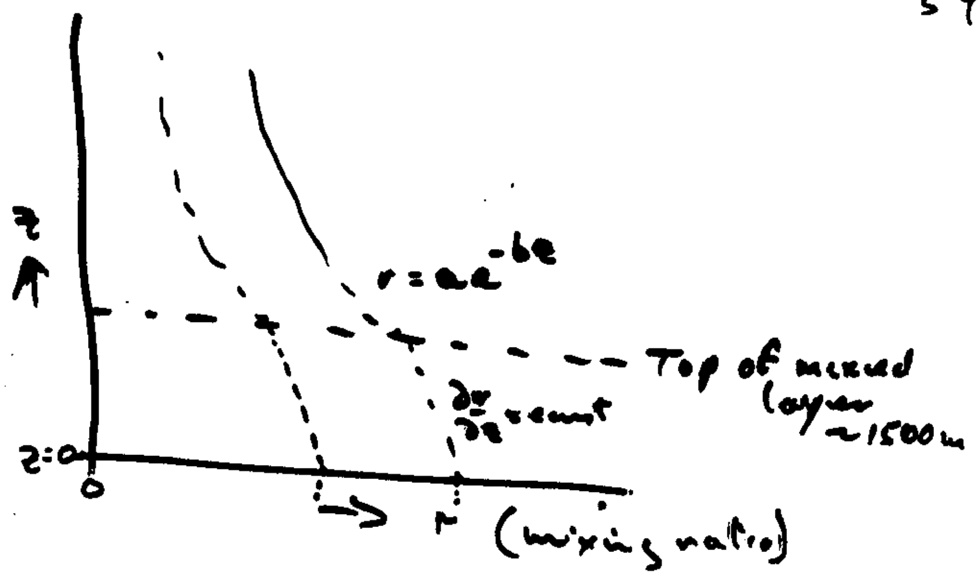
z
r = ae^-bz
Top of mixed layer ~1500 m
∂r/∂z = const
z=0
0
→ r (mixing ratio)

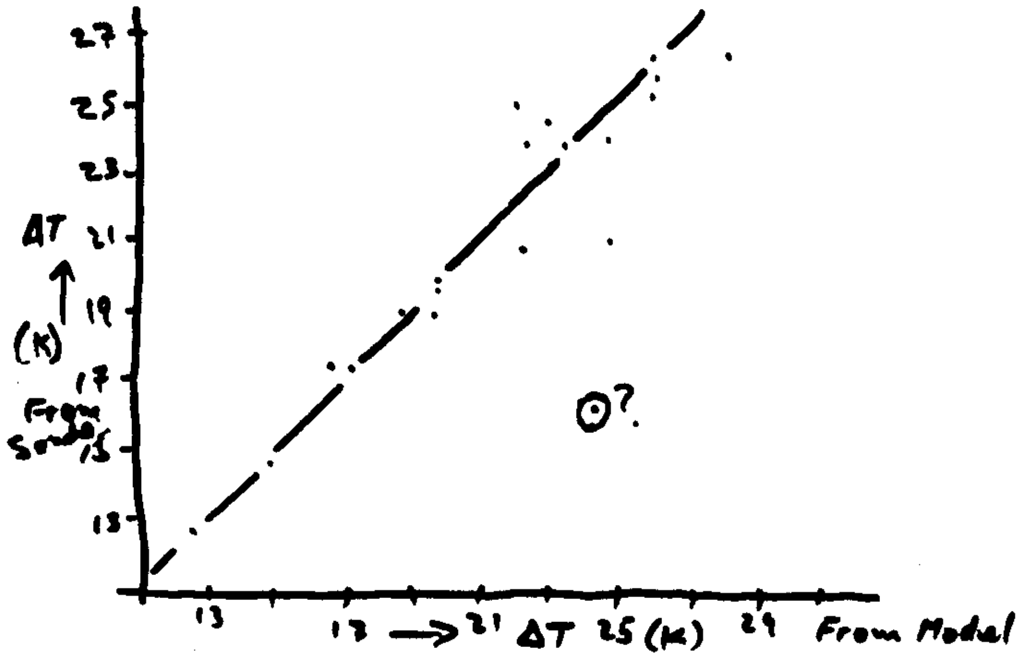
27
25
23
21
19
17
15
13
ΔT (K)
From Sonde
13
17
21
25
29
→ ΔT (K)
From Model
⊙?

34

5.11

Vertical profiles of atmospheric temperature, humidity and radiance contribution, Niamey 16 July 1982

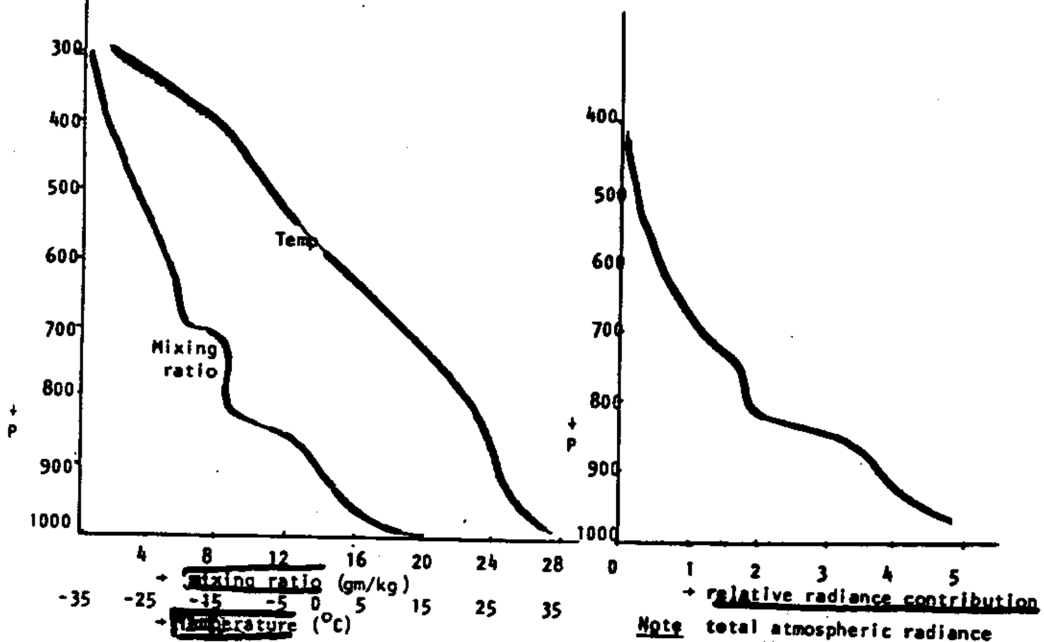

Note total atmospheric radiance contribution 29%, surface contribution 71%

5.10

Vertical profiles of atmospheric temperature, humidity, and radiance contribution, Niamey 25 October 1982

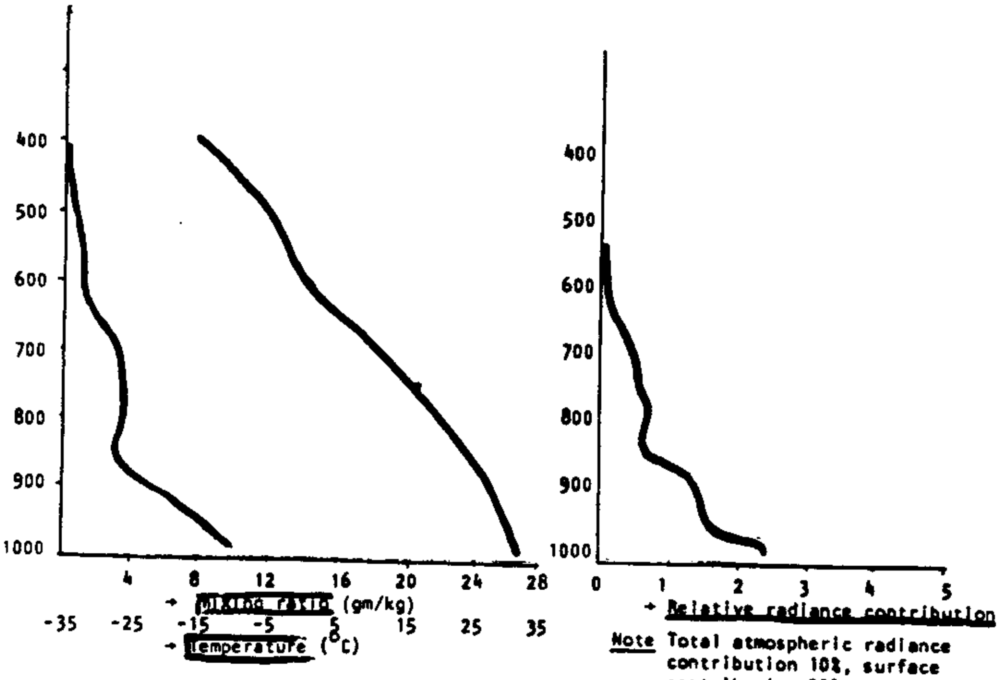

Note Total atmospheric radiance contribution 10%, surface contribution 90%

Split window methods

If we have two radiometers in the atmospheric window (say 10·5 to 11·5 and 11·5 to 12·5 μm) the atmospheric correction will be different in each channel because of $k_1(\nu)$, $N_B(\nu)$

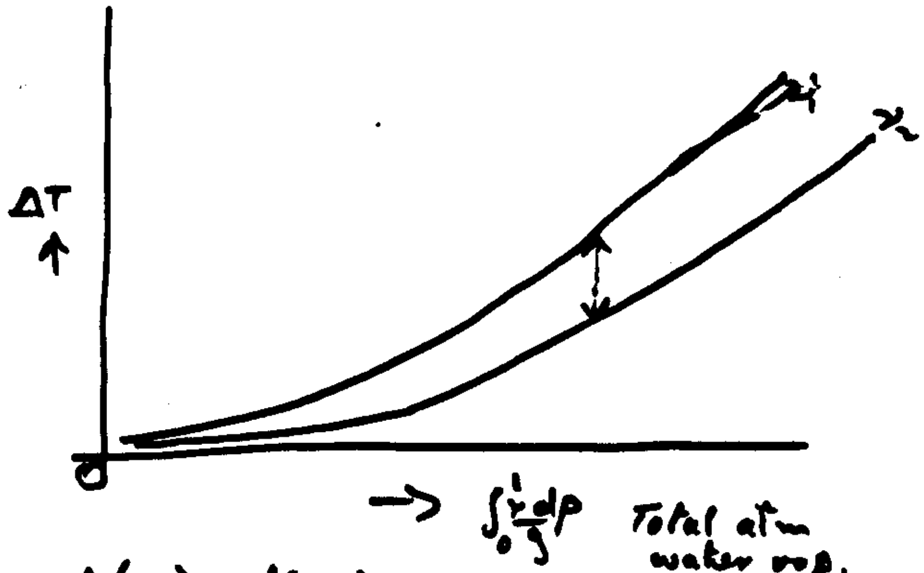

$$\Delta(\Delta T) = f(\Delta T)$$

$$\text{Know } (T_{M_1} - T_{M_2}) = (T_s - \Delta T_1) - (T_s - \Delta T_2)$$
$$= (\Delta T_2 - \Delta T_1)$$
$$= \Delta(\Delta T)$$

ASSUMES $\epsilon_{\nu_1} = \epsilon_{\nu_2}$?

Corrections good to ±2°C or 15% whichever is the lower

Micro-wave soundings of the surface of the earth. (passive) 5.13

$$N_{BT_\nu} = \epsilon N_{B\nu}(T_s)$$

$\epsilon = \epsilon_\nu$(ROUGHNESS, SOIL MOISTURE, MOISTURE IN VEGETATION)

Difficult to disentangle.
Perhaps through using several frequencies.

SLOT I

① VIS — LOCATE

IR — LOCATE

IDENTIFY CLOUDS HAVING TOPS WITHIN A SPECIFIED TEMP. RANGE

②

IR. ONE CLOUD TYPE

③ VIS. ONE CLOUD TYPE

④ → LOCATE CLOUD PATTERN TO ② SLOT I FOR a 1×1° SQUARE

TWO GROUND PATTERNS

Measure dislocation to derive wind vector

GO TO 4
REPEAT FOR EACH 1°×1° SQUARE
GO TO 2
REPEAT FOR EACH CLOUD TYPE

SLOT 2
(30 min after I)

VIS

IR

AS SLOT I

VISIBLE SOUNDINGS OF THE SURFACE OF THE EARTH

Spectral data.
Full band data.

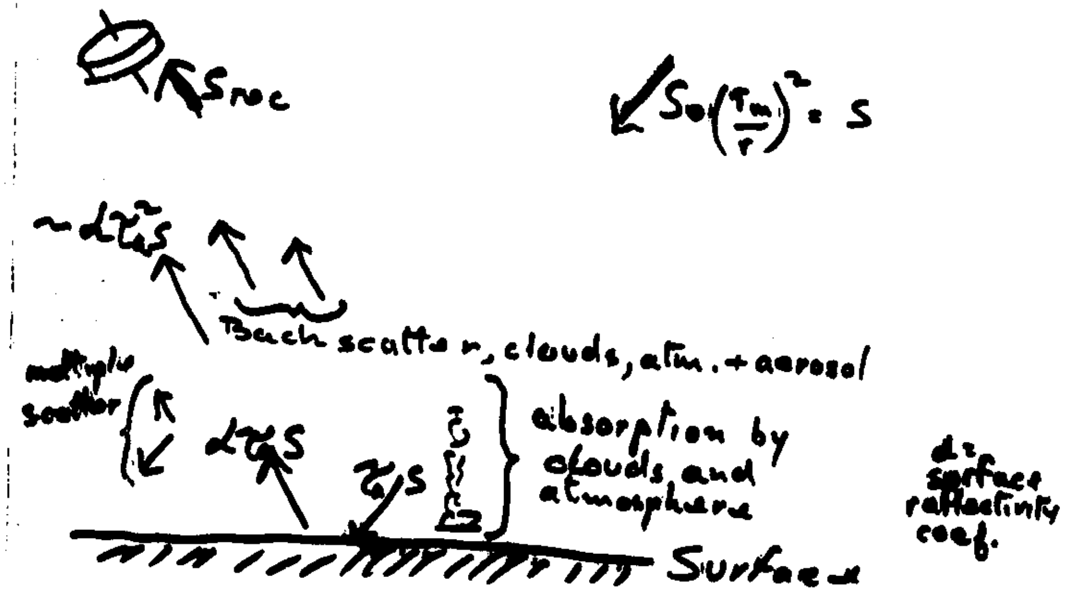

$\frac{S}{S_{rec}} \approx$ Global albedo

ENERGY BUDGET (surface)

$$R_N = L\downarrow + S\,\underbrace{\tau(1-\alpha)}_{?} - L\uparrow$$

$L\downarrow$: calculate from $T(z)$, $H_2O(z)$, include emission from CO_2, O_3

S: solar data

$L\uparrow$: calculate from T_s, ϵ

$?$. $S\tau(1-\alpha)$

The value of α can be estimated from "clear sky" conditions by calculating the scattering and absorption by H_2O, O_2, O_3 etc.

In cloudy or turbid conditions atmospheric absorption is assumed to remain a constant fraction of back-scattering & various empirical relationships have been derived which have some success under specified climatic conditions only.

surface cover

$\alpha = \alpha(\nu, \text{COVER}, \text{HUMIDITY})$

If spectral data is available we can take advantage of the α, ν relationship to identify types of cover

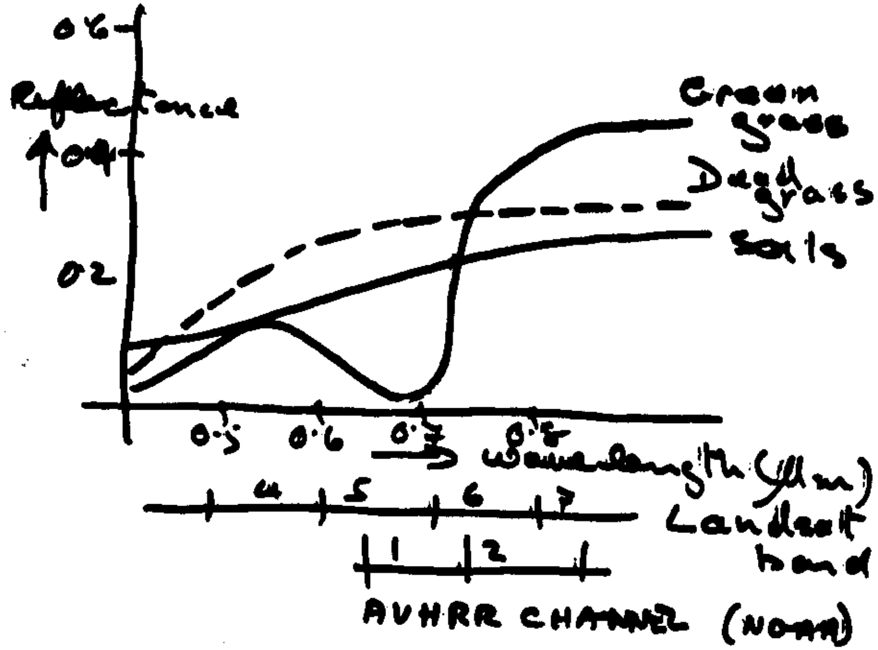

To minimise atmospheric effects the ratios of reflectance are usually used, such as

$$\frac{\text{Near IR} - \text{Red}}{\text{Near IR} + \text{Red}}$$

as vegetation indices.

Windfinding from satellite

6·4

Assume that clouds move with the wind prevailing at about the level of their tops. Derive the wind from the cloud movement between consecutive slots (30 min interval) and ascribe the height according to the cloud top temperature and climatology.

Surface winds over the ocean

6·6

Active satellite microwave (radar) has been used to estimate surface winds over the ocean.

Surface wind is well correlated with surface roughness on a scale of a few cm. The backscattering of microwave is also correlated with roughness on this scale. So, the intensity of back scatter is related to the surface wind. The doppler shift and polarisation of the returned signal indicate the direction of the wind.

Possible accuracy $\pm 2\,m\,s^{-1}$

$\pm 20^\circ$

RAINFALL ESTIMATION FROM SATELLITE DATA

VISIBLE
INFRA-RED
MICRO-WAVE

MICRO-WAVE – active + passive
look possible

Microwave is the only method in which the radiometric measurement may be directly related to the water content of a cloud.

Polar orbiting satellites in 1990's may be equipped with up to 20 microwave channels from 18 to 180 GHz. 12 channels close to 60 GHz O_2 band (temperature), 4 ch. close to 180 GHz H_2O band (water vap. + ? rainfall)

Microwave emission from land surfaces is so dependant on surface state that interpretation of near surface data over land is difficult.

Over oceans the sources are

sea
atmosphere H_2O vapour
atm. H_2O liquid. ⟸

Emissivity depends on drop size, ice/water. Small drops (few/μm) are almost transparent. As $D \to \lambda$ absorption & emission become strong.

Field of view ~30 km > shower size could give problems in some zones

Observations at two frequencies having different relative sensitivities for w.v and liquid water can help separate the signals.
Best estimates are, for ocean measurements to within a factor of 2.

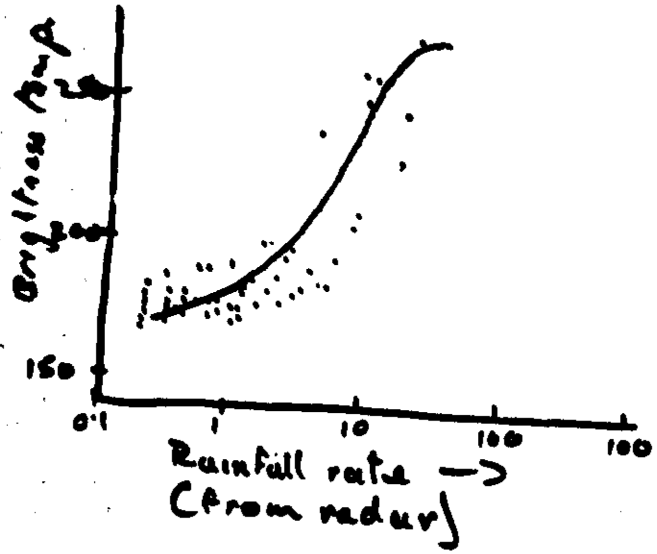

Results biased by time of overpasses as no prospects for such instruments on GEOS. [Spat. resol'n ~ 100's km]

VIS + IR methods

① No direct information on rain rate available

Two fundamental methods

① Cloud index

② Cloud dynamics (life history)

Cloud index

a) **Subjective**

Use high quality I.R. + VIS photographic images or colour monitor display to identify cloud types [Polar orbit. satellite]

Classify

St	0	CLOUD INDEX I
Sc	1	
⋮		
~~As~~	5	
⋮		
Cb	9	

Rainfall rate mm/hour

$= I \times S \times C \times T$

C Climatological factor $= \frac{\text{annual rainfall}}{\text{annual raindays}}$

T Topographical factor = altitude of site × local increase of rain rate per km.

S Synoptic factor = interpolated rainfall (adjusted for altitude) from adjacent raingauge sites.

This is the basis of a technique used by Barrett (Bristol)

i) Requires skilled interpretation – labour intensive

ii) Requires climatological background data

iii) Requires high resolution imagery [P.O.]

Reports significant improvement over linear interpolation, particularly in rain from mid-latitude synoptic scale rainfall.

b) Objective

Relate rain with bright (VIS) and cold (I.R.) cloud (and W.V. data also)

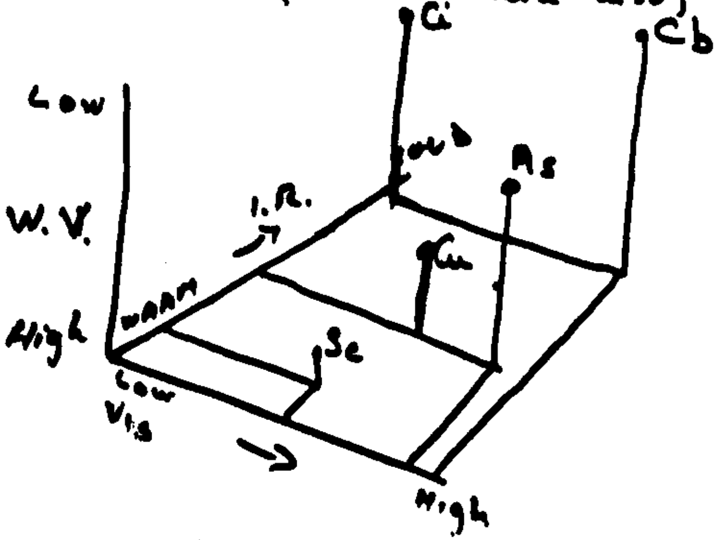

Within a zone or synoptic situation associate a rainfall rate with a cloud type.

Can only be used in daylight as most of the W.V. data is redundant

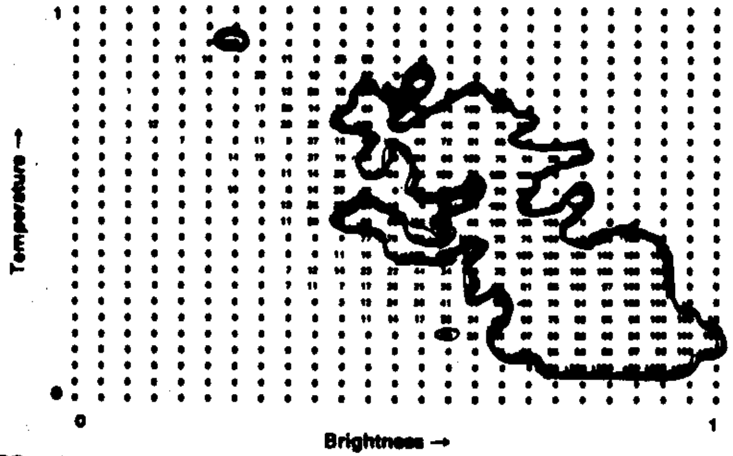

FIG. 6.4 The conditional probability of rain, in percent, from the rain and no rain arrays of Fig. 6.3. For any element this probability is all R as a percentage of all R plus all N. The 50% optimum boundary is sketched. From Lovejoy and Austin, 1979a.

RAINFALL PROBABILITY

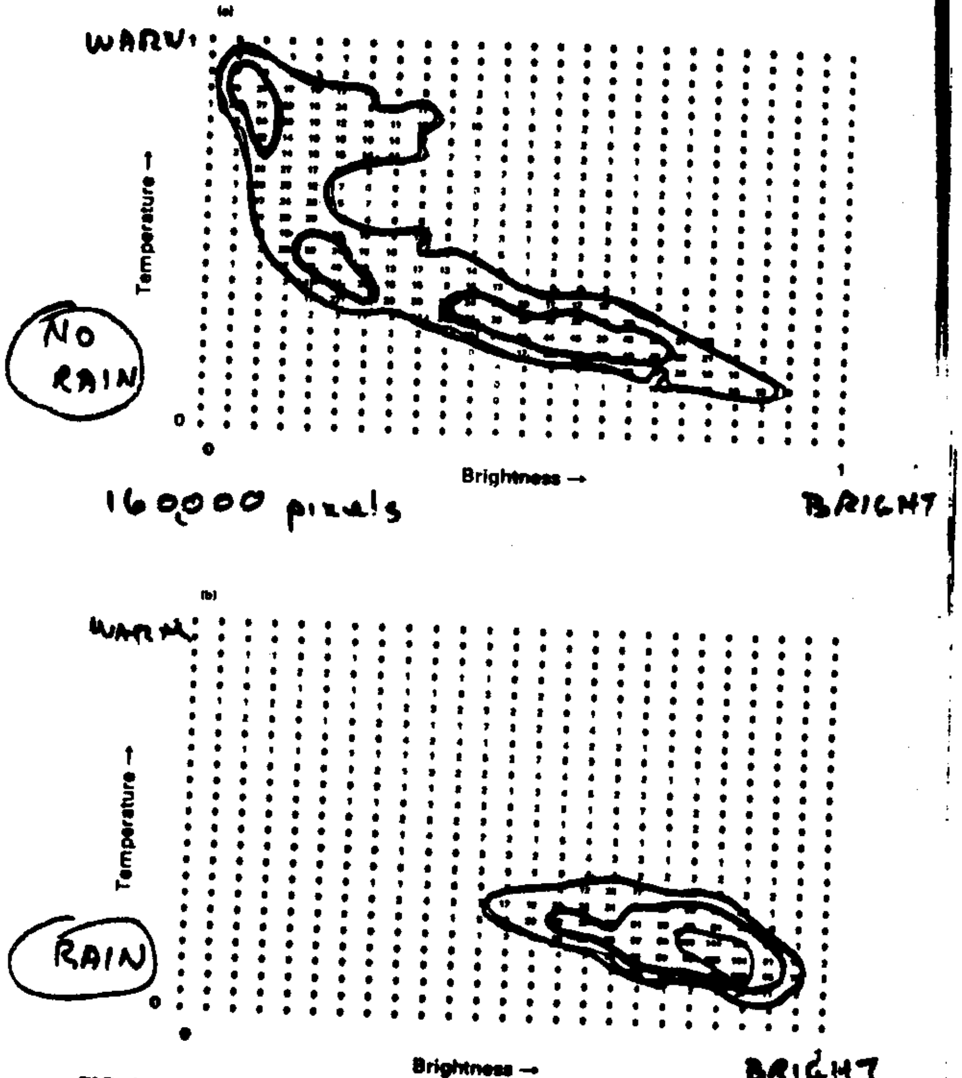

FIG. 6.3 *Joint frequency distribution of SMS-1 visible and infrared data for a 400 × 400 km box centred at 09°00′N, 22°40′W in the eastern tropical Atlantic Ocean, 1300 GMT 5 September 1974. Data have been normalized to a scale 0–1. (a) No rain case (N class). (b) Rain case (R class). After Lovejoy and Austin, 1979a.*

43

Life history methods

Convective clouds T<-30°C

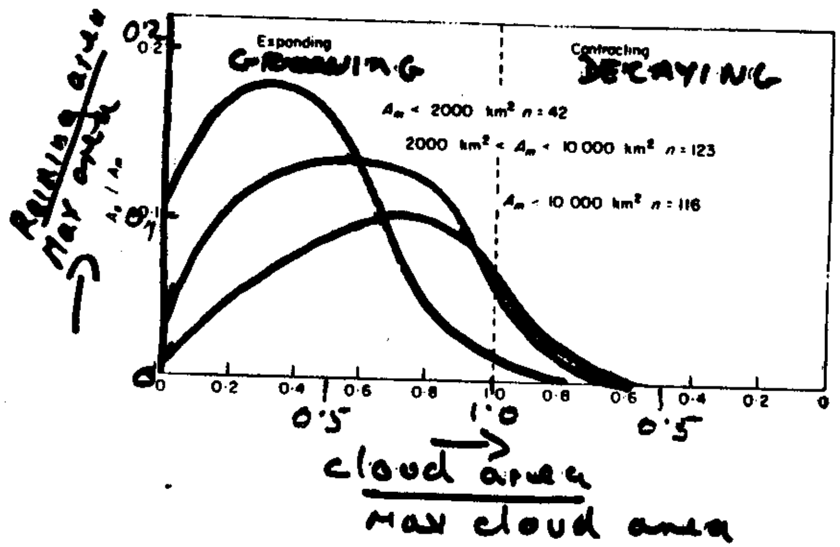

— $A_m > 10{,}000\ km^2$

$2{,}000 < A_m < 10{,}000\ km^2$

— $A_m < 2{,}000\ km^2$

7.8

$R = a_0 + a_1 \frac{\partial R}{\partial t}$

Woodley, Griffith

Stout, Martin, Sikdar.

Good results over areas for which the coefficients were determined. Poor mobility.

$\div$

7.9

R. U.

Estimation of rain from S.C.s

Use knowledge of synoptic + mesoscale features of S.C.s. to improve rainfall estimation.

Correlation of rainfall amounts at sites round Niamey from large scale convective systems (1982)

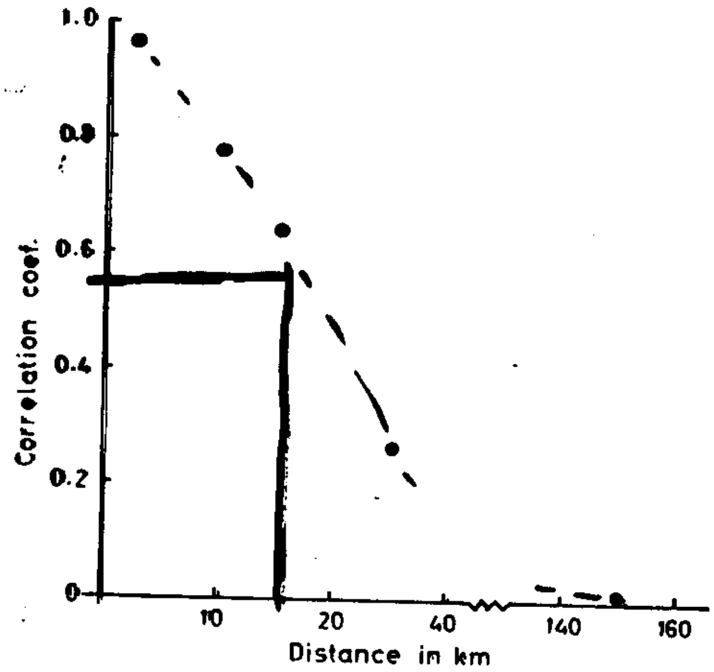

RAINFALL PATTERNS IN SQUALL LINES

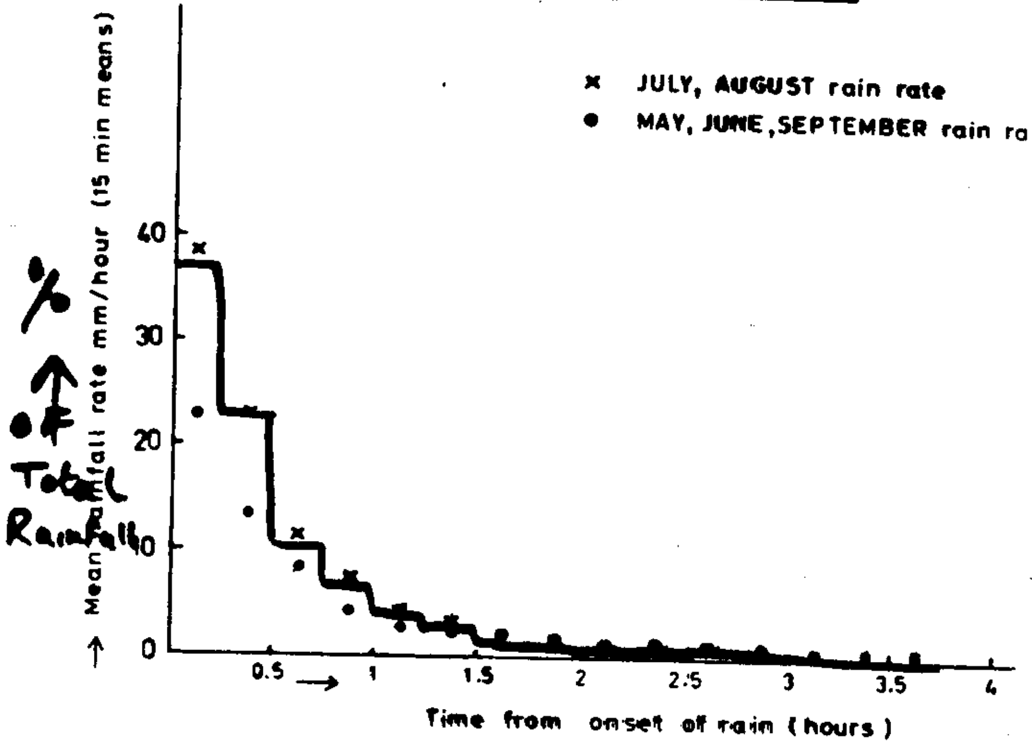

Mean rainfall rate in squall lines affecting Niamey (rain rates are averaged over 15 minute intervals).

95

SQUALL LINE CHARACTERISTICS

VARY RAPIDLY WITH TIME

VARY RAPIDLY WITH DISTANCE

GIVE MOST RAIN AT NIGHT

SATELLITE RAINFALL ESTIMATION

1. DAILY, SINGLE PIXEL

   MUST FOLLOW CLOUD DEVELOPMENT

   $$R = \sum_{day}\left(a_0 + a_1 \frac{\partial A}{\partial t} \cdot \frac{1}{A} + a_2 \frac{\partial T}{\partial t}\right)$$ FOR EACH PIXEL

2. DAILY, LARGE AREA (AREA $\gg$ STORM AREA)

   $$\bar{R} \approx \sum_{day}\left\{\frac{\text{area of cold cloud}}{\text{total area}}\right\}$$

3. 10 OR 30 DAY PERIODS, SINGLE PIXEL

   $$R = \sum_{period}(\text{COLD CLOUD})$$ FOR EACH PIXEL

   = DURATION OF COLD CLOUD

Median and interquartile ranges of rainfall corresponding to the duration of cold cloud (< -60 °C) over Niger.

a) 1 to 31 July 1985.

Cloud duration (hours)	Rainfall (mm)		
	Med	Q_1	Q_3
0 to 4.5	7	1	17
4.5 to 9.5	31	12	65
10.0 to 19.5	80	55	118
20.0 to 29.5	94	63	108
> 30	105	83	115

Expected rainfall variability within a 10 x 10 km square, ten day totals (mm).

Med	Q_1	Q_3
12	7	16
29	19	38
36	30	44
57	43	68

c) 11 to 20 July 1985.

Cloud duration (hours)	Rainfall (mm)		
	Med	Q_1	Q_3
0	4	0	10
0.5 to 4.5	11	4	26
5.0 to 9.5	26	13	45
10.0 to 14.5	43	25	77
15.0 to 19.5	65	47	83

●
1 – 2
3 – 4
5 – 6
7 – 8

Soil moisture and evaporation estimates from satellite data

Micro-wave – theoretically possible, little progress to date.

Energy budget methods using VIS + IR

$$R_N = H + \lambda E + G$$

$$R_N = S(1-\alpha) + L\downarrow - L\uparrow$$

$$H = \rho c_p \frac{(T_s - T_a)}{r_a} \;;\; \lambda E = \rho \frac{c_p}{\gamma} \frac{(e_s - e_a)}{r_a}$$

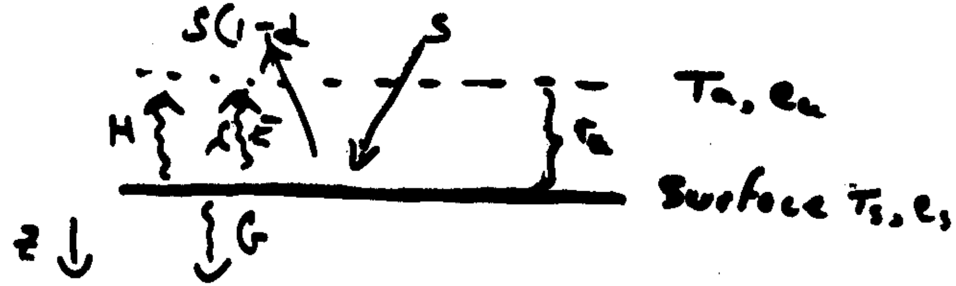

$$G = -k \frac{\partial T}{\partial z}\Big|_{z=0} \;,\; c\frac{\partial T}{\partial t} = \frac{\partial}{\partial z}\left(k \frac{\partial T}{\partial z}\right)$$

$$r_a = f((T_s - T_a), u)$$

7,22

Quantity	Source	Variability
$S(1-\lambda)$ absorbed solar radiation	} satellite ?	minutes/hour
$L\downarrow$ incoming L.W	satellite (from T, H_2O profiles)	hours
$L\uparrow$ outgoing L.W	satellite (from T_s)	minutes/hour
ρ air density	~ constant	—
C_p " spec. ht	"	—
T_s ground surf. temp	satellite	minutes/hour
T_a air temp	synoptic	minutes/hour
r_a aerodynamic resistance	?	minutes/hour
U air speed	synoptic	minutes/hour
γ psychrometric constant	constant	—
e_s vap. pres at surface	?	minutes/hour
e_a vap. pres of air	synoptic	minutes/hour.
$\frac{\partial T}{\partial z}\Big\vert_{zero}$	?	minutes/hours
k thermal cond. of soil	f(soil type + soil moisture) ?	hours/days
C thermal capacity of soil	f(soil type and soil moisture) ?	hours/days

Unknowns

r_a, e_s, $\frac{\partial T}{\partial z}\Big\vert_{zero}$ } vary within the day

k, C } constant within the day

3 Solution methods

1/ Europe – growing crops

($T_s - T_a$) small, r_a estimated from U, ($T_s - T_a$), roughness aerodynamic formulae.)

$$e_s = (e^{sat}_{T_s} - e_a)\frac{r_s}{r_s + r_a}$$

r_s (stomatal or canopy resistance)

$$\int_{day} G = 0$$

Explicit soln

Area means.

2/ Represent each variable by its Fourier components, using at least 6 observations per day solve for all unknowns [Univ. of S'hamp]

Gives **Good** $H+\lambda E$
Poor $H/\lambda E$
Poor soil moisture

3/ Assume that all daily variables for fluxes can be represented by their mean values.

e.g. $H = \rho \frac{C_p}{r_a}(\overline{T}_s - \overline{T}_a)$ etc

and $\overline{T}_s, \overline{T}_a$ etc are represented by $\left(\frac{T_{s\,max} + T_{s\,min}}{2}\right)$ etc.

So use 2 obs/day

Evaluate r_a in dry season when $E = 0$

Represent $\lambda E = \frac{\rho C_p}{\gamma} \frac{(e_\delta - e_a)}{r_\delta + r_a}$

when δ is the depth of dry soil

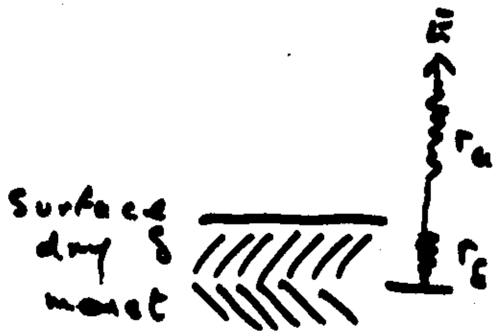

$k_1\ C_1$
$k_2\ C_2$ } Solve $C\frac{\partial T}{\partial t} = \frac{\partial}{\partial z} k\left(\frac{\partial T}{\partial z}\right)$ for Gower 12 hours

δ is defined from $\bar{E}$ since last rainfall and the soils field capacity

r_δ from diffusion resistance of soil

[Rosema]

Gives plausible results but not yet validated or adequately sensitivity tested.

Readings empirical methods (SLIDES) 7.126

① Soil moisture.

- via thermal inertia.

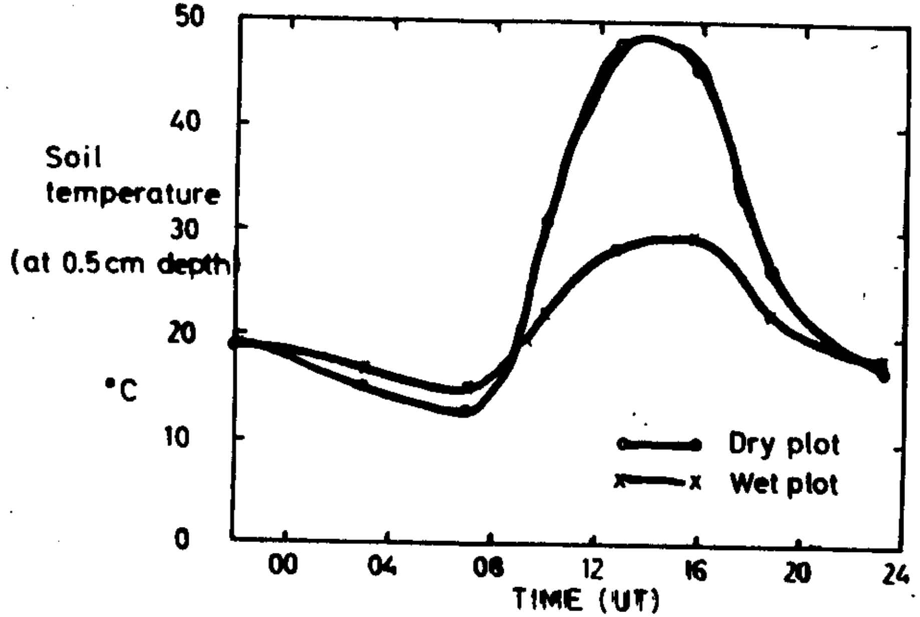

Diurnal soil temperature variation
(Wet and dry test plots at Niamey, Niger, 11-12-81)

Soil surface temperatures

Drying curves

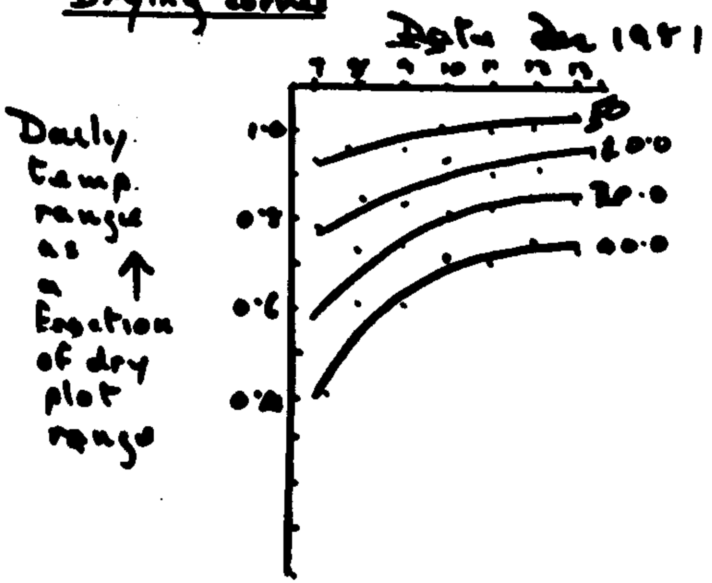

Plot irrigated on 6 Dec.

Average daily range of dry plot ≈ 35 K

$K = \frac{k\text{-cond}}{c\text{-vol heat cap.}}$

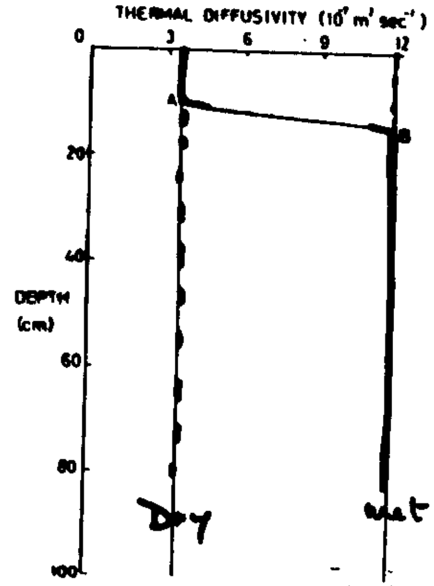

A TWO-LAYER MODEL OF THERMAL DIFFUSIVITY

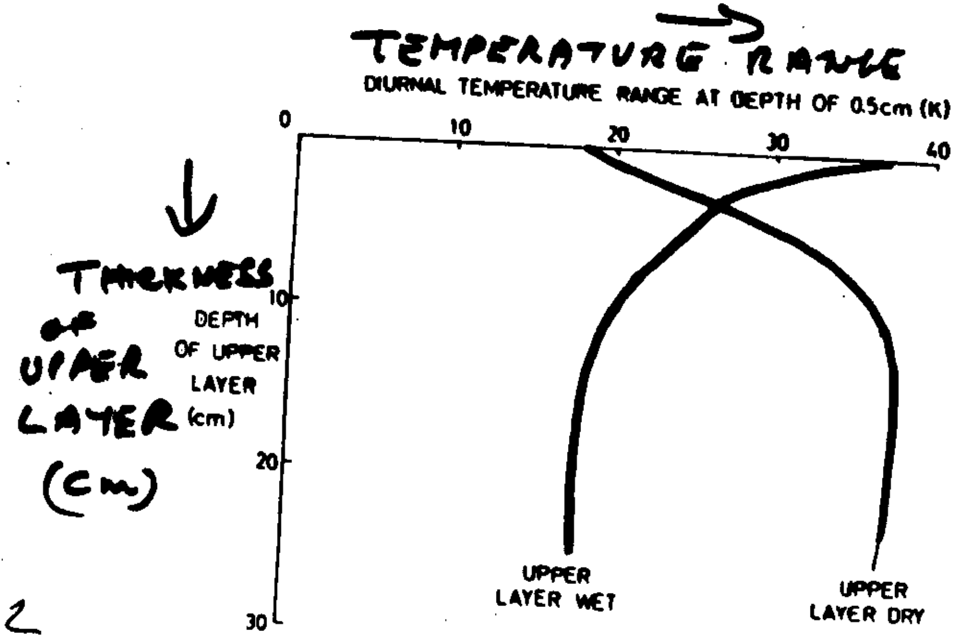

CLOUD DATA FROM METEOSAT VIS

EVAPORATION.

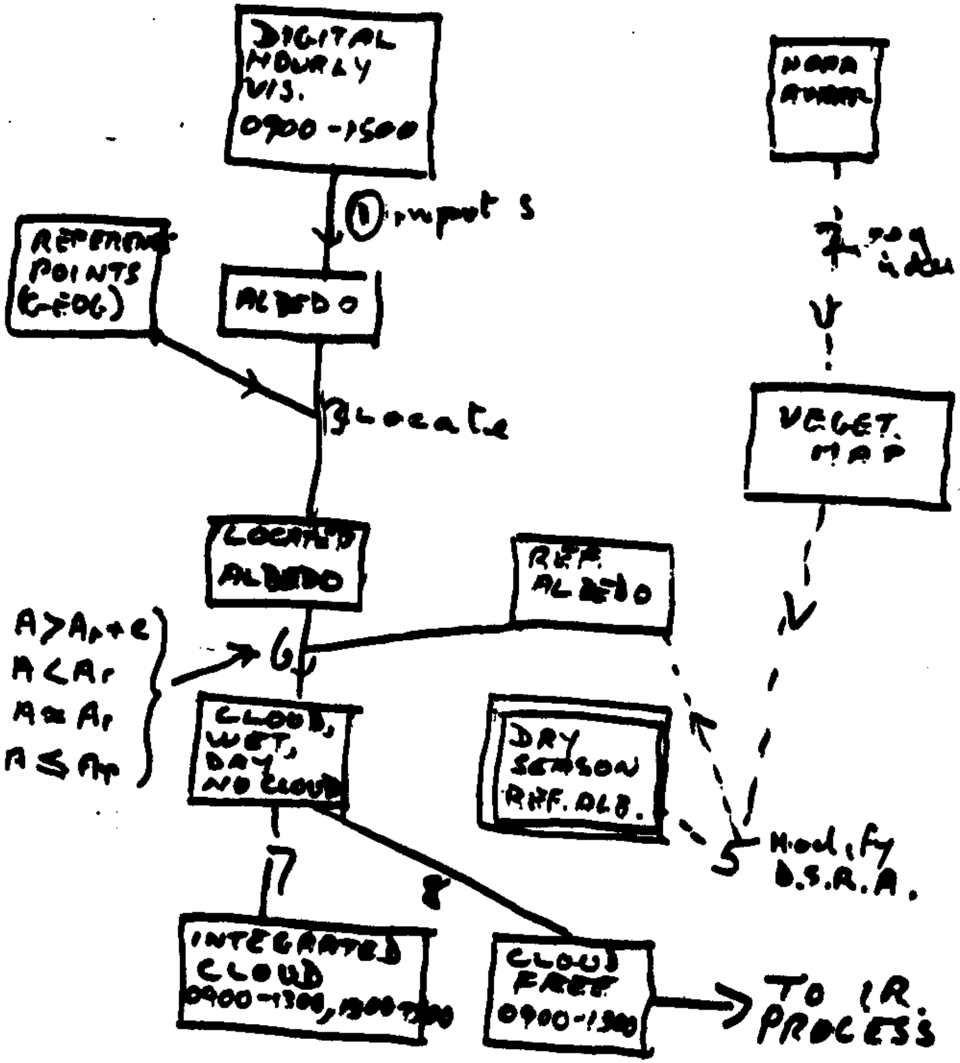

Soil moisture drying curve
Niamey, May 1982

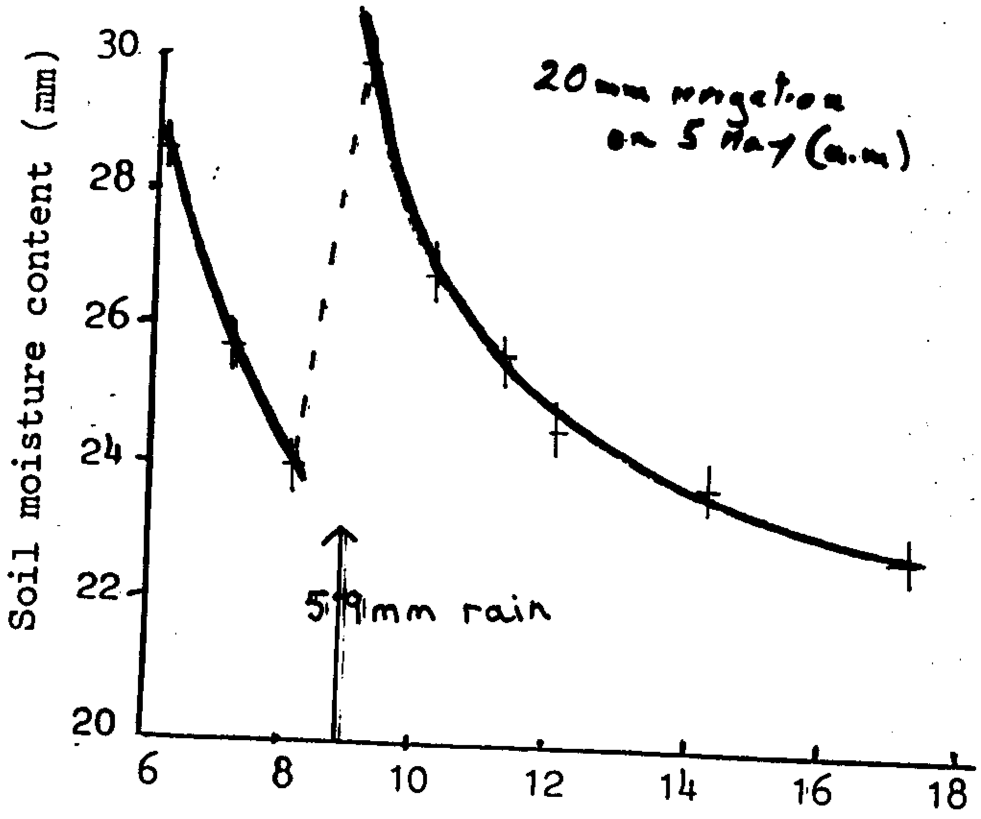

EVAPORATION (mm) 3.1 1.3 → 3.1 1.1 0.8 0.6 0.4 ←0.8→

$E_d = \frac{a}{d}$ d: days since rainfall

Soil moisture (SM)

$SM = R - \sum_{1} E_d$

Subject to SM $\not>$ Field capacity x depth

for $R < a$ mm $R = 0$

$\sum E_d \not>$ s.m.

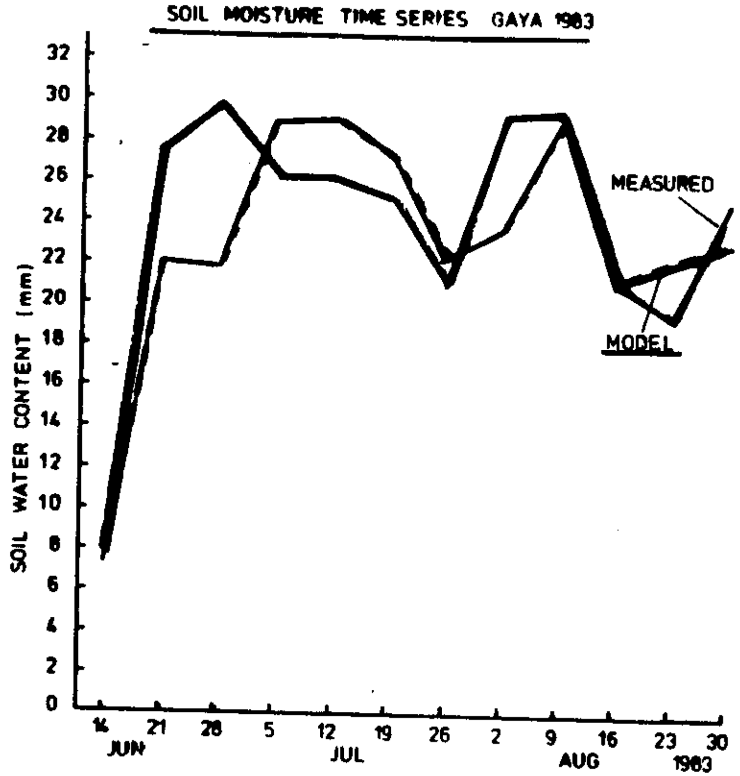
SOIL MOISTURE TIME SERIES GAYA 1983
SOIL WATER CONTENT (mm)
32
30
28
26
24
22
20
18
16
14
12
10
8
6
4
2
0
MEASURED
MODEL
14
21
28
5
12
19
26
2
9
16
23
30
JUN
JUL
AUG
1983

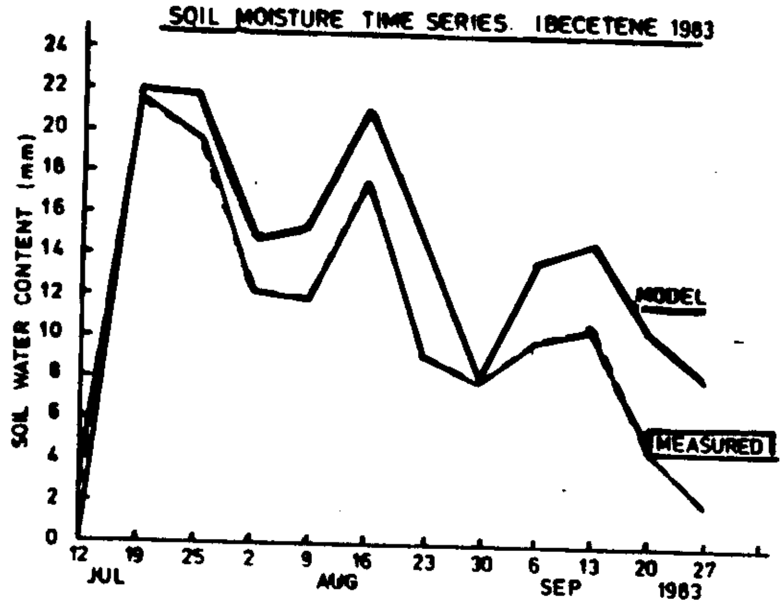
SOIL MOISTURE TIME SERIES. IBECETENE 1983
SOIL WATER CONTENT (mm)
24
22
20
18
16
14
12
10
8
6
4
2
0
MODEL
MEASURED
12
19
25
2
9
16
23
30
6
13
20
27
JUL
AUG
SEP
1983

JJ

Radar.

Principles of radar

The radar eq.

Scattering by spherical particles

- Principles + problems of rain-rate measurement

A satellite application of radar

Measurements of motion in storms

Validation of remotely sensed data

Radio Detection and Ranging

λ = 0·1 to 100 cm (micro-wave)

Uses

Storm detection
Wind finding
Rainfall estimation
Cloud physics research
Turbulence studies
Sea state

Principles

Emit a ~~wave~~ pulse and judge the position and range of the target by the direction from which the echo comes and the time from emission to reception

Components

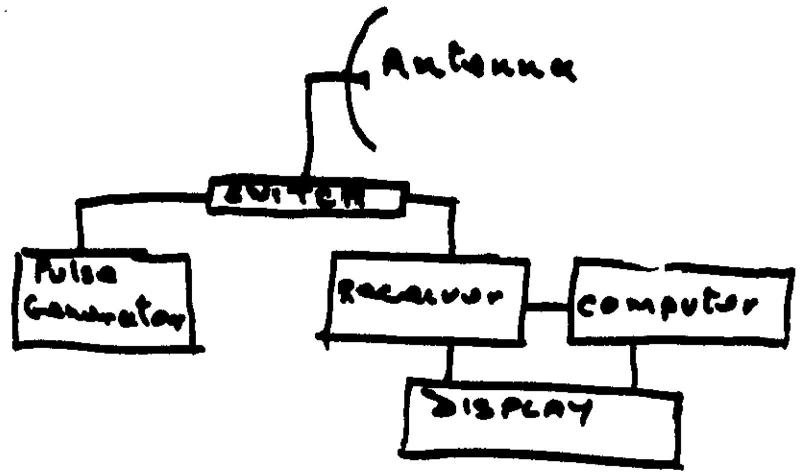

Pulse generator

Single or dual freq
λ in range 1 to 20 cm
Pulse length μs (~20 to 500 m)
Pulse repetition freq ms

Switch

Disconnects rx. from tx during emission

Receiver

Tuned amplifier
Range compensated
Doppler shift

Antenna

Serves to transmit and receive
Parabolic, or section there-of.
Focussing power $f(D, \lambda)$
May lock-on, rotate or nod

P.P.I.

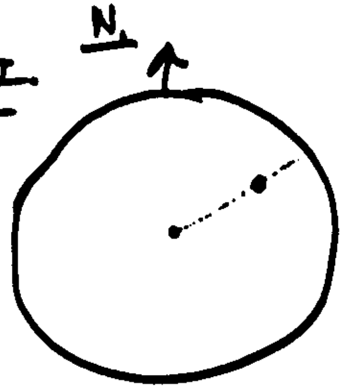

ROTATING ANTENNA and TIME BASE

OFF CENTRE FACILITY

R.H.I.

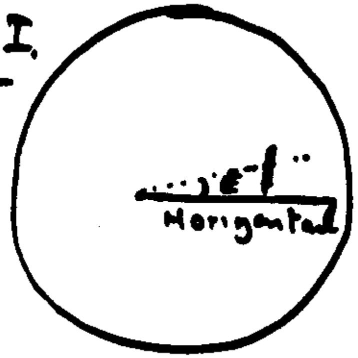

NODDING ANTENNA AND TIME BASE

E = angle of elevation

COLOUR MONITOR

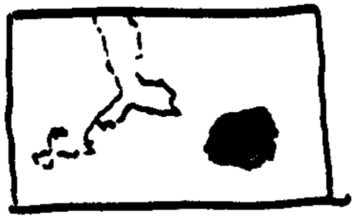

Radar characteristics

Minimum range $\geq$ pulse length/2
(switch cannot open until tx ends)

Maximum range

- Transmitted power
- Back-scattering "power" of target
- Pulse repetition freq.
- Sensitivity and noise characteristics of receiver
- Earth's curvature

Distance of target Limited by pulse "rise time"

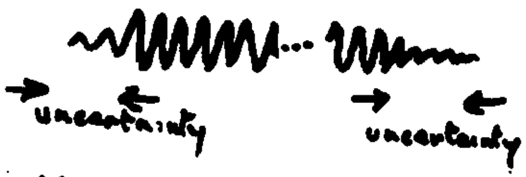

1/10 $\mu s \equiv 30m$

Azimuth or elevation of target

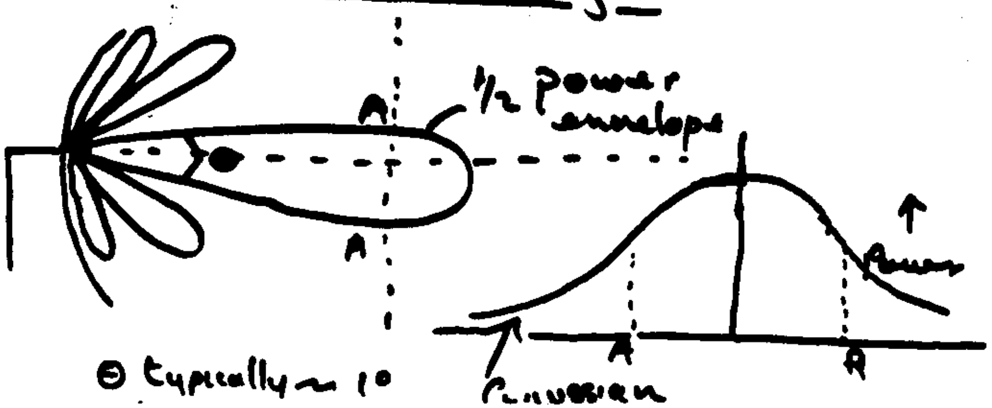

θ typically ~ 1°

For greater directional accuracy a rotating or nodding source is used so that as the axis of the beam scans across the target the return signal peaks.

This can give directional accuracy to $(10^{-2})°$

Refraction of the radar beam

Due to the decrease of pressure and humidity with height the radar beam is refracted towards the earth's surface.

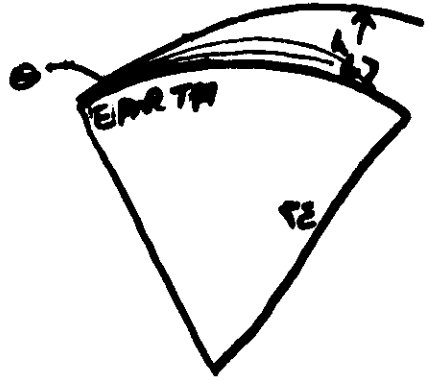

Ducting if $\frac{\partial T}{\partial z}$ and/or $-\frac{\partial q}{\partial z}$ are large

Refraction of E - [redacted] radiation

Fig 8.3

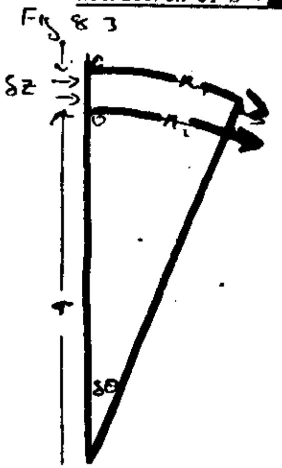

Consider a plan wave front OO propogating in a stratified medium. If n decreases with height the wave front will tend to tilt as it propogates.

$$\delta\theta = \frac{c\,\delta t}{n_1}\cdot\frac{1}{r} = \frac{c\,\delta t}{n_2}\frac{1}{(r+\delta z)}$$

$$r n_1 = (r+\delta z)\left(n_1 + \delta z\frac{\partial n}{\partial z}\right)$$

$$0 = n_1\delta z + r\,\delta z\frac{\partial n}{\partial z} + \delta z^2\frac{\partial n}{\partial z}$$

$$r \approx -n\Big/\frac{\partial n}{\partial z}$$

$$r \approx -n\Big/\frac{\partial n}{\partial z}$$

$$\text{in air } r \approx -1\Big/\frac{\partial n}{\partial z}$$

In air n ≈ 1.0003, So $r = \left(-\frac{\partial n}{\partial z}\right)^{-1}$

$$n = a\rho_a + \frac{b\rho_w}{T}$$

$$n = a\rho_a + \frac{b\rho_w}{T}$$

	Visible	Microwave
a	$\sim 2.23\times10^{-4}$	$2\cdot23\times10^{-4}$
b	0	1·77

EX

Show $$\frac{\partial n}{\partial z} = \frac{-P}{RT^2}\left[\frac{\partial T}{\partial z}\left(a+\frac{bq}{T}\right) - b\frac{\partial q}{\partial z} + \frac{g}{R}\left(a+\frac{bq}{T}\right)\right]$$

Hence find the temperature and humidity laps rates near the earth's surface which would keep a radar beam // to the surface.

The radar eq —

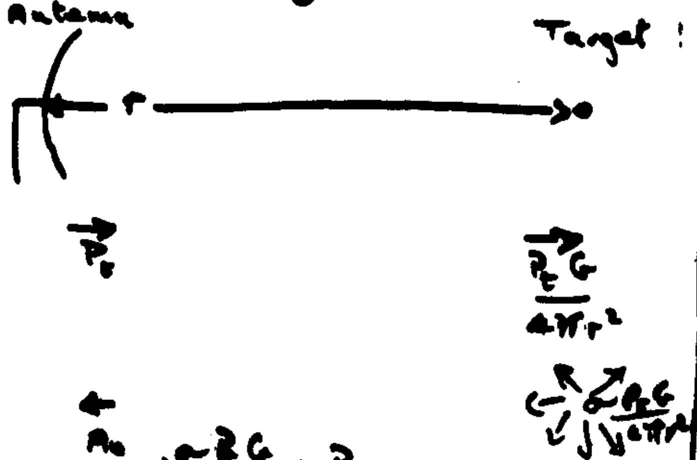

P_t = peak power transmitted

$G \sim A_e\frac{4\pi}{\lambda^2}$

A_e = affective antenna area ≈ ½ actual antenna area

σ back scattering cross section of target

$$\frac{A_e}{4\pi r^2}\cdot\frac{\sigma P_t G}{4\pi r^2} = P_r$$

$$P_r = \frac{P_t\,\sigma\,\lambda^2 G^2}{(4\pi)^3 r^4}$$

Typically $\begin{cases} P_t \sim 10^6\,\text{w} \\ A \sim 4\,\text{m}^2 \\ \lambda \sim 0{\cdot}1 \to 0{\cdot}001\,\text{m} \\ P_r(\text{min}) \sim 10^{-15} \end{cases}$

$G = \frac{A_e 4\pi}{\lambda^2}$ refers to the beam axis for a Gaussian power distribution & an extended target

$$G = \frac{A_e 4\pi}{\lambda^2}\cdot\frac{\pi^2}{32\ln 2}$$

<u>Uses</u>
Wind finding
Storm warning
Rainfall measurement
Sea state & ...

8·10

Scattering / size/λ relationship (M:

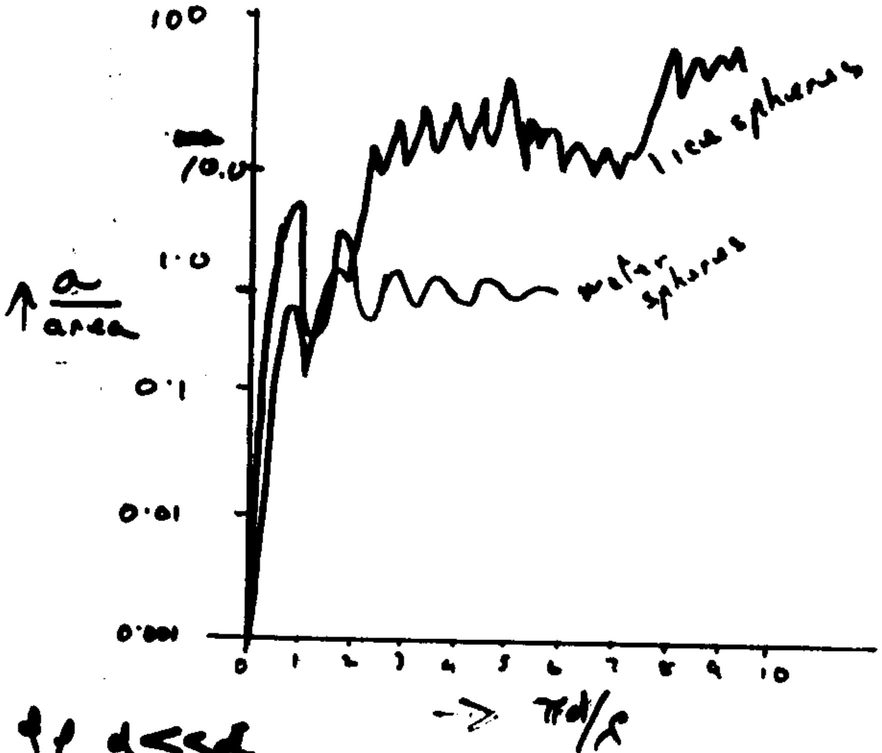

If $d \ll \lambda$

$$\sigma = \frac{\lambda^2}{\pi}\left(\frac{\pi d}{\lambda}\right)^6\left(\frac{n'^2-1}{n'^2+2}\right)^2$$

where n' is the complex refractive index

$$= \frac{\pi^5}{\lambda^4} K^2 d^6$$

with $\left(\frac{n'^2-1}{n'^2+2}\right)^2 = K^2 \approx 0.93$ water ≈ 0.20 ice

$$= \frac{\pi^3}{\lambda^4} K^2 \frac{m^2}{\rho^2} \cdot 36$$

in terms of mass

Scattering

Back scattering cross section σ

The cross section of the isotropic scatterer which would back-scatter the same fraction of the incident energy as the actual particle does. The σ may be a small fraction or many times the actual cross sectional area.

Scattering by spherical particles

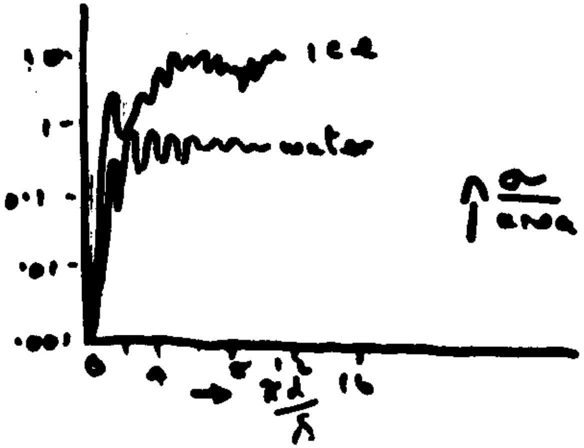

If the drop diam. $d \ll \lambda$

$$\sigma = \left(\frac{\lambda^2}{\pi}\right)\left(\frac{\pi d}{\lambda}\right)^6\left(\frac{n'^2-1}{n'^2+2}\right)^2$$

where n' is the refractive index

putting $\left(\frac{n'^2-1}{n'^2+2}\right)^2 = K^2$

$$\sigma = \frac{\pi^5}{\lambda^4} K^2 d^6$$

or in terms of mass

$$\sigma = \frac{\pi^3}{\lambda^4} K^2 \frac{m^2}{\rho^2} \cdot 36$$

<u>Power received from a volume of spherical particles filling the beam</u>

$$P_r = \frac{P_t G^2 \lambda^2 \theta^2}{(4\pi)^3 r^4 \, 32 \ln 2} \cdot \underbrace{\frac{h}{2}\,\frac{\theta \pi r^2}{6}}_{\text{volume irradiated}} \cdot \frac{\pi^5}{\lambda^4} K^2 \sum_{\text{unit vol}} (d)^6$$

$$= \frac{c K^2}{r^2} \sum d^6$$

where c is a constant of the radar

So *if* we know the drop size distribution in a cloud, *if* the drops were all ice (or water) and *if* they were spherical we could measure the liquid water content from P_r (ignoring attenuation)

<u>Effects of non-spherical particles</u>

Fig 8·7

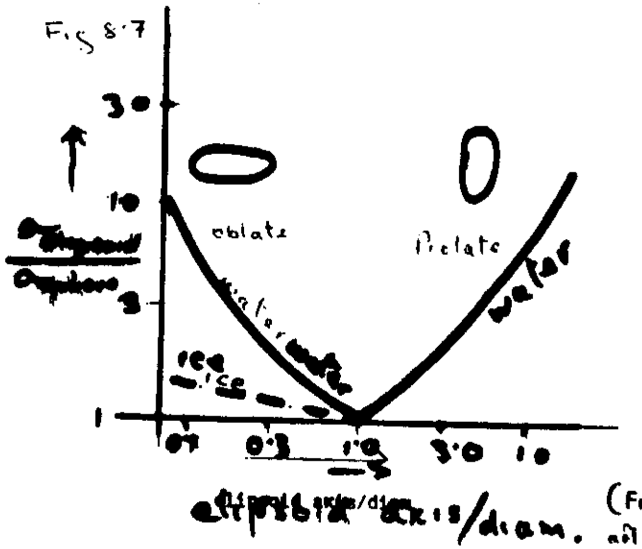

10 cm radar

(From Batten Radar Atlas)

Backscatter by melting ice spheres

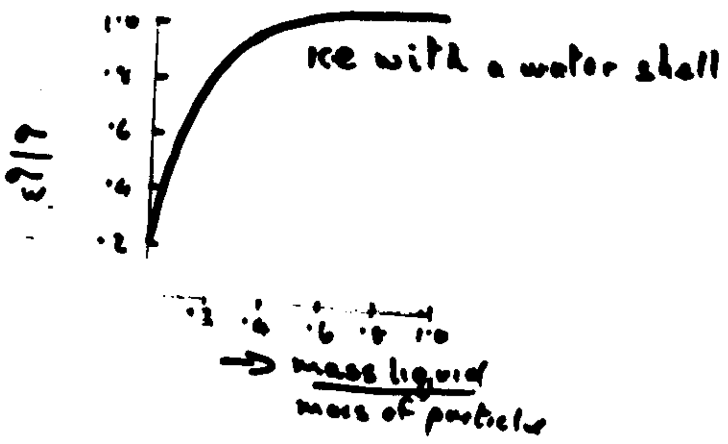

Rain-rate measurement by radar

$$P_r = \frac{c}{r^2} K^2 \sum_{\substack{\text{unit}\\ \text{vol}}} d^6$$ for an assembly of spherical particles

to measure rain rate we must take account of:

non-spherical particles

is K ice or water

possibility of non Rayleigh scatter

rain rate / dropsize distribution relationships

Σd^6 does not define the drop size distribution.

We substitute Z for Σd^6 and seek the relationship between the rainfall rate (R) and Z, the radar reflectivity factor

Drop size distribution

This is mainly determined by coalescent growth and the spontaneous break-up of large drops

Fig. 9.1 (From Doviak)

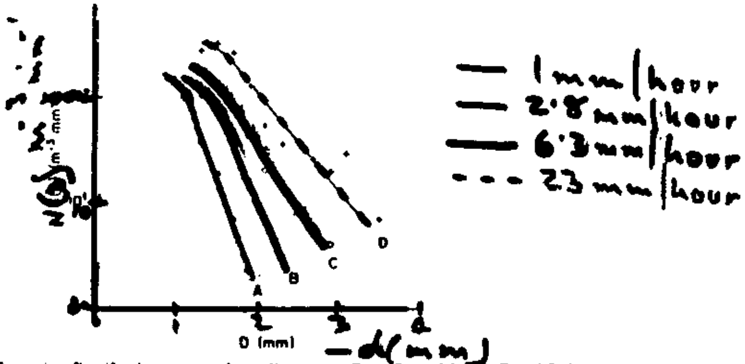

Raindrop size distribution versus drop diameter. (Data from Marshall and Palmer, 1948.) Curves ABCD are for rainfall rates of 1.0, 2.8, 6.3, and 23.0 mm hr⁻¹, respectively.

The data fits a curve

$N(D) = N_0 \exp(-\Lambda D)$ $\Lambda = 4.1R^{-0.21}$

$N_o = 8 \times 10^{-3} m^{-3} mm^{-1}$

where R is the rain-rate.

$$N(D) = N_0 \exp(-\Lambda d)$$

$$\Lambda = 4.1\, R^{-0.21} \qquad R = \text{rain rate}$$

$$N_0 = 8 \times 10^{-3}\, m^{-3}\, mm^{-1}$$

A computed drop size distribution by Srivastova (1971) assumed that drop size was determined by coalescent growth and spontaneous break-up and showed that the final distribution was independant of the initial distribution state but depended on the initial liquid water content.

Fig. 9·2

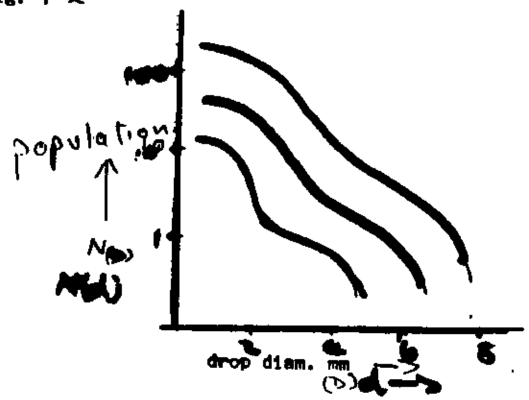

From Doviak

Rain rate and drop size are connected by the terminal velocity of the drops in still air and complicated by vertical air motion. Observed terminal velocities are shown below.

Fig. 9.3

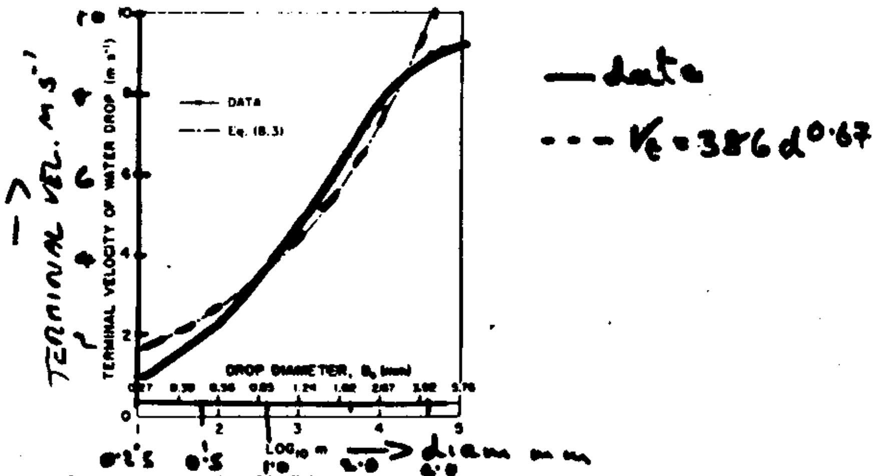

. Terminal velocity (solid line) of distilled water droplets in stagnant air at 76-cm-Hg pressure, 20° Centigrade, and 50% relative humidity, as function of the mass m (in micrograms) or the equivalent spherical diameter D. (Data from Gunn and Kinzer, 1949.)

still air, 1 atm, 20°C

Rain rate + drop size

Number of drops falling thro' unit area in time δt of size d to $(d+\delta d)$

$$= N(d)\, V_t(d)\, \delta d\, \delta t$$

each drop is of mass $\frac{1}{6}\pi\rho_w d^3$

$\therefore$ Rain rate

$$= \int_0^\infty V_d N(d)\, m\, dd$$

$$= \frac{\rho_w \pi}{6}\int_0^\infty d^3 N_d V_d\, dd \quad \text{as a mass}$$

or Rain rate

$$= \frac{\pi}{6}\int d^3 N_d V_d\, dd \quad \text{as a depth}$$

Substituting for N_d, V_d & integrate

$$R = \frac{\pi N_0}{\Lambda}\left[9.65 - \frac{10.3}{1+\frac{600}{\Lambda^4}}\right] \text{m s}^{-1}$$

Cloud water content and drop size

Mass of drops of size d to $(d+\delta d)$

$$\delta M = \frac{\pi}{6} d^3 \rho_w N_d\, \delta d$$

So cloud water density $(M) = \int \delta m$

$$= \frac{\pi \rho_w}{6}\int_0^\infty d^3 N_d\, dd$$

If $N(d) = N_0 \exp(-\Lambda d)$

$$M = \frac{\pi \rho_w N_0}{\Lambda^4}$$

Radar reflectivity Z

$$Z = \int_0^\infty N_d\, d^6\, dd$$

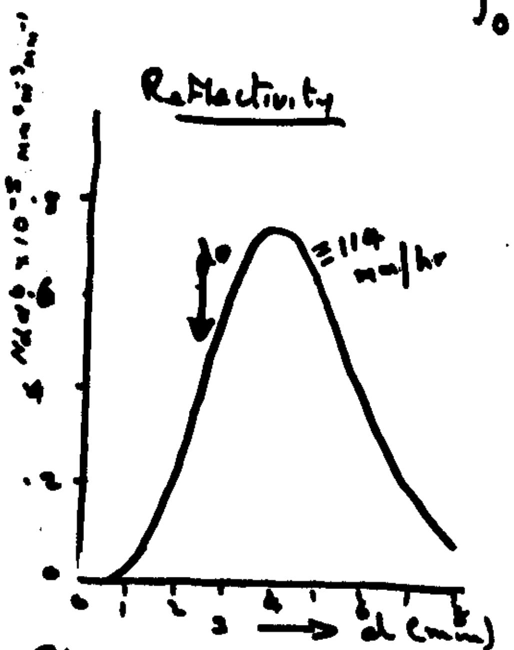

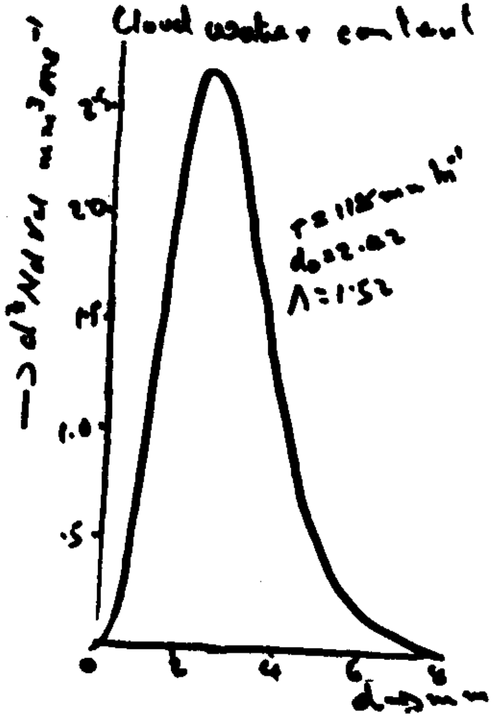

BUT !

Even with model distributions & spherical drops we have a two parameter distribution and only one measurement

So back to empircal relationships

As the N(D) depends on the type of rain, so do the emperical relationships

Using M-P for rain from stratoform cloud

$$Z = 200 R^{1.6}$$

For orographic cloud

$$Z = 31 R^{1.71}$$

For Cb

$$Z = 486 R^{1.37}$$

See Batten for ≈ 70 other relationships.

DUAL PARAMETER METHODS

a) Dual wavelength.

The σ is a function of λ so the two λ give different Z values and these can be interpretted in terms of the drop size distribution. A short wavelength is chosen for the higher reflectivity however attenuation may become a problem.

b) Dual polarization

The difference in reflectivity of vertically and horizontally polarized radar beams arises from the non-spherical component of the drops. This is related to drop size and together with the Z values can be related to the drop size distribution

c) Reflectivity and attenuation at different wavelengths. Both the attenuation coef and the radar reflectivity factor can be related to Λ and N_0 so drop size distribution can be determined.

Almost absolute, but of little operational value.

d) Single wavelength $Z \neq Z'$

Active radar on satellites

Problems

1) Poor surface resolution

$$d = \frac{1.2\lambda}{D} \approx \frac{1.2\times10^{-2}}{1}$$

$\approx$ 12km at 1000 km

$\approx$ 400km at 36,000 km.

2) Low returned power.

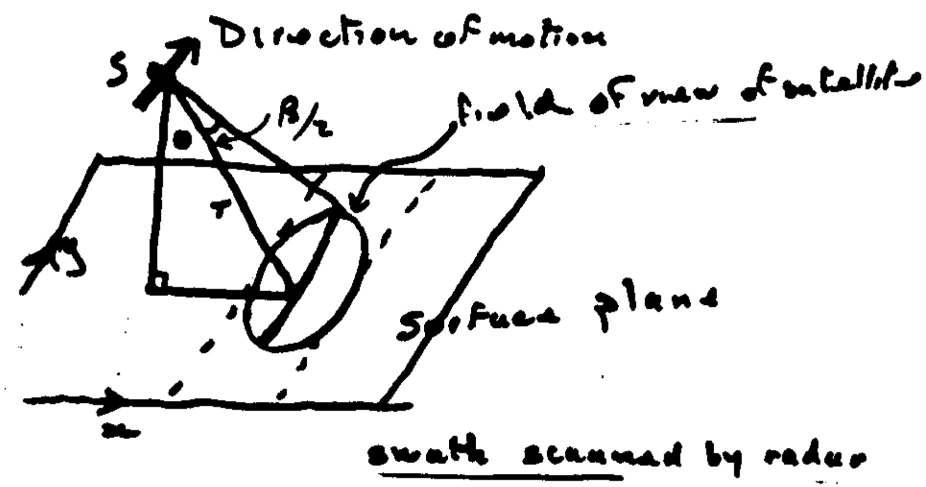

x resolution $\frac{\text{pulse length}}{2\cos\theta}$

Y resolution $r \sin\beta/2$

The S.A.R. (SEASAT).

When a pulse is transmitted and received its power/time curve may resemble

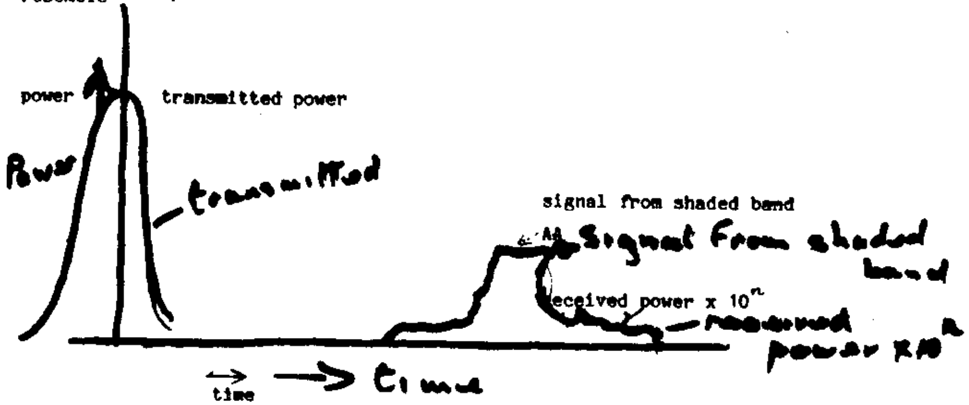

In the SAR both the received power and the x direction resolution are increased by coding the pulse signal by changing its frequency slightly throughout the duration of the pulse.

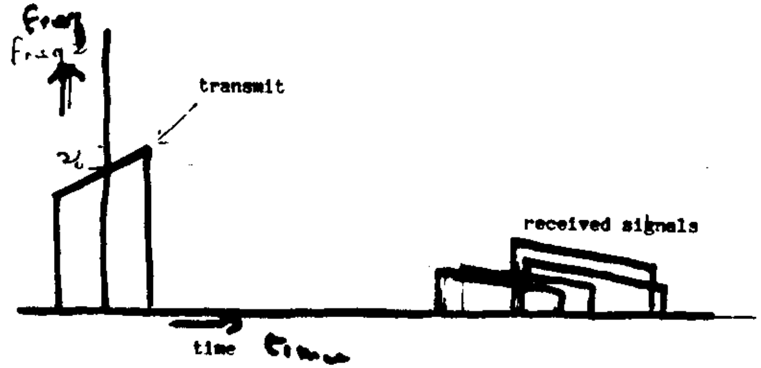

The received signal is then delayed according to its frequency so the whole pulse is compressed after reception, thus increasing power and resolution. This technique is known as the CHIRP.

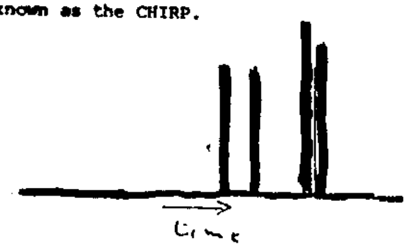

Satellite moving at speed v in y direction emitting pulses at S_1, S_2

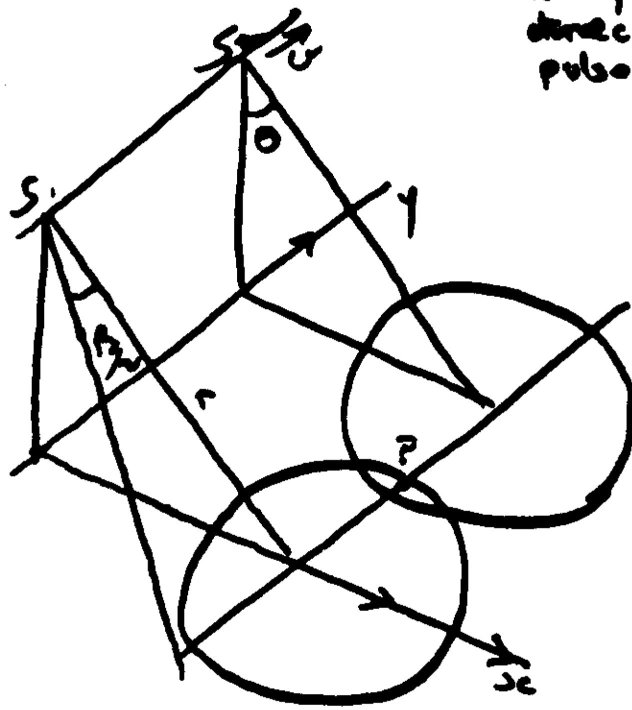

A point must be viewed by at least two pulses

So max. synthetic aperture (A_s) is S_1S_2

$$S_1S_2 = r\sin\beta \sim r\beta$$
$$= A_s$$

and the resolution of the synthetic aperture $\beta_s = \frac{1.2\lambda}{A_s}$

$$= \frac{1.2\lambda}{r\beta}$$

But $\beta = \frac{1.2\lambda}{A_r}$

$\therefore \beta_s = \frac{A_r}{r}$ angular resolution

spatial resolution

$$= \underline{\underline{A_r}}$$

Limited by no. of pulses necessary to perform the analysis and by the loss of power if A_r too small

Pulse repetition frequency

min $\frac{v}{1.5r\beta} = \frac{vA_r}{1.5r\,1.2\lambda} \approx \frac{7\times10^{3}\times1}{1.5\times1.2\times10^{-2}\times10^{6}} \approx 10^{-1}\ s^{-1}$

max $\frac{c}{2r} \approx \frac{3\times10^{8}}{3\times10^{6}} \approx 10^{2}\ s^{-1}$

N.B. the higher P.R.F. the better the s/n ratio

Doppler radars in storm research

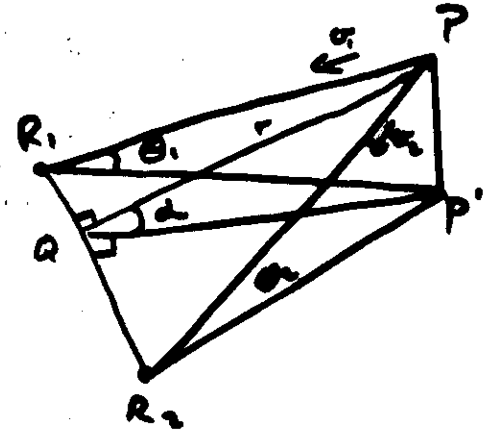

$R_1 R_2$ radars
P common target
P' projection of P on horizontal
r = PQ normal to R_1R_2
θ_1, θ_2 elevations of P from R_1, R_2
v_1, v_2 doppler vel. towards R_1, R_2
α angle between R_1PR_2 plane and horizontal

Using doppler determine v_1, v_2. We require velocities of air in cylindrical coordinates based on axis R_1R_2 in the plane R_1PR_2 and $\perp$ to it.

v_1, v_2 contain the motion of the raindrops due to gravity so

$$w = 2.65\,Z^{0.114}\left(\frac{\rho}{\rho_0}\right)^{0.4}\ m\,s^{-1}\quad \text{(Atlas)}$$

so put $v_1', v_2' = v_1 - w\sin\theta_1,\ v_2 - w\sin\theta_2$

Now we can resolve v_1, v_2 along and $\perp$ to r, and repeat for a grid of points in the R_1PR_2 plane.

Repeat for other planes.

Use eq. of cont. in cyl. coords to obtain winds $\perp$ to cylindrical planes. Convert to normal coords.

R_1R_2 50 to 100 km

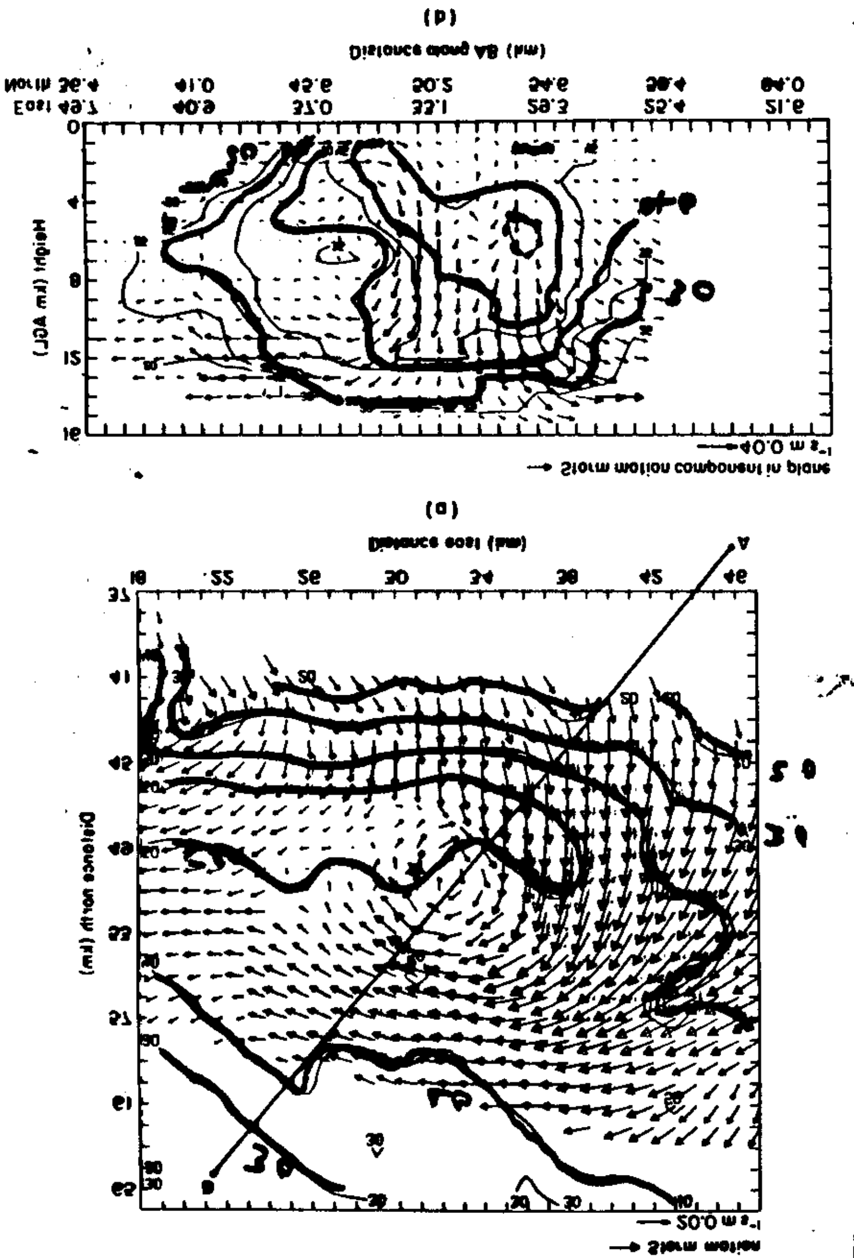

Validation of remotely sensed data

Point v area measurement

Study spatial variability

Calibrate in a statistical sense

Intermediate scale measurements

Mans impact on climate

i.e. errors in "ground truth"

e.g. rain fall

68

INTERNATIONAL ATOMIC ENERGY AGENCY
UNITED NATIONS EDUCATIONAL, SCIENTIFIC AND CULTURAL ORGANIZATION

INTERNATIONAL CENTRE FOR THEORETICAL PHYSICS
34100 TRIESTE (ITALY) - P.O.B. 586 - MIRAMARE - STRADA COSTIERA 11 - TELEPHONES: 224281/2/3/4/5/6
CABLE: CENTRATOM - TELEX 460392 - I

H4.SMR/164 - 13

WORKSHOP ON CLOUD PHYSICS AND CLIMATE

23 November - 20 December 1985

ATMOSPHERIC CLOUD PHYSICS MEASUREMENTS -II
(Extra lecture notes)

C. SAUNDERS

University of Manchester, U.K.

Calibrated Thermometer

Mercury or Alcohol

Accuracy 0.1°c

Thermocouple

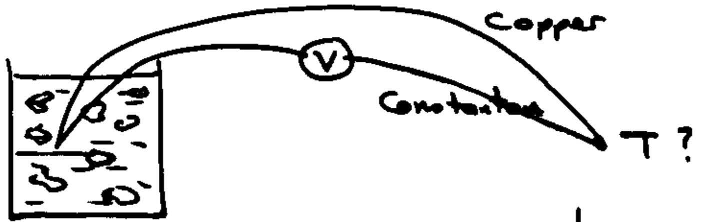

Constant Temperature Bath. Ice/water at 0°c.

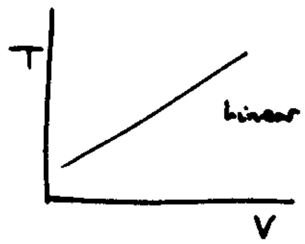

Accuracy 0.01°c

Thermistor

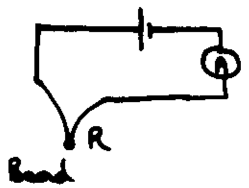

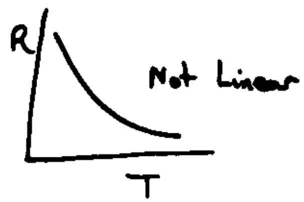

Accuracy 0.1°c

Platinum Resistance Thermometer

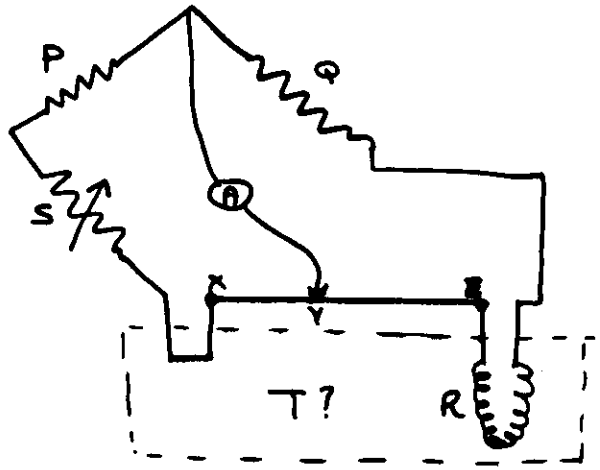

$$\frac{P}{Q} = 1 = \frac{S + (r\,XY)}{R + (r\,YZ)} \qquad \text{For } A = 0$$

r = resistance / length of wire XZ.

Manufacturers give R/T data in form of polynomial.

Humidity Measurements

1) Wet and Dry bulb.
(Sling psychrometer)

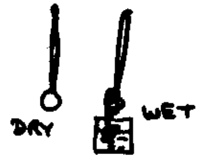

2) Lyman α Absorption. 121nm (Kyle)
(Fast Response, £2000/sensor, optics prone to NaCl damage.)

3) Capacitance.

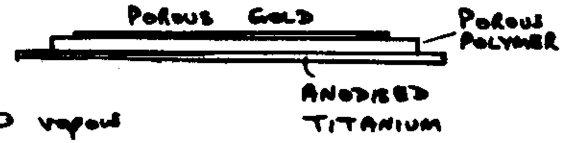

Polymer absorbs H_2O vapour
k_{POLY} changes. $C = 500pf \pm 1pf / \%$ RH change
Linear response. (2 seconds) Contaminant Sensitive
Cost £50 from Lee Integer, Vaisala.

4) Carbon Hygristors

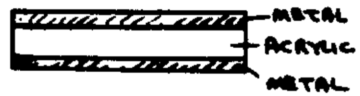

2 × 6 cm.

Acrylic/carbon absorbs H_2O which changes R.
Response Time 0.2 s.

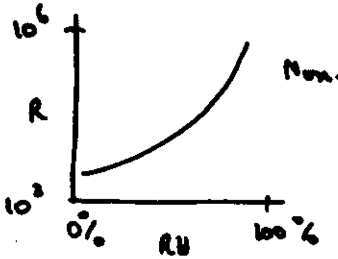

Non-linear

Linearising Circuit

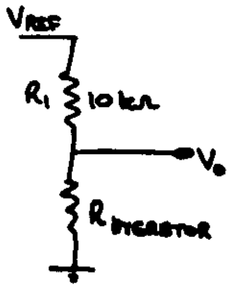

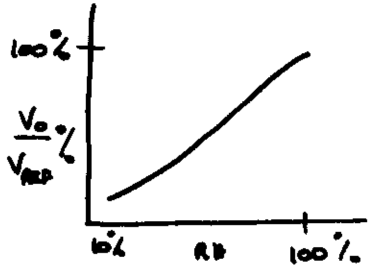

5) Direct Capacitance Method.

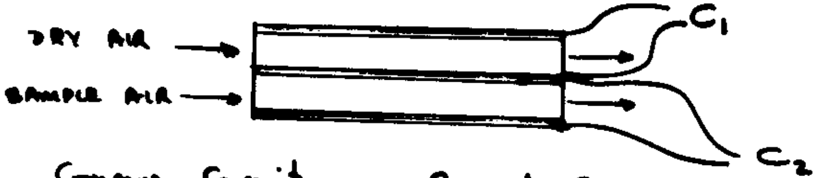

Compare Capacitances C_1 and C_2
$(\varepsilon - 1)$ for dry air $= 6 \times 10^{-4}$
$(\varepsilon - 1)$ for H_2O vapour $= 1.6 \times 10^{-4} \rho$
$\rho \equiv g\, m^{-3}$.

Dew Point (Frost Point)

Cambridge hygrometer

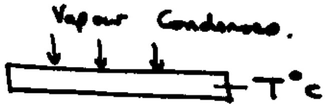

Cooled, then heated surface

Liquid Water Content

1) Psychrometric Method. See Wishart pp 3 and 22
2) Rotating Impactor. Need Collision Efficiencies.

2-D Probes (OAP)

(Two-Dimension) (Optical Array Spectrometer)

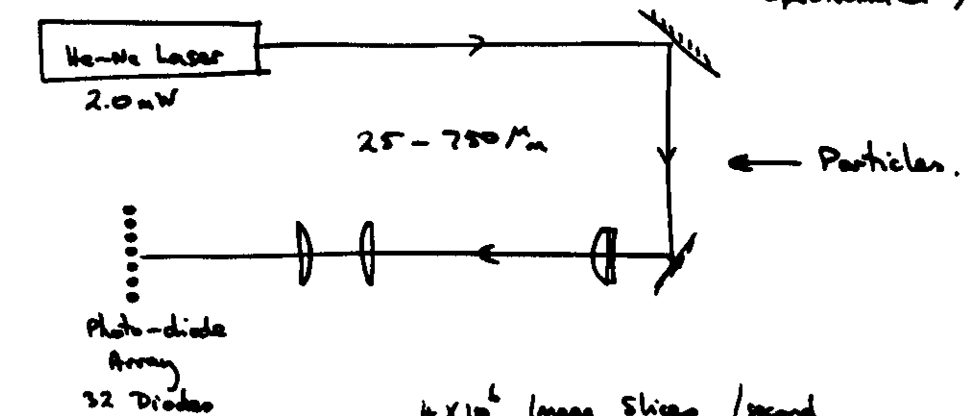

4×10^6 Image Slices / second

$\equiv$ 250 nsec.

OAP-2D-C

Air Speed = 100 m sec^{-1}

$\therefore$ Minimum Detectable Size = 25 μm

OAP-2D-P

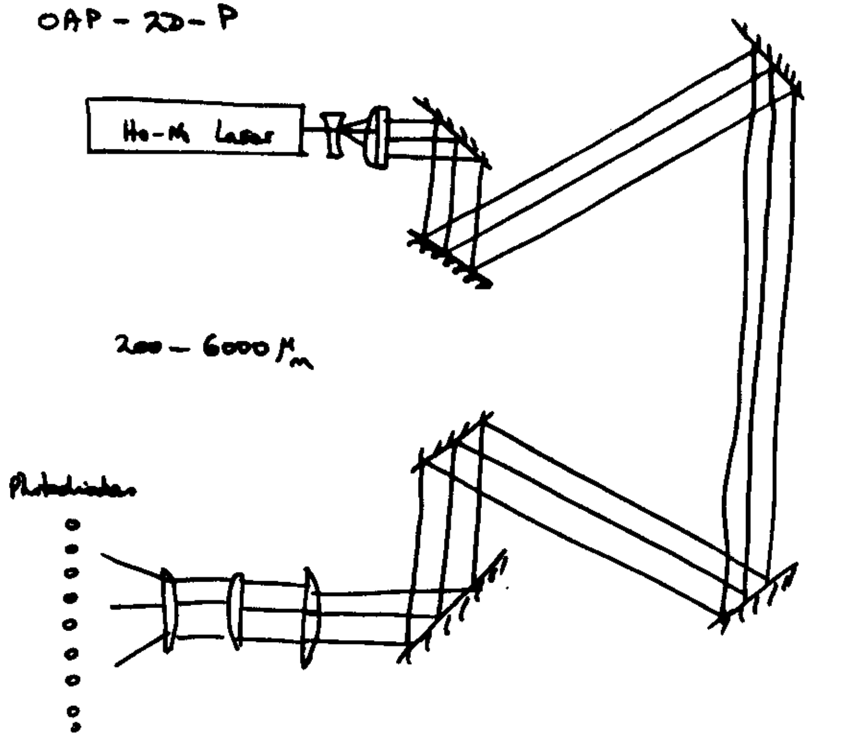

3

radar pulses. Studies of hydrometeors using airborne imaging devices correlated with one or more radars observing the same region of cloud or precipitation as the aircraft will lead to further understanding of storms.

- Are automatic particle-counting and sizing instruments giving an accurate representation of the cloud being observed? By giving the scientist a "look" at the cloud, imaging devices serve as a check on the integrity of data coming from other counting and sizing instruments. Data from electronic and electro-optical devices may be influenced by electronic noise, icing, or collection efficiency problems that might otherwise go undetected if the data look reasonable. Automatic sizing instruments give the size of the projected image; the measured size depends on orientation of the particles. This orientation can often be determined with imaging instruments. The accuracy and interpretation of impressions or replicas can also be checked by comparison with images obtained using imaging devices.

We will describe three imaging devices currently in use— the two-dimensional optical array spectrometer probe of Particle Measuring Systems (PMS), Boulder, Colorado; the NCAR particle camera; and the airborne holography system of Science Applications, Inc., El Segundo, California.

The Optical Array Spectrometer Probe

The PMS two-dimensional array spectrometer probe, developed under the direction of Robert Knollenberg (of PMS), is a unique variation of the optical array particle-sizing probe described in the article by A. Heymsfield in this issue. In the sizing probe, the particles pass through a parallel light beam from a continuously radiating laser and a shadow is cast on a linear array of light sensors (photodiodes) located in the beam. The size of each particle is determined by electronically counting the number of sensors with light extinguished below a 50% intensity threshold by the shadow. In the two-dimensional probe, the entire array of sensors is sampled at a "slice" rate proportional to the true airspeed. By use of a high-speed, front-end data storage register, each sensor can transmit up to 1,024 bits of shadow information for each particle. A series of "image slices" is recorded across the shadow to develop a true two-dimensional image.

Figure 1 illustrates the data format for a dendritic ice crystal. All together in the basic probe there are 32 sensors in the linear array, each imaging a portion of the light beam 25 μm in diameter. Because of the shadow cast by the particle, the light level falls to the threshold of detectability (50%

Fig. 1 Star-shaped dendritic ice particle passing across optical array of PMS two-dimensional probe is imaged as a matrix of zeros and ones, depending on absence or presence of light (at 50% extinction) on the optical sensors during each slice.

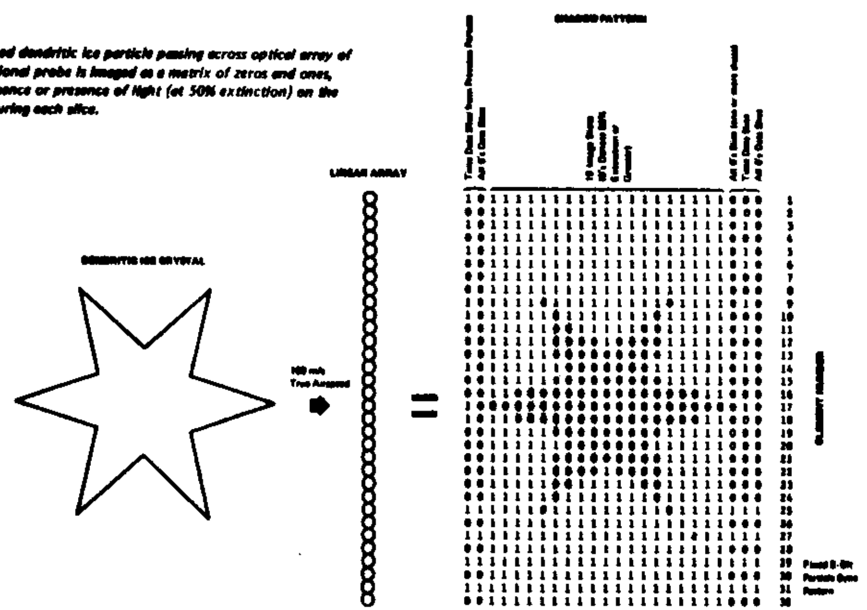

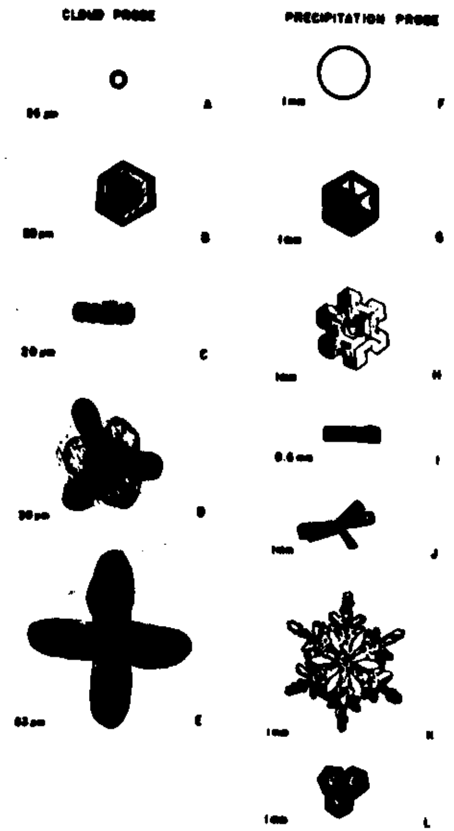

Fig. 4 Parts A - E are tracings of ice crystal microphotographs for sizes smaller than 100 µm as they would appear if viewed from above or focused on the optical array of the probe. Parts F - L are ice crystals larger than 300 µm as they would be focused on the optical array of the precipitation probe.

Parts B-E of Fig. 4 show tracings of ice particles smaller than 100 µm in length, which one would expect to be sized by the cloud probe. The plate ice crystal (B) is generally oriented with its long axis horizontally aligned to the array, and its cross section is therefore read as nearly spherical. The depth of field will be the same as that for a sphere of equivalent diameter, it will be sized properly, and the calculated concentration will be correct. But consider the column in part C. Its long axis will be horizontal in the atmosphere, but its orientation will be random when it passes through the linear optical

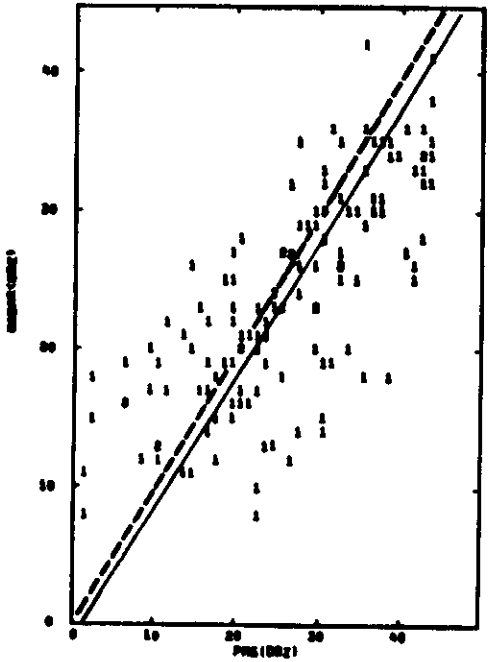

Fig. 5 Radar reflectivity factor measured by NSSL radar (dBZ = 10 log Z) and calculated from PMS precipitation probe in nearly the same region of the cloud. Each 1 point is a 1 km average, and a 2 point indicates two 1 km points on top of each other. The dashed line is at 45°, and the solid line is a least-squares curve through the data points.

PROBE / RADAR Comparison in rain.

array. Therefore, it will be read at values ranging from its full length (20 µm) to its width (6 µm) when passing through the array. A 100 µm column with a similar length-to-width ratio may be sized anywhere from 100 µm to about 30 µm. The distributions can be "transformed" on the basis of this random columnar crystal orientation (Heymsfield and Knollenberg, 1972) if all the particles are columnar.

Other problems may be associated with measuring the columnar particle in part C. Assume that it passes through the array at its full length. Even if in perfect focus on the array, its cross-sectional area per channel will be $6 \times 20 = 120\ \mu m^2$, compared to the channel cross-sectional area of $20 \times 20 = 400\ \mu m^2$. Therefore, the reduction of light intensity will be 120/400 = 30%, not enough to trigger the flip-flop switch or to register a count as a particle. In addition, the

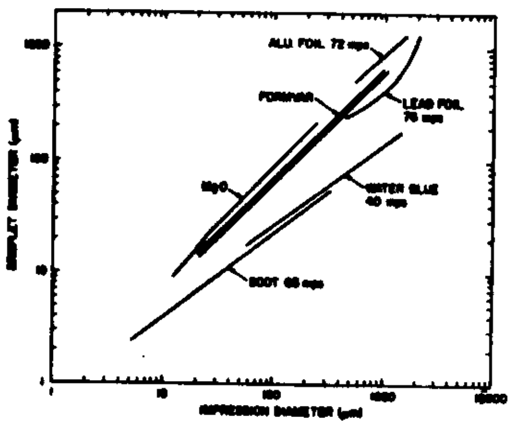

Fig. 1 Relation between droplet diameter and impression diameter for various sampling media.

Fig. 2 Drop impressions in soot layer. (Photo courtesy of J. Dye, NCAR.)

Slide Impactors

• *Oil-Coated Slides*. One of the earliest measurements of cloud droplet sizes was made by Fuchs and Petrjanoff (1937). A clean glass slide coated with a mixture of light mineral oil and petroleum jelly was used to capture cloud droplets and keep them submerged until they had been photographically recorded. The method was improved and used in an aircraft by Mazur (1943), who saturated the mineral oil with distilled water to prevent the droplets from diffusing into the oil.

Slides coated with castor oil were used in the first extensive set of measurements of droplet sizes in cumuliform clouds by Weickman and Aufm Kampe (1953). With this method it was possible to collect droplets as large as 200 µm in diameter with no apparent shattering if the impact velocity was less than 100 m/s.

A large amount of droplet data was obtained by an automated sampler designed by Brown and Willett (1955). In their sampler three slides coated with silicone oil moved in rapid succession through an airstream and were photographed under a microscope in a cold cabin. The results for mean droplet distributions in trade-wind and summertime U.S. continental cumuli were reported by Braham, Battan, and Byers (1957) and by Battan and Reitan (1957).

These methods gave us the first details of the droplet spectrum at different geographical locations. A disadvantage of using them is that the sample must be recorded immediately, a procedure which is difficult in turbulent air. It is also necessary to know the exact time that elapsed between sampling and recording in order to apply diffusion corrections.

• *Magnesium Oxide Method*. Another widely used method involves coating a clean glass slide with a thin film of magnesium oxide. Droplets impinging on the film leave round holes which are proportional to their size.

This technique was developed and calibrated by May (1950) for drop diameters between 10 and 240 µm. For droplets larger than 20 µm in diameter, the ratio of droplet diameter to impression diameter was found to be 0.86; it remains constant with droplet size. Data reduction requires the investigator to examine the slide surfaces by microscope with a strong transmitted light and record the images photographically. This method is not affected by drop diffusion and droplets cannot coalesce, so the samples can be preserved. One disadvantage is that this layer is rather fragile in texture and can break off because of buffeting by the airstream. Another is that drops below 8 µm in diameter cannot be sized with certainty because the texture and grain size of the magnesium oxide interfere. Squires and Gillespie (1952) used this technique in a gun-type sampler which could be reloaded in about 50 s during flights. They exposed ten rods 3 mm wide (yielding a high collection

The foil impactors provided our first drop-size distributions for precipitation-sized particles (>250 μm in diameter) in natural clouds. Yet there are still problems with these devices. One is that it is difficult to obtain a representative sample of large drops if they occur in low concentrations. Increasing the sampling volume yields an overexposure of the smaller drops, resulting in overlapping of the imprints. Moreover, during icing conditions instrument reliability depends on how successfully deicing elements were employed. It is not always possible to make a clear distinction between liquid and solid hydrometeors from impressions obtained in a mixed-phase cloud. Calibration of imprints is not available for solid particles. Under all conditions, data handling and analysis are tedious and subjective.

Replicator Devices

Replicator devices have been widely used in cloud physics studies. They are mechanized sampling devices using the well known Formvar technique to capture and permanently encapsulate cloud particles (see MacCready and Todd, 1964; Spyers-Duran and Braham, 1967; Spyers-Duran, 1972a). They utilize a Mylar tape (usually a 16 mm polyester leader) which is coated with a solution of Formvar plastic and chloroform. (For airborne use, chloroform is preferred since it is nonflammable.) The continuously moving ribbon of Formvar is exposed in a cloud through a sampling slit several millimeters wide and then carried into a drying compartment where the plastic sets quickly. There, the encapsulated particles evaporate, leaving behind permanent replicas which can be sized and counted after suitable magnification. Since it is possible to obtain a continuous record through a cloud, the replicas can provide small-scale resolution of changes in cloud microstructure. Recently developed devices have the capability of viewing the replicas shortly after exposure so that tape speed and Formvar thickness can be adjusted in flight, as reported by Christensen, Keller, and Hallett (1974). Another major advantage of this method is that simultaneous recording of cloud droplets and ice crystals is possible (see Fig. 5).

Basically these devices are simple; however, they require a great deal of design compromise. In designs in which coatings

(a)

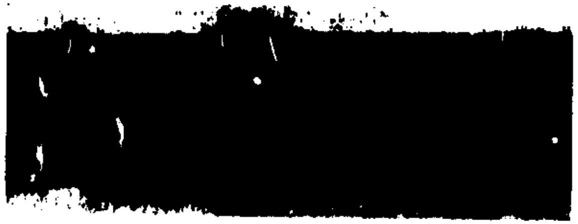

(b)

Fig. 4 Impressions of precipitation-sized particles in a lead foil exposed on the University of Chicago Lodestar aircraft (a), and in aluminum foil exposed on the South Dakota School of Mines and Technology T - 28 aircraft (b). Smallest diameter is 250 μm. (Sample a, courtesy of E. Brown, NCAR; sample b, courtesy of C. Knight, NCAR.)

Fig. 5 Replicas of supercooled droplets (A), a snow pellet (B), and ice crystal columns (C).

RADKE – TURNER ICE CRYSTAL PROBE

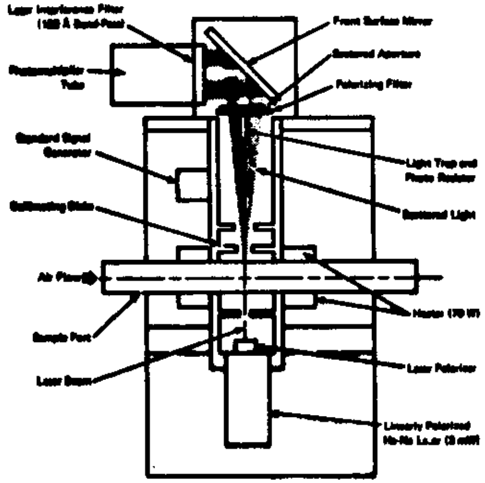

Fig. 1 Schematic representation of the University of Washington's automatic optical ice particle counter.

system so that linearly polarized infrared light is incident on particles passing through the sample pipe. The light sensor (a solid-state device) detects the infrared light that is scattered at an angle of 90° (actually a cone of light around a scattering angle of 90°) after the light passes through an optical system containing a polarizing filter set for maximum extinction.

It can be seen from the description of the two instruments that the UW-IPC detects forward-scattered light while the Mee-IPC detects light scattered at an angle of 90°. As we will see below, this difference becomes important in discussing the mechanisms for the detection of ice particles in the two systems.

Mechanisms for Ice Detection

There are three possible mechanisms for the detection of ice particles in the two devices described above (see Turner and Radke, 1973, for a more detailed discussion):

- The rotation of the plane of polarization of the light beam, produced by the birefringent property of ice, as it passes through the ice particles
- The detection of specularly reflected light from the external faces of ice crystals
- The detection of light scattered at a preferred angle by the ice particles.

Owing to the birefringent (or double refracting) property of ice, linearly polarized light that is transmitted through ice will, generally, be rotated in such a way that although the light

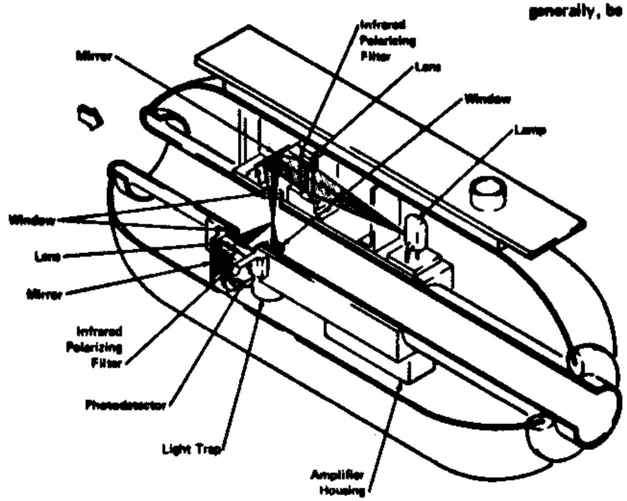

Fig. 2 Schematic diagram of the Mee Industries automatic optical ice particle counter. The pod is 45.7 cm (18 in.) long and 17.8 cm (7 in.) in diameter. The cylindrical opening in its center is 5.1 cm (2 in.) in diameter.

26

STATIC DIFFUSION CHAMBER FOR CCN

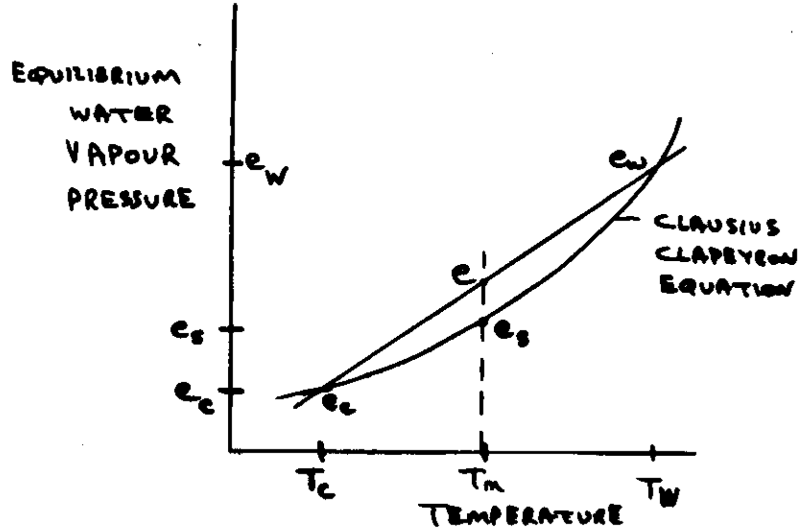

Saturation Ratio, $s_w = \left(\dfrac{e_w - e_c}{2} + e_c\right)\Big/ e_s$

$s_w = (e_w + e_c) / 2e_s$

Supersaturation % $= (s_w - 1) \times 100$

$$S_w = \left(\frac{(e_w + e_c)}{2e_s} - 1\right) \times 100 \quad \%$$

Camera views drops.

Ice Nuclei Detection.

Deposition Nuclei : Filters + Static Diffusion Chamber or Continuous Flow Chamber below water Saturation.

Condensation Freezing Nuclei : Continuous Flow chamber above water saturation.

Contact Nuclei : Drop Freezing (Vali)

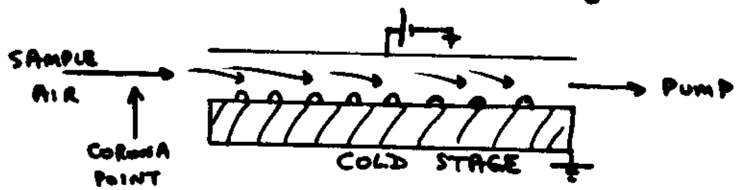

Charged nuclei are deflected in field onto supercooled (pure) water drops.

Immersion Nuclei Sample Drop Freezing (Vali)

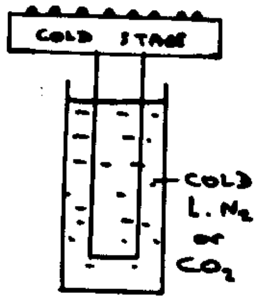

Cool drops containing the nuclei and watch for them to freeze. Note the number freezing at each temperature.

Contact Nuclei Spray Technique

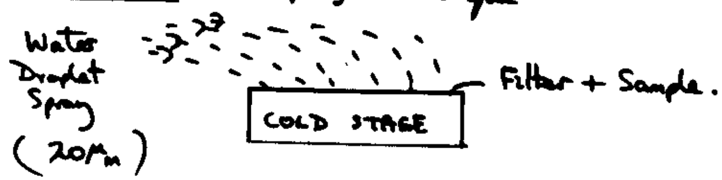

Diffusion Battery

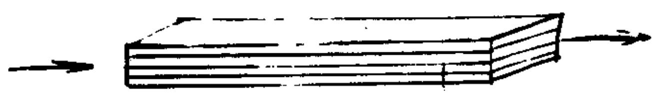

Many plates. Small particles diffuse to the plates and are captured. Only the large particles pass through.

Cascade Impactor

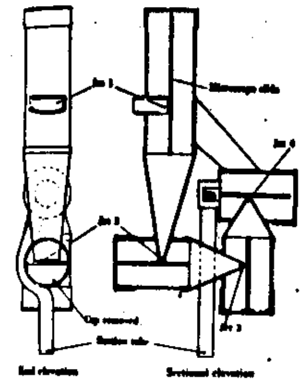

Fig. 2. Diagram of cascade impactor

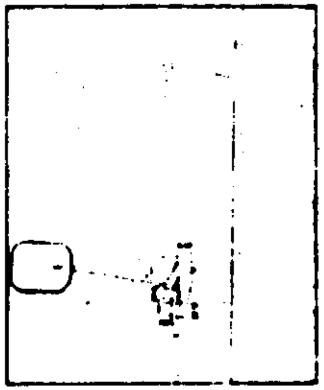

Fig. 3. Field sampling suspension

Aircraft Measurements

a) Vertical Wind . ~ 1 second (100m) resolution.

i) Cheap method: Slow down and let the plane "follow" the air vertical velocity. Find the vertical velocity from the altimeter rate of change.

ii) Accurate method : $W_{ag} = W_{ap} + W_{pg}$

W_{ap} = Air vertical velocity with respect to plane.
W_{pg} = Plane " " " " " ground.
W_{ag} = Air " " " " " " .

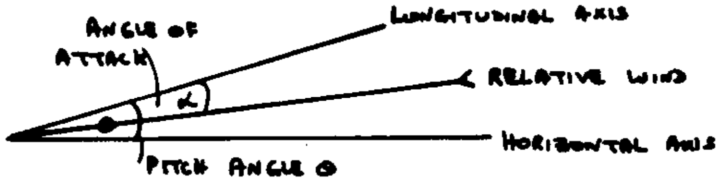

$$W_{ag} = \underset{\substack{\uparrow \\ \text{True Air Speed}}}{TAS} \sin(\theta - \alpha) + \int \underset{\substack{\uparrow \\ \text{Vertical Acceleration}}}{a_z}\, dt$$

$$TAS = IAS \left(\frac{0.1309\,(^\circ k)}{\text{Pressure Alt in " of Hg}} \right)$$

IAS = Indicated Air Speed. (from Pitot Tube)

Pitch, θ, Vertically stabilised accelerometer. (VSA)

α, Vane on nose boom, or side of aircraft.

W_{pg}, from the VSA.

b) Horizontal Wind . Doppler System + Yaw Vane.

$V_{ag} = V_{ap} + V_{pg}$ ← 'plane relative to ground

Wind = Air relative to ground ; ↖ Air relative to plane

Doppler radar → V_{pg} . TAS + Yaw Vane Angle → V_{ap}.

7

CLOUD SEEDING

Objective To increase ice particle concentration.

Aims 1) Ice clouds are more efficient than water clouds at producing precipitation. [Increased Rainfall]

2) To reduce damage to crops from hail. [Hail Suppression.]

1) To Increase Precipitation:

a) Cloud physics study of clouds — is there water available in the cloud? Can this water be frozen by seeding? Will the precipitation fall where you want it?

Increase buoyancy / Dynamic Seeding eg Florida.

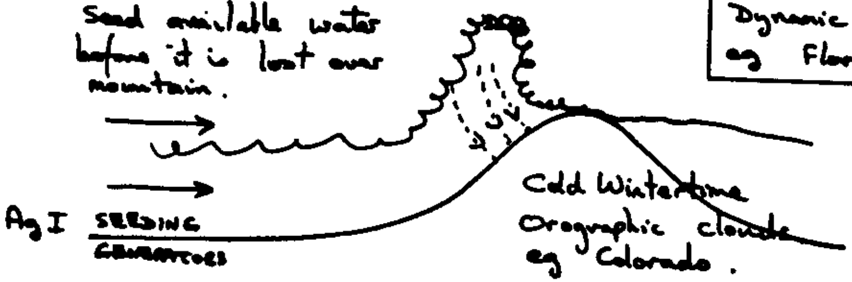

2) To Reduce Hail:

Methods 1) Total Glaciation — Ice Crystals blow away. > 10 gm AgI / min / km^2. Too Expensive.

2) Beneficial Competition. Many small particles compete for available water — so insufficient water for large hail to grow.

Works best for storms with warm cloud bases — frozen-drop embryos are efficient hail producers — so artificially seeded frozen-drop embryos give competition. Storms with cold bases have graupel embryos which start on small crystals higher up — competition seems inadequate. [eg Colorado]

Cloud Seeding (2)

Agents AgI – NH_4I – Acetone. (Better epitaxial fit than AgI.) Still active 90km downwind. (hrs) No deactivation.

Cheaper is Titanium Oxide coated with AgI (20% cost)

Pyrotechnic Flares at cloud base — 400 Xtals / l after 4 mins. Aggregates in 13 mins. Traced by glider. 10^{11} particles / gm of AgI.

Burn a AgI – acetone mixture on the ground or on aircraft generators. (400gm / hr.)

Top seeding, $-14°C$, 16 – 20,000', into feeder towers. 50gm droppable pyrotechnic flares.

Tracers To check whether seeding agent would get into the cloud at the right place.

eg Tag AgI with Titanium Dioxide. Detect on captured precipitation with ion probe analysis.

Other Methods

Carbon black, 0.1 μm particles — absorb solar energy.

Cool by releasing compressed air or gas.

Warm Rain — Hygroscopic seeding — NaCl — Langmuir chain reaction — drop breakup. Models show need for ≥ 10 ms^{-1} updraught. No results yet.

Fog — Helicopter Downwash — mixing.
— Water jets to wash-out fog.